INVESTIGATION OF THE PARTIALLY IONISED INTERSTELLAR MEDIUM ASSOCIATED WITH THE HII REGIONS

ABDUL QAIYUM

ABSTRACT

THESIS SUBMITTED FOR THE DEGREE OF

Doctor of Philosophy

IN

PHYSICS

TO

ALIGARH MUSLIM UNIVERSITY,

ALIGARH

1983

T 2821

T 2821

ABSTRACT

A detailed study to explain the intensities of radio-recombination lines of partially ionised hydrogen, carbon and of other elements from NGC 2024, Orion A and W3 is reported here. For that purpose we work out the details of the reaction Cl II + H_2 $\longrightarrow$ HCl II + H and photo-dissociation HClII + $h\nu$ $\longrightarrow$ H II + Cl, as a source for the production of H II in the inter-stellar clouds. Further, based upon the large number of gas-phase, gas-grain reactions and other relevant atomic and molecular processes, a chemical balance is set up to evaluate the position dependent electron density and density of ionised species from which line emissions are considered here.

A thermal balance is also set up between heating and cooling to calculate the temperature structure of the regions in question. A large number of heating processes are considered and their relative importance is also studied here. Investigations on the importance of far infra-red radiation (FIR) field from the dust-grain in HII region on the cooling in HI region at low temperature is also reported here. In particular we have performed detailed calculations for cooling at low temperature, $T_e < 100$ K, as only these regions are affected in the presence of FIR.

To calculate the line-intensity, statistical equilibrium corresponding to each position, is solved and thereby departure

coefficients from thermodynamic equilibrium (b_n) are calculated. The best fit of the observed recombination line-intensities over the frequency spectrum (0.6 GH_Z to 15 GH_Z) are used to derive the physical parameters of the clouds for solar as well as depleted abundance. It may be added that position-dependent temperature and density is being studied in detail for the clouds in question to calculate the line-intensities, for the first time here in this work.

It is found that cool region of narrow hydrogen lines (H^o) lie in between CII and HII regions, sharing some portion with CII region but slightly displaced towards the boundary of HII region. The depth of ionisation of heavy elements are large and they share the whole of CII region and also have some region in common with the molecular region. The temperature and density are not constant over the line-emitting regions. Two regions of neutral hydrogen along a line of sight is predicted theoretically and column densities are found to agree well with the observed one. The calculated column densities of the molecule in general depend upon the assumed abundance. But column density of OH agrees well with the observed one for both abundances, while column density of CO for the assumed size of the cloud is closer to the observed value for solar abundance.

The best fit of the carbon lines yield a density range $2x10^4$ to $4x10^5$ cm^{-3} for solar and $5x10^4$ to $2x10^6$ cm^{-3} for depleted

abundances. The ratios of α and β lines of carbon, α lines of S and C, and H and C at the same frequencies are compared with the observations. It is found a moderate depletion of C and S and heavy depletion of Mg, Si and Fe lead to a fairly good agreement.

It is further concluded that a slight more depletion will give a high hydrogen density range and consequently temperature obtained from the thermal balance would be $\gtrsim$ 300 K, due to which the detection probability of the lines would be low. This may be one of the reasons of the absence of the carbon recombination lines in the neighbourhood of many HII regions.

INVESTIGATION OF THE PARTIALLY IONISED INTERSTELLAR MEDIUM ASSOCIATED WITH THE HII REGIONS

ABDUL QAIYUM

THESIS SUBMITTED FOR THE DEGREE OF

Doctor of Philosophy

IN

PHYSICS

TO

ALIGARH MUSLIM UNIVERSITY,

ALIGARH

1983

T2821

Certified that the work presented in this thesis is the original work of Mr. Abdul Qaiyum, done under my supervision.

(Dr. S.H. Razaullah Ansari

Department of Physics,
Aligarh Muslim University,
Aligarh (U.P.)
India.

C O N T E N T S

		Page
ACKNOWLEDGEMENTS		
Chapter 1:	INTRODUCTION	1
	TABLE 1.	9
	FIGURES 1. and Diagram 1	
Chapter 2:	ABUNDANCE CALCULATION	10
	2.1 Introduction	10
	2.2 Flux and its Attenuation	11
	2.3 Ionisation and Dissociation Rates in a Medium Close to an Early Type Star.	14
	2.4 Chemical Reactions and Recombinations	15
	2.5 Chemical and Ionisation Equilibrium	16
	2.6 Results and Discussion	20
	2.6.1 Ionisation Structure	20
	2.6.2 Abundances of molecules and neutral hydrogen atom	25
	TABLES 2.1a —— 2.9	31
	FIGURES 2.1(a) —2.4(b) and Diagram 2	
Chapter 3:	THERMAL STRUCTURE	51
	3.1 Introduction	51
	3.2 Heating Mechanism	53
	3.2.1 Heating due to photo-electrons from dust grains	53
	3.2.2 Cosmic ray heating	58
	3.2.3 Heating due to H_2 formation and its dissociation	60
	3.2.4 Heating by photo-ionisation of heavy elements	61

			Page
	3.2.5	Chemical heating	62
	3.2.6	Gravitational contraction ..	62
	3.2.7	Gas-grain interaction	63
3.3	Cooling	....	64
	3.3.1	Level population and cooling rate	64
	3.3.2	Induced transition	66
	3.3.3	Cooling by atoms, ions and molecules	67
3.4	Numerical results and discussions		72
	3.4.1	Effect of density and UV radiation on photo-electron heating	72
	3.4.2	Effect of Far Infra-red Radiations on cooling	74
	3.4.3	Relative importance of various heating and cooling mechanisms and temperature distribution	78 87
TABLES	3.1	....	
FIGURES	3.1 — 3.8		
Chapter 4:	INTERPRETATION OF RADIO-RECOMBINATION LINES FROM PARTIALLY IONISED MEDIUM ADJACENT TO HII REGIONS	....	89
4.1	Introduction	....	89
4.2	Statistical Equilibrium	....	91
4.3	Brightness Temperature	....	98
4.4	Characteristics of the carbon emitting region	....	105
4.5	SII — Region	....	112
4.6	H^{o} —— Region	....	117
TABLES	4.1a — 4.5	....	120
FIGURES	4.1(a)—4.5		
Chapter 5:	SUMMARY AND CONCLUSION	....	129
	REFERENCES	....	135
	List of Author's publications (attached in the flap at the back)	....	144

ACKNOWLEDGEMENTS

It is with much pleasure that I acknowledge the support and patient guidance of my thesis supervisor, Dr.S.M.R. Ansari. His constant encouragement, advice to prevent serious errors but yet allowing me to discover methods of approaching problem for myself, and support while working on it are very much appreciated.

I wish to extend my thanks to Mr.Badr-e-Alam for many stimulating discussions, reading this manuscript, and making constructive comments that has contributed both to its scope and depth. It is through our many discussions that my knowledge and understanding of astrophysics has been developed. I gratefully acknowledge Edward B. Churchwell for sending his thesis from which I have been benefited much.

I am grateful to Professor Mohammad Zillur Rahman Khan, Chairman Department of Physics, for the facilities provided in the department and financial assistance for computational purposes.

A special word of gratitude is extended to all my teachers, colleagues, and scholars of the department. Especially I am deeply indebted to Dr. Israr Ahmad and Dr. M.S.Z.Chaghtai for encouragement in this work and for a advice on a number of scientific and personal matters. I have also been benefited

greatly from suggestions and co-operations with Dr.Rahimullah Khan, Dr.Mushtaque Ahmad, Mr. M.A. Alvi, Mr.Mohammad Imtiazul Haq and Mr.Mohd.Ali Ansari.

My greatest thanks must go to my parents, family members, and to those relatives and friends without whom this work would not have been completed. Finally I am deeply grateful to my wife, Tahira Khatoon, who has preserved through many moods while working on this problem and writting this thesis.

I acknowledge financial support from the 'Council of Scientific and Industrial Research' and 'University Grants Commission' New Delhi. I am particularly grateful to Mr.Mukhtar Husain Siddiqi for careful typing of this thesis.

(ABDUL QAIYUM)

CHAPTER 1

INTRODUCTION

To study an astrophysical object it is necessary to consider two types of behaviour: the microscopic which deals with the interaction between the individual particles of the medium and the macroscopic, that gives the properties of the object as a whole. Evidently, the two behaviours are not independent of each other. The study of the individual processes of microscopic nature helps one to determine the macroscopic properties of the object as well. However, these microscopic processes are not always required to understand the general behaviour of stellar and interstellar matter. For example, in stars and some of the interstellar medium, local thermodynamic equilibrium (LTE) can be assumed safely and consequently no detailed knowledge of microscopic processes is required to calculate the macroscopic properties of the gas, i.e. state of ionization, temperature, atomic and molecular density etc. Evidently in the gas or plasma for which LTE does not hold, the knowledge and contribution of individual processes become rather quite important to calculate the above mentioned parameters of the cloud. Interstellar matter is an example of such a gas or plasma in which LTE can not be presumed. Therefore the atomic and molecular processes involved in the medium need considerable attention.

The interstellar gas consists mainly of condensations or clouds, which are being continuously formed and dissolved by a variety of processes. The thermal properties and physical conditions inside these clouds are of fundamental importance, since these objects are known to be the actual sites of proto-star formation and chemical evolution of complex molecules.

A major step forward in the study of interstellar matter was, in fact, made with the discovery of the first interstellar spectral line in the radio range, namely, the famous 21-cm hyperfine line of atomic hydrogen (Wild 1952). This discovery led to the possibility of detecting other spectral lines by radio astronomical techniques. Kardashev (1959) first predicted that the radio recombination lines of hydrogen could be detected from the H II region with the equipment available at that time. Following this prediction Dravskikh and Dravskikh (1964) at Pulkavo Observatory first detected the radio recombination line at 5762 MHz for the level transition n = 105 $\longrightarrow$ 104 in Orion A and M 17.

In the beginning the research workers concentrated almost extensively on the observation and interpretation of these lines from the classic bright radio H II regions. However later observational advances especially in radio and infra-red astronomy, offered new opportunities for studying the interstellar gas under a variety of previously inaccessible conditions. With further improvements in the sensitivity of telescopes and

receivers, it became possible in the last decade to use radio recombination lines as a tool to explore a much broader range of phenomena in galactic and extragalactic medium. Recent area of investigations includes the study of Planetary nebula, the nuclei of some radio galaxies, and the distributed ionized gas in the galactic and extra-galactic planes. Beside studying the *thermodynamic structure of ionized regions*, recombination lines have been used for diagonistic purposes, as diverse as the investigations of magnetic fields, abundance determination and kinetic studies of galactic structures.

The carbon recombination line emission was first detected by Palmer *et al.* (1967) from the cold transition region between Orion A and its background molecular cloud, and subsequently from the neutral matter associated with many other H II regions (see Qaiyum and Ansari 1979). This new type of cool object was later identified as CII clouds. From this new object, narrow lines of hydrogen and also recombination lines of other heavy element(s) have been observed. Moreover, the observations are no longer limited to single dish measurements at centimeter wavelengths but have been made now virtually over the entire radio spectrum.

During the last decade the physics of formation and transfer of radio recombination lines in both hot and cold gas has been thoroughly described and many troublesome questions have been settled. It is now recognized that observed radio-line emission depends sensitively on LTE effects, on the density

and density structure of various species in the line emitting region, on temperature and temperature structure , on the geometry and beam effects, and on the velocity field within the region (Brown et al.1978). The lines are sensitive to so many properties of the regions in which they are formed that they can be regarded as a blessing, for carrying detailed information about the region. Therefore, radio recombination lines from ionized species offer a direct method with the help of which the studies of the structure and physical conditions within various components of the interstellar medium are carried out.

In contrast to the observational situation, which is yet to be fully explored, the theoretical aspects of the recombination line emission is well understood now. Considerable efforts have also gone into quantifying the relevant atomic processes but there are areas that need still additional theoretical work. On one hand, the relevance of the internal processes for overall dynamical evolutions needs to be examined and on the other, dependance of the line emissions in the clouds on the detailed distribution of atomic constituents, especially of the carbon, hydrogen, other most abundant heavy elements and their ions along with that of molecules is to be investigated thoroughly. Moreover, relationship between thermal and chemical effects, ionized species, molecules and dust should also be studied. In this thesis we attempt to carry out these problems in detail.

As a matter of fact there is no fundamental difference between the analysis of radio recombination lines from H II regions and those from Planetry nebulae, the ionized gas in galactic nuclei or the ionized gas seen along the line of sight. However, there are important differences between the recombination lines from H II regions and those from cool, partially ionized clouds (CII regions). The site chosen for theoretical calculation and its comparison with the observations are the regions adjacent to the fully ionized hydrogen regions where a hot O-type star is supposed to be embedded within or is in vicinity of the cloud. The flux of UV radiation depends upon the spectral type of the star. The variation in the luminosity as a function of spectral type is shown in Figure 1. A large number of physical processes are considered in constructing the realistic model of such interstellar clouds, for instance W3, NGC 2024 and Orion A. The calculations are performed both for solar ($A_\odot$) and depleted (A_D) abundances tabulated in Table 1.

In the following chapter 2 we discuss the various atomic and molecular processes that are important to the abundance calculation of atomic and ionic species of hydrogen, carbon and other heavy elements and also some of the important molecules: H_2, CO, OH, CH^+, H_2CO to name a few (see Tables 2.1—2.5). Here we calculate as follows. A chemical equilibrium is set up between formation and destruction processes of a particular species to solve for the abundance structure,

especially that of ions of hydrogen, carbon and other heavy elements (mg, Si, S and Fe), at a particular position in the region. To determine the ionisation structure, the photo-ionisation by ultraviolet radiations ($\lambda \geq 912A^{o}$) from the nearest hot stars of HII and X-ray background, and cosmic ray ionisation and ionisation by ion, atom and molecular exchange reactions are considered. As a matter of fact, the aim of this thesis is also to show that the densities of electrons and ions are not constant over the whole region of line emission, and the line emitting regions of hydrogen, carbon and other heavy elements and also of molecular clouds are not identical spatially, though associated with each other.

In Chapter 3, a thermal balance is set up between heating and cooling to obtain the temperature at a particular position of the region. Thermal balance is solved in a self-consistant way until convergence is achieved. For this purpose, all possible heating mechanisms (H_2 formation on the grains and its photo-dissociation, photo-electrons from the dust grains, photo-ionisation of heavy elements, cosmic ray ionisation, gravitational collapse, and chemical reactions) are studied and taken into account. The cooling is considered mainly from hyperfine transitions of C, O, Si, Fe and some of their ions, and from rotational transitions of molecule 12_{CO} and its isotopes by considering all the relevant electronic, atomic and molecular collisions.

The effects of background radiations that include $3^{o}K$ radiation and far infra-red radiations from dust grains are also studied.

It may be mentioned here that like the densities of various species the temperature too is not constant over the whole region of line emission. There is large difference between temperatures and temperature structures of the inner and outer regions of the cloud for both the assumed abundances.

Chapter 4 includes the basic line formation theories, calculation of the contribution to the line intensities from different regions and study of the characteristics of the line-emitting regions. We then interpret the line intensities of hydrogen, carbon and other heavy elements. The line intensity calculation involves temperature, and densities of electron and ionised species directly and also indirectly through departure coefficients from thermodynamic equilibrium (b_n). Therefore, we divide the cloud into equally thick isothermal and homogeneous thin slabs. Statistical equilibrium corresponding to density and temperature of each slab of the cloud is solved to determine the b_n factor at each position. The line-intensity is calculated along a particular line of sight by integrating over the whole region.

A best fit of recombination line intensities is also carried out taking the total hydrogen density n_H, emission measure (EM) of HII regions and the cloud size as a free and

independent parameters. The characteristics of the regions are also tabulated.

The last section is devoted to the summary and conclusions inferred from our theoretical calculations.

Table 1

Heavy element abundances

Atom	Solar	ζ Oph	λ Sco	Adopted Depleted
He	.1	-	-	.1
C	3.7×10^{-4}	7.4×10^{-5}	1.7×10^{-4}	1.1×10^{-4}
N	1.15×10^{-4}	2.2×10^{-5}	2.9×10^{-5}	2.5×10^{-5}
O	6.8×10^{-4}	1.8×10^{-4}	1.4×10^{-4}	1.6×10^{-4}
Mg	3.5×10^{-5}	1.1×10^{-6}	7×10^{-6}	2.1×10^{-6}
Si	3.5×10^{-5}	8.1×10^{-7}	2.8×10^{-6}	1.5×10^{-6}
S	1.62×10^{-5}	8.3×10^{-6}	1.3×10^{-5}	1.0×10^{-5}
Fe	2.5×10^{-5}	2.7×10^{-7}	1.3×10^{-6}	5.8×10^{-7}
Cl	3×10^{-7}			10^{-7}*

* Jura & York (1978)

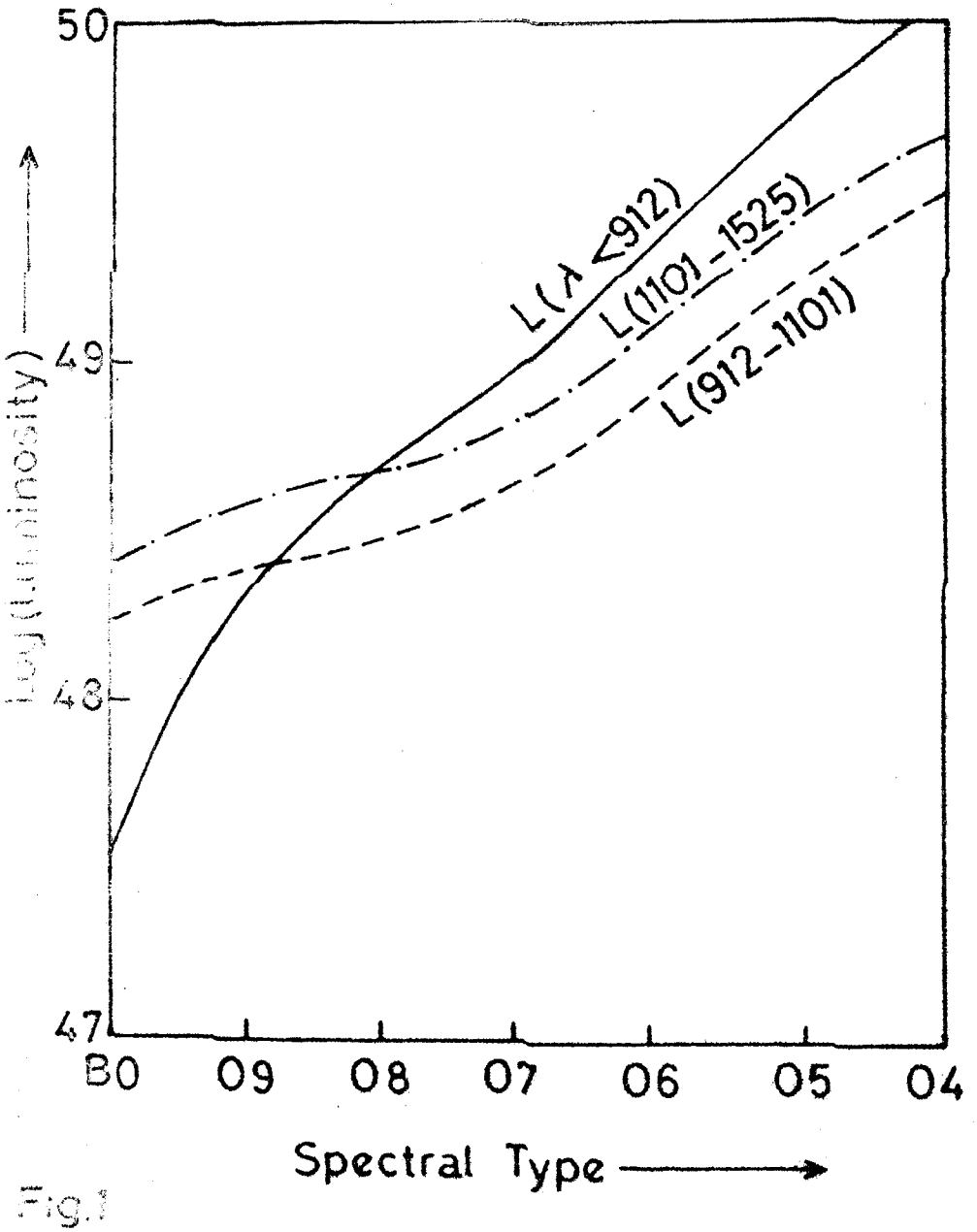
50
49
48
47
log(Luminosity)
L(λ<912)
L(1101-1525)
L(912-1101)
B0
09
08
07
06
05
04
Spectral Type

Fig.1

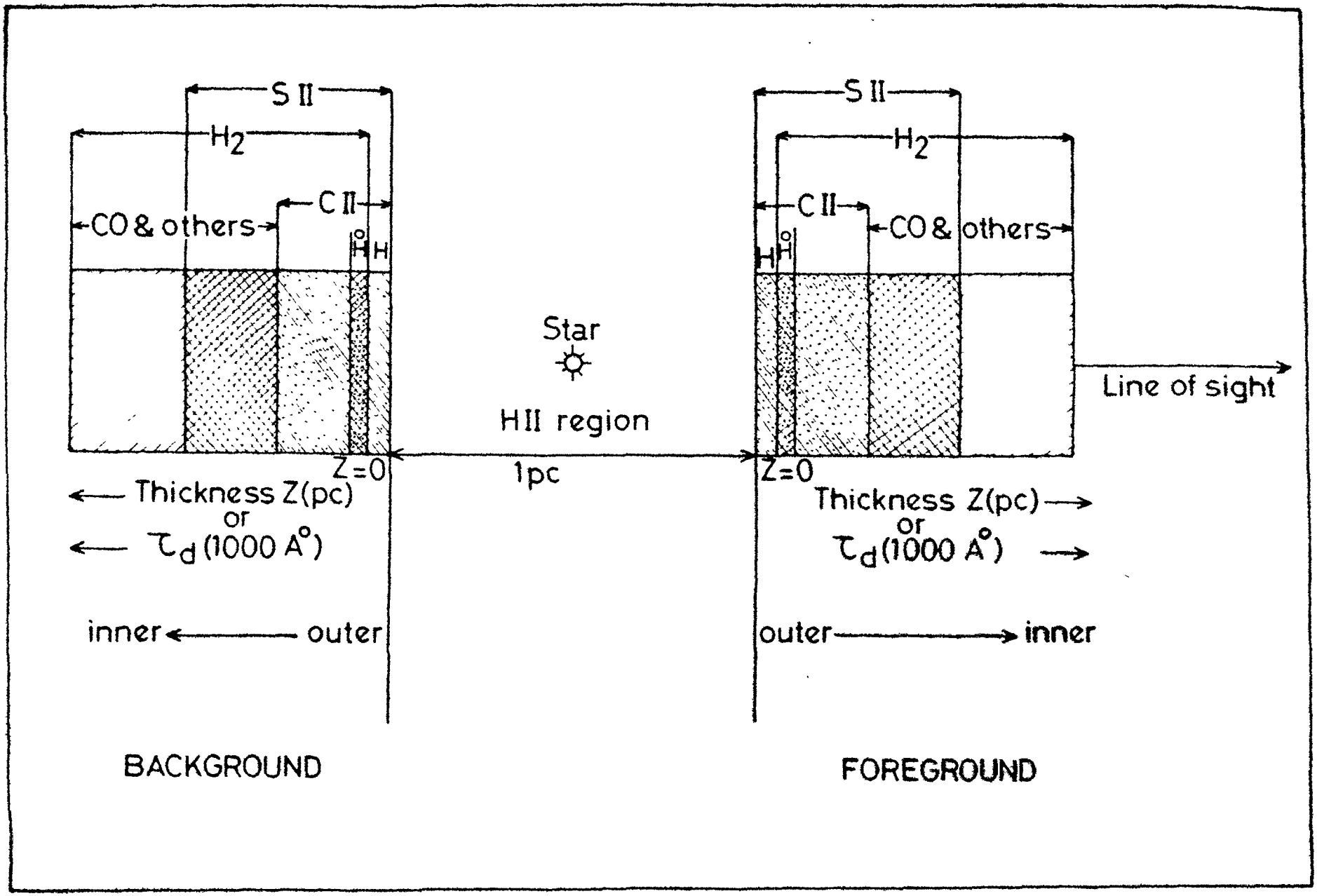
S II
H2
C II
CO & others
H°
H
Star
HII region
1pc
Z=0
Thickness Z(pc)
or
τd (1000 A°)
inner
outer
BACKGROUND
S II
H2
C II
CO & others
H°
H
Line of sight
Z=0
Thickness Z(pc)
or
τd (1000 A°)
outer
inner
FOREGROUND

Diag. 1

FIGURE CAPTIONS

Fig.1. Ultraviolet photon luminosity as a function of spectral type for zero age main sequence stars with log g = 4.0 in the range $\lambda < 912$ A^{o}(——), 912 $A^{o} < \lambda < 1101$ A^{o}(- - - - -) and 1101 $A^{o} < \lambda <$ 1525 A^{o} (—— : ——)

Diag.1. Schematic diagram of the model used in computation.

CHAPTER 2

ABUNDANCE CALCULATION

2.1 Introduction

Recent observations in radio and ultraviolet range have established the presence of many species of polyatomic molecules, radicals and their ions in the interstellar clouds. de Jong et al.(1980), Viala et al.(1979) and Gerola & Glassgold (1978) have proposed various formation and destruction mechanisms and have calculated the abundance of molecules, atoms and their ions to explain the presence of these species. All these attempts were mostly confined to the dark clouds where it is supposed that the clouds are exposed to the cosmic ray background and to the mean interstellar UV radiation field ($\lambda \geq 912 A^{o}$).

Recent observations of carbon recombination lines establish that cool and partially ionized medium, from where carbon lines are emitted, form the interface between the fully ionized gas (i.e. HII region) and a neutral (molecular) cloud. Evidently HII regions are intimately related to molecular clouds. Therefore, in the present work an attempt is made to study the ionisation and molecular structure of the clouds associated with the HII regions such as Orion A, NGC 2024 and W3. Here, beside discussing in general ionisation and molecular structure, we emphasise more on the ionisation structure of hydrogen, carbon and other heavy elements from which the recombination lines are emitted.

2.2 Flux and its Attenuation

For the calculation of photo-dissociation and photo-ionisation rates, the exciting star of associated HII region is supposed to be the main source of ultraviolet radiation field ($\lambda \gtrsim 912 A^{o}$). This radiation field depends naturally upon the spectral type and star's size. Based upon non-LTE models of Auer & Mihalas (1972) and the stellar radii given by Mezger et al.(1974), the luminosity of Lyman continuum photons of Zero-age main sequence stars for the wavelength range 912-1101 A^{o} and 1101-1526 A^{o} is plotted against the spectral type in Figure 1. These ranges are roughly the relevent ranges for the ionisation of C, Mg, Si, S and Fe in particular and photo-dissociation and ionisation of the most of the important molecules in general considered in this work.

Auer & Mohalas (1972) find that effective gravity for O-type stars ranges between $3.9 < \log g < 4.2$. Therefore 4.0 is probably a reasonable mean value. Churchwell et al.(1974) and Sarazin (1976) concluded that exciting star of HII region NGC 2024 has an effective temperature $\backsim$ 37000 k. The flux F corresponding to the temperature $\backsim$ 37000 k and log g = 4.0 at a distance of 0.5 pc from the star position may be approximated by (Qaiyum and Ansari 1979).

$$F = \chi_{F}\ 1.76 \times 10^{-4}\ \text{Photons cm}^{-2}\ \text{Sec}^{-1}\ \text{Hz}^{-1}. \qquad 2.1$$

Churchwell et al.(1974) have also studied the continuum luminosity of HII regions Orion A and W3, which are $\gtrsim 8$ to that of NGC 2024. The accomodation factor χ_F in expression 2.1, therefore, takes care of the fluxes for Orion A and W3. The value of $\chi_F = 1.0$ corresponds to the flux from NGC 2024 star and its value taken equal to 10 gives an upper limit for the radiations from the stars of Orion A and W3.

The photo-destruction of neutral species involves the spectrum between 912Å and 2000 A^o but the region near 1000A^o is especially important because most of the important atoms and molecules considered here (to name a few C, S, Fe, OH, H_2O and CO) have ionisation and dissociation limits around this wavelength. Astronomical observations indicate that the extinction by dust grain is large and increases with $\sim \frac{1}{\lambda}$ (Winnewisser et al. 1974). As a matter of fact, the absorption of radiation is also due to photo break-up of atoms and molecules. Taking into account the optical depth $\tau_\lambda(Z)$, that includes the absorption or extinction by dust, atoms and molecules, we get the following general expression for the flux (Qaiyum and Ansari 1979)

$$F_\lambda(Z) = \chi_F \, 4.4\times10^{-5} \, e^{-\tau_\lambda(Z)} \Big/ (0.5+Z)^2 . \qquad 2.2$$

Now, the exact extinction by the dust grain around 1000 A^o is not known but the contribution is assumed to be

largely from the smaller grains. Depending upon the assumed size, shape, type and number density n_g of a grain, extinction $\langle n_g \sigma_g \rangle^{ext}$ may vary by an order of magnitude. The attenuation depends upon the anisotropy factor and albedo also. OAO$_2$ observations of the diffuse galactic light (Witt & Johnson 1973, Lillie and Witt 1976) suggest that dust grains have large albedo $a_\lambda = 0.6 - 0.7$, and anisotropy factor $\epsilon_\lambda = 0.7$ for wavelengths around 1000A^o. The attenuation along a ray is $(1 - \epsilon_\lambda a_\lambda)\, \tau_\lambda^{ext} + \tau_\lambda^{at}$. It could be written as $\tau_d(Z) + \tau_\lambda^{at}(Z)$. The observations of the extinction and gas to dust ratio indicates that (Spitzer & Jenkins 1975)

$$\tau_\lambda^{ext}(Z) = \left[1 + \frac{E(\lambda - v)}{3E(B-v)}\right] \times \frac{N_H(Z)}{2.72 \times 10^{21}} \qquad 2.3$$

$$E(1033A^{\circ} - v) = 10\, E(B-V) \quad \text{(Savage 1975)} \qquad 2.4$$

$$\langle \sigma_g\, n_g \rangle^{ext} = 2.27 \times 10^{-21} N_H \quad \text{(Bohlin 1975)} \qquad 2.5$$

and

$$N_H(Z) = \int_0^Z n_H(z')\, dz'$$

where the total hydrogen number density $n_H = n(H) + n(H_2)$ and atomic or molecular absorption is

$$\tau_\lambda^{at}(Z) = \sum_X \int_0^Z n_X(z')\, \sigma_\lambda(X)\, dz' \qquad 2.6$$

and a_λ is approximated as

$$a_\lambda \simeq \frac{22.5}{\sqrt{\lambda(A^\circ)}} \qquad 2.7$$

2.3 Ionisation and Dissociation Rates in a Medium Close to an Early Type Stars

The photo-ionisation and/or dissociation rates are calculated using the radiation flux $F_\lambda(Z)$ and adopting one dimensional transfer approach of Werner (1970). Then, the rate $\zeta_X(Z)$ of species X at a position Z is given as:

$$\zeta_{X(Z)} = \int_{\nu_1(X)}^{\nu_0} F_\nu(Z)\, \sigma_\nu(X)\, d\nu \qquad 2.8$$

where $\sigma_\nu(X)$ is the cross-section for ionisation and/or dissociation of the species X at frequency ν, $\nu_1(X)$ is the frequency corresponding to ionisation and/or dissociation limit of the species X. ν_0 is the Lyman limit. The ionisation and/or dissociation rates of atoms and/or molecules are tabulated in Table 2.1. The references for the cross-sections are mentioned against each reaction in the corresponding table. It should be mentioned here that in some of the molecules and atoms the cross-sections are not continuous functions of the frequency. Their rates are written as the sum of two rates

corresponding to two different limits. In some cases the range of frequency not contributing significantly to the total rates are neglected without mentioning it specifically in the table. Wherever $\tau_\lambda^{at}(Z)$ contributes negligibly, it is omitted from the rates. In the following the rates are tabulated in unit of $\chi_F/(0.5+Z)^2$, where Z is the position co-ordinate in pc measured from the boundary of the HII region, which is usually presumed as 0.5pc.

2.4 Chemical Reactions and Recombinations

Most of the molecules are formed through gas-phase reaction but some of these could also be formed efficiently due to gas-grain reactions. The experimental and theoretical basis for gas-phase reactions are more firmly established than that for gas-grain reactions. However, in our scheme of calculation both the gas-phase and gas-grain reactions are considered. In the theory of formation and destruction numerous subsidiary species are also involved which are not listed and compared on account of non-availability of observational data.

More than 40 molecules have been observed excluding isotopic species. However, there are important physical conditions which indicate that only relatively few species needed to be dealt with explicitly. In particular, the thermal

and chemical evolution of the clouds depend only upon the smaller number of species which mainly determine the ionisation structure, thermal properties and molecular formations in the cloud. For example, H and H_2 determine the various cooling and heating mechanisms and they are also important for various other chemical reactions. Similarly CI, CII, CO, and other heavy elements turn out to be the most important coolant. Some of these species are the main sources of electron density, which in turn plays a specific role in the chemistry of molecules. The rates are tabulated in Tables 2.2 to 2.5.

2.5 Chemical and Ionisation Equilibrium

As mentioned earlier the typical clouds considered here are associated with the HII regions. As a result these clouds are supposed to be exposed to ultraviolet radiations from the nearest hot stars of HII regions. The atoms and molecules having ionisation/dissociation energy less than 13.6 ev are mostly destroyed by these ultraviolet flux ($\lambda \geqslant 912 A^{\circ}$). Inside the cloud the gas-phase reactions (Cf. Tables 2.3 & 2.4) dominate over other mechanisms (Cf. Tables 2.1, 2.2 & 2.5). Although hydrogen away from HII regions can not be ionised by ultraviolet radiation of their hot stars, yet the observed recombination line of hydrogen show the existance of an appreciable fraction of ionised hydrogen in the cool regions of ISM. A lower limit set for the ionisation rate of hydrogen,

from the observed intensity of recombination lines of hydrogen, is $\zeta_H \backsim 10^{-14}$ Sec^{-1} (Walmsley 1974, Qaiyum 1976).

Cravens & Dalgarno (1978) calculated that 2 MeV cosmic ray proton may penetrate a hydrogen column density $N_H = 9\times10^{20}$ cm^{-2} while loosing most of its energy by ionisation. An upper limit set for the rate of ionisation by these protons is 2×10^{-15}sec^{-1} (Spitzer & Tomasko 1968). This set of depth and rate of ionisation can not explain the abundance of ionisation in the medium. However, the additional flux, other than 2 MeV proton, due to cosmic ray protons with energies E > 10 MeV may penetrate to a greater depth > 1.6×10^{22} Cm^{-2} (Cravens & Dalgarno 1980) but corresponding calculated rate of ionisation of hydrogen $\zeta_H \backsim 6.8\times10^{-18}$Sec^{-1} (Spitzer & Tomasko 1968) and $\zeta_{H_2} \backsim (1.5\text{-}3.0)\times10^{-17}$Sec^{-1} concluded from the observations of OH and HD (O'Donell and Wattson 1974, Glassgold & Langer 1976, Black & Dalgarno 1977) are too low to explain the intensity of recombination lines of hydrogen.

Following the conjecture of Jura (1974) we worked out the details of the ionisation of hydrogen using chlorine chemistry (Qaiyum & Ansari 1979). Our clouds of interest consists of the total hydrogen density $n_H \gtrsim 10^4$ Cm^{-3}. For this order of density, molecular hydrogen H_2 should be sufficiently abundant to react with any ion XII as XII + H_2 —— XHII + H, thereby dominating the cloud chemistry (Black & Dalgarno 1973, Herbst & Klemperer 1973, Clavel et al 1978 and De Jong et al 1980).

Although carbon is ionised in the medium but we can not consider its reaction with H_2 because the latter is endothermic. Since the medium of interest is a low temperature region, therefore the possible reactions are restricted by exothermicity. On the other hand chlorine with ionisation potential 12.97 ev, reacts with H_2 exothermically (Weiss, Lawrence & Young 1970) to give HCl II. The photodissociation of this HCl II gives ionised hydrogen. The reactions are as follows:

$$ClII + H_2 \longrightarrow HClII + H + 0.17(ev) \qquad (A1)$$

$$HClII + h\nu \longrightarrow HII + Cl \qquad (A2)$$

The abundances are calculated using the steady state balances:

$$P_X(n_X(Z), T_e(Z)) = D_X(n_X(Z), T_e(Z)) \qquad 2.9$$

$$n_e(Z) = \sum_X^i n_X^i(Z) \qquad 2.10$$

In these equations P_X and D_X are the production and destruction rates for the species X of density $n_X(Z)$ at a position Z; $n_e(Z)$ and $n_X^i(Z)$ are the density of the electron and of ions i of element X at a distance Z. All the formation and destruction mechanism are defined in the preceding sections,

For simplicity we have computed cloud models of uniform hydrogen number density $n_H = n(H) + 2n(H_2)$; the variation in

the chemical composition of the cloud arises from the attenuation of UV radiations which ionises and dissociates the gas constituents.

The fraction $f = 2n(H_2)/n_H$ of the molecular hydrogen is calculated using the equation (Walmsley 1974)

$$\frac{df}{d\,\tau_\lambda(Z)} = e^{2\,\tau_\lambda(Z)}\, A\,(1-f)^3 + f\,(1-f) \qquad 2.11$$

$$A = \frac{R^2 n_H^2}{\tilde{\sigma}\,\beta^2 I^2}$$

In this expression R is the recombination rate of atomic hydrogen on grain surface to form molecular hydrogen H_2. I, the rate of dissociation for H_2 at the exposed surface of the cloud, is equal to 2.7×10^{-7} sec^{-1}, $\beta = 4.2\times10^5$ cm^{-1} and $\tilde{\sigma}$ is the average geometric cross-section. $\tau_\lambda(Z)$ is the effective optical depth at 1000A° as defined previously.

The computations presented here are for $n_H = 10^4$ cm^{-3} and for the total column hydrogen density $N_H = N(H) + 2N(H_2) = 5\times10^{22}$ cm^{-2} To simplify further chemical equilibrium is presumed to have been attained. The geometry of the cloud is plane-parallel. Our calculations may appear to be over simplified but it permits at least a step towards the understanding of the physical conditions and physical processes operating in the cloud.

2.6 Results and Discussion

2.6.1 Ionisation structure

As discussed earlier the constituent of the gas and its ions are very much dependent upon the strength of the molecular hydrogen (H_2) at every point in the cloud. The growth and dependence of f on R is discussed by Qaiyum & Ansari(1979) (see Figure 1 there). H_2 is also an important attenuator of the radiation. When hydrogen is completely converted to H_2, the absorption of radiation can block 30% and 20% of the ultraviolet radiation band responsible for the ionisation of C and S respectively. Beside the dust and molecules, C,S and S_i atoms are the most important absorbers of radiation.

The importance of atomic absorption can be visualized from the comparisons of Figures 2.1(a) and 2.1(b) that gives the information about the depth and the range of ionisation of carbon and of other heavy elements at $n_H = 10^4 cm^{-3}$ for both the assumed abundances, $A_\odot$(solar) and A_D(depleted). Although dust absorption for both abundances is same, yet 10% level of ionisation of carbon corresponds to dust optical depths, τ_d=7 and 9 for $A_\odot$ and A_D respectively. This is due to the fact that in the case of A_D the atomic absorption is less than that

for $A_\odot$ at the same depth, by the same factor with which the abundances are depleted. Further inside the cloud the ionised fraction of carbon is very small and its ionisation is only due to gas-phase reaction or cosmic ray protons.

The other heavy elements having ionisation potential less than the carbon are ionised to a greater depth than the carbon. Their depths of ionisation depend too upon the abundances assumed. For $A_\odot$ the depth of ionisation for S and Si are less than that for A_D, because of the self absorption. But the ionisation structure of Mg and Si are not appreciably different for both the abundances because of the low ionisation cross-section that contributes to the atomic absorption. Consequently, the electron density varies with position, depending upon the ionisation structure of hydrogen, carbon and of other heavy elements. After the ionisation edge of carbon, the electron abundance falls sharply to the value of the sum of the abundances of the heavy elements. In the core of the cloud the abundance of electron is governed by the gas-phase reactions.

The ionisation structure of hydrogen is studied here extensively and computations have been carried out for the more likely values of hydrogen density in the cloud: $n_H = 5\times10^3, 10^4, 2\times10^4$ and 5×10^4 cm^{-3} and the rates of H_2 formation $R=5\times10^{-18}$, 10^{-17}, 3×10^{-17} and 5×10^{-17} $sec.^{-1}$ The results of these computations are presented in Tables 2.6 and 2.7. It may be

noted here that these are slightly different from those of Qaiyum and Ansari (1979) because of the new rates of chlorine reactions with H_2 (Raouf et al.1980, Smith and Adams 1981) used here.

The effect of R on $n(H_2)$ and ionisation of Cl and H atom is shown in Figures 2.2 and 2.3. This dependence is rather pronounced. The effect of R on the ionisation of carbon is not shown here, since it is negligible. First, we observe (see Figure 2.3) that the region of ionised chlorine ClII and H_2 are almost separated from each other, since with the increase in the number density $n(H_2)=\frac{1}{2}$ f n_H the destruction of ClII increases due to dominant reaction ClII with H_2. Second, as compared to carbon, chlorine is ionised in a very thin shell. This is due to the fact that in addition to electron recombination, ClII is mostly reduced by reacting with H_2 (reaction A1). The molecule so formed dissociates into HII and chlorine (reaction A_2). Thirdly, we also see that CII and H_2 regions have some volume in common, depending upon the rate R.

From Figure 2.2 we notice that the ionisation of hydrogen is also strongly dependent on R. With high values of R the peaks are shifted towards the origin i.e. the boundary of the HII region, and the area under the curve (proportional to the emission measure EM) also increases with R. Besides, the positions of the peaks are nearly coincident with the corresponding points of intersection of the ionised chlorine and of

f- curves shown in Figure 2.3. Evidently, at the point of intersection $n(H_2)$ and n(ClII) are just optimal to give the peak in the n(HII) curve, though before or beyond that point, one or the other number density is low enough to reduce the production of n(HII).

The dotted curves in the Figure 2.2 are for A_D assumed here. Notice, that position of the peaks for both abundances coincide. It is also clear from the same figure that the ratio n(HII)/n(CII) is inflated approximately by the same factor as the carbon is depleted, that is the ionisation of hydrogen, n(HII) remaining nearly the same for both the abundances. In other words ionisation of hydrogen depends weakly on the assumed abundance of Cl. This can be explained as follows. In the case of depleted abundance, n_e is also depleted almost by the same factor as carbon, thereby decreasing the probability of the following reactions:

$$\begin{aligned} HClII + e &\longrightarrow H + Cl \\ H_2ClII + e &\longrightarrow H + HCl, \end{aligned} \qquad \text{I}$$

and consequently increasing the probability of the ionisation of hydrogen according to the following reactions,

$$\begin{aligned} HClII + h\nu &\longrightarrow HII + Cl \\ H_2ClII + h\nu &\longrightarrow HClII + H \ . \end{aligned} \qquad \text{II}$$

From the Table 2.6 we see that emission measures for carbon, hydrogen and other heavy elements increase with increasing n_H. However, the ratio of emission measures EM(HII)/EM(CII) increases first and then decreases. It means the increase in EM of hydrogen and carbon are not in the same proportion. The initial increase in the ratio can be simply understood as follows. With the increase of n_H, H_2 molecule becomes quite abundant, since $n(H_2) \propto n_H^2 (1-f)$, while $n(CII) \propto n_H$ only. Thus reactions II lead to the more production of HII compared to CII, thereby increasing the ratio of their emission measures. For sufficiently high n_H i.e. high n_e, reactions I are realised more than the reactions II, thus suppressing the production of HII, while n(CII) still remaining proportional to n_H. This leads to the decrease of the emission measures.

Another point to be mentioned here is that the ratio $\sum_X EM(X)/EM(CII)$, where X stands for Mg, Si, S and Fe, is fairly constant, though having a slightly increasing trend. This ratio is greater than the ratio of their total abundance to carbon $\sum_X n(X)/n(C)$.

From the Table 2.7 it is clear that ionisation of hydrogen and therefore emission measures of the species increase with the increase of R. This is because, in the region where Cl is sufficiently ionised, H_2 is also available sufficiently due to high value of R to form HClII thereby producing HII by realising reactions II.

2.6.2 Abundances of molecules and neutral hydrogen atom

Although we intend to present first in the following section a detailed calculation of the abundances of the molecules in the clouds associated with HII regions, we also discuss the association of the molecular region with those emitting the radio recombination lines of carbon, hydrogen and other heavy elements. Besides, our cloud model leads to some ideas concerning the observational aspects of some of the molecules. The results of the abundance calculation are summarized in Figures 2.4(a) and 2.4(b). A first glance at these figures and also at Figures 2.1(a) and 2.1(b) leads one to the following conclusions:

i) The regions of ionised carbon CII and hydrogen HII are well separated away from the associated (adjacent) molecular region other than H_2. They are themselves not only associated with each other but have also some region in common (see Diagram 1).

ii) The heavy elements other than carbon are ionised to a greater depth and have some domain common with the molecular region. Therefore, the properties and parameters derived from the ionised heavy elements and molecules may be approximately the same.

iii) The most abundant molecule is CO after H_2 and it takes more than 90% of the carbon beyond 0.2 pc of the cloud depth,

while carbon atom (Figs.2.1(a) and 2.1(b)) and its ion decreases sharply. The other abundant molecules plotted here are OH, O_2, H_2O, CH, CH_2 and H_2CO. The abundances of these molecules are appreciable only in the interior part of the cloud i.e. either just about 0.2 pc or bit deeper than this depth. This is due to the reason that for $Z < 0.2$ pc all the molecules have high rates of photo-ionisation and/or dissociation in the presence of large flux of UV radiations from the nearest hot stars.

iv) There is significant difference between the calculated abundances of molecules for the case of solar and depleted abundances.

We reiterate that grains play a pivotal role in the molecular formation. The molecular formation processes are shown in a block diagram (Diagram 2). We discuss them in the following. As we proceed towards the interior of the cloud, most of the hydrogen is converted to H_2 through sticking on the grain surface and UV bands through which H_2 molecule dissociates are self-shielded by H_2. The cosmic ray ionisation of H_2 produces H_2^+, which reacts efficiently with H_2 to form H_3^+. With the formation of H_3^+, the carbon and oxygen hydride cycles start and they end up with the final products of CH, CH_2 (carbon hydride), OH and OH_2 (oxygen hydride) formation. Moreover, CH and CH_2 are also formed by radiative association of C^+ with H_2 while CH and OH are also formed efficiently by

the reaction of C and O with H on the surface of grain. In the core of the cloud O_2 is also highly abundant (Figs.2.4(a) and 2.4(b)) and it is mainly formed by the reaction of O with OH. The most observationally and theoretically studied molecule of interstellar medium is CO which is mainly formed by the reaction of CH and CH^+ with O, and OH with C and C^+. The abundance of H_2CO is confined in the core of the cloud (Figures 2.4(a) and 2.4(b)) and it is mainly formed through the intermediate molecules of carbon hydride cycle CH_3 and CH_3^+ either by the electronic recombination, charge exchange, reaction with hydrogen or with combination of all these processes.

We present in Table 2.8 the column densities N(X) of species X for the four cloud models ($n_H = 10^3$, 10^4, 10^5, and 10^6); the observational values are tabulated in Table 2.9 for comparison. From these tables we observe the following:

i) For a single homogeneous cloud model two neutral hydrogen (H) regions corresponding to two values of N(H) in Table 2.8 exist along a particular line of sight. The magnitudes of these N(H) at $n_H \sim 10^4$ cm^{-3} are comparable to the two observed N(H) values for NGC 2024 and Orion A (see Table 2.9). These two components of the neutral hydrogen of differing column densities embedded in a molecular cloud depend upon the kind of UV radiations falling on the exposed

surface. The portion exposed to UV radiation from the nearest hot star will have greater column density of neutral hydrogen (because of the high dissociation rates) as compared to the portion exposed to cosmic background radiation, where radiation density is low enough to dissociate the H_2 molecules only in a very thin region.

ii) The highly abundant and also most observationally and theoretically studied molecule in the interstellar medium is CO as mentioned above. Its calculated column densities for both abundances are presented in Table 2.8 and compared with the observational values mentioned in Table 2.9. The calculated column densities $^{N}(CO)$ at different n_H are approximately equal but they differ for solar and depleted abundances, more or less by the factor of carbon depletion. Since N(CO) is approximately same for all n_H, one can not infer the hydrogen density n_H of the molecular region by just comparing the calculated $^{N}(CO)$ with the observational values, unless the size of the molecular region is specifically known. We may mention that we have restricted ourselves here only to the calculation of the column densities. We also intend to study in future the profile structure of CO molecule that explains in detail the behaviour and conditions of the molecular cloud. The observed values of N(CO) lie between the calculated values for solar and depleted abundances but they are closer to the case of solar abundance.

iii) As shown in Figures 2.4(a) and 2.4(b) the second important abundant molecule is OH. The calculated column density of OH decreases with the increase of n_H, because of the reaction of oxygen with OH to form O_2 (see reaction 5, Table 2.4). The calculated column densities for $n_H > 10^4$ cm^{-3} are comparable to the observed values (Table 2.9), for both solar ($A_\odot$) and depleted abundances (A_D). The column density N(OH) for $A_\odot$ is slightly less than in the case of A_D because of the depletion of oxygen, since OH is mainly destroyed by O, producing O_2, the depletion of O leading to the decrease of OH destruction. It should be emphasized that in our calculation of N(OH) we have taken into account both the gas-phase reactions and formation of OH on the grain surface. Calculation with either of the processes will not lead to results comparable with observations.

iv) The computed column densities of CH at high densities are greater by an order of magnitude than the observed values. It is probably due to the use of over estimated reaction rates of the formation of CH on the grain surface that dominates in the core of the cloud over the gas-phase reaction. If reaction rate of C and H on the grain surface would have been taken equal to that of O and H then the result obtained would have been very near to the observed values. In the outer region the CH formation through the gas-phase reaction $C^+ + H_2 \longrightarrow CH_2^+$ (see Table 2.3, item 15) dominate over the formation through

grain surface (see Table 2.2, item 2). But this region is not contributing to the total column density, because CH is destroyed by the UV flux from the nearest exciting star of HII region. We have, in particular, not considered the destruction of CH by reactions with nitrogen N which can be a dominant destruction process at large densities in the interior of the cloud. Moreover, reactions of CH_2^+ and CH_3^+ with N can also reduce the CH_2^+ and CH_3^+ densities and consequently the formation of CH.

v) The column densities of H_2O and O_2 can not be compared with the observations as there are no values available in the literature for the regions considered here. The computed column densities for these molecules are not very much different for both the assumed abundances. The column densities also depend very weakly on the assumed values of n_H.

vi) The column density of H_2CO decreases with the increase of n_H because in the interior of the cloud where it is abundant it is mostly destroyed by the reaction of O with H_2CO at high n_H (see reaction 9, Table 2.4). The column densities for both solar and depleted abundances differ by an order of magnitude and the calculated values of $N(H_2CO)$ is comparable to the observed one for depleted abundances.

Table 2.1

Photo-ionisation and dissociation rates

	Photo-reactions	Rates $(sec^{-1})\ \chi_F / (0.5+Z)^2$	References for cross-sections used in calculating the rates.
1.	$C + h\nu \longrightarrow C^+ + e$	$2.25\times10^{-7}\ \exp(-0.9\ \tau_d(Z) - \overset{at}{\tau_\lambda}(Z))$	Henry (1970) Carter & Kelly (1976)
2.	$Mg + h\nu \longrightarrow Mg^+ + e$	$9.2\times10^{-8}\ \exp(-0.62\ \tau_d(Z) - \overset{at}{\tau_\lambda}(Z))$	Dubau & Wells (1973)
3.	$Si + h\nu \longrightarrow Si^+ + e$	$2.5\times10^{-6}\ \exp(-0.66\ \tau_d(Z) - \overset{at}{\tau_\lambda}(Z))$	Chapman & Henry(1972)
4.	$S + h\nu \longrightarrow S^+ + e$	$1.4\times10^{-6}\ \exp(-0.81\ \tau_d(Z) - \overset{at}{\tau_\lambda}(Z))$	Chapman & Henry(1971,1972)
5.	$Fe + h\nu \longrightarrow Fe^+ + e$	$2.2\times10^{-7}\ \exp(-0.64\ \tau_d(Z) - \overset{at}{\tau_\lambda}(Z))$	Kelly (1973)
6.	$Cl + h\nu \longrightarrow Cl^+ + e$	$2.5\times10^{-7}\ \exp(-\tau_d(Z) - \overset{at}{\tau_\lambda}(Z))$	Peach (1967) & McGuire(1968)
7.	$H_2 + h\nu \longrightarrow H + H$	$0.113\ \exp(-0.9\ \tau_d(Z) - \overset{at}{\tau_\lambda}(Z)) \sqrt{N(H_2)}$	Stecher & Williams (1967) Allison & Dalgarno (1972) Stephens & Dalgarno(1972)
8.	$HCl + h\nu \longrightarrow H + Cl$	$4.2\times10^{-7}\ \exp(-0.8\ \tau_d(Z) - \overset{at}{\tau_\lambda}(Z))$	Jura (1974)
9.	$HCl^+ + h\nu \longrightarrow H^+ + Cl$	$1.5\times10^{-6}\ \exp(-0.57\ \tau_d(Z))$	Raftery & Richards (1973)

Table 2.1(Continued)

	Photo-reactions	Rates (sec^{-1}) $\chi_F / (0.5+Z)^2$	References for cross-sections used in calculating the rates.
10.	$CH + h\nu \longrightarrow CH^+ + H$	$4.3\times10^{-7}\exp(-0.91\ \tau_d(Z) - {}^{at}\tau_\lambda(Z))$	Walker & Kelly (1972)
			Solomon & Klemperer (1972)
	$\longrightarrow C + H$	$2.1\times10^{-7}\ \exp(-0.51\ \tau_d(Z))$	Elander & Smith (1973)
11.	$CH^+ + h\nu \longrightarrow C^+ + H$	$6.9\times10^{-9}\ \exp(-\tau_d(Z) - {}^{at}\tau_\lambda(Z))$	Solomon & Klemperer (1972)
12.	$C_2 + h\nu \longrightarrow C + C$	$1.3\times10^{-8}\ \exp(-0.8\ \tau_d(Z) - {}^{at}\tau_\lambda(Z))$	deJong et al.(1980)
13.	$CN + h\nu \longrightarrow C + N$	$2.4\times10^{-7}\ \exp(-0.83\ \tau_d(Z) - {}^{at}\tau_\lambda(Z))$	Solomon & Klemperer (1972)
14.	$CO + h\nu \longrightarrow C + O$	$7.5\times10^{-9}\ \exp(-\tau_d(Z) - {}^{at}\tau_\lambda(Z))$	Cook et al.(1965)
			Solomon & Klemperer (1972)
15.	$OH + h\nu \longrightarrow OH^+ + e$	$1.1\times10^{-8}\ \exp(-1.1\ \tau_d(Z) - {}^{at}\tau_\lambda(Z))$	Barsuhn (1977)
	$\longrightarrow O + H$	$2.3\times10^{-7}\ \exp(-1.1\ \tau_d(Z) - {}^{at}\tau_\lambda(Z))$	de Jong et al.(1980)
16.	$O_2 + h\nu \longrightarrow O_2^+ + e$	$9.3\times10^{-7}\ \exp(-1.1\ \tau_d(Z) - {}^{at}\tau_\lambda(Z))$	Matsunaga & Watanabe (1967)
	$\longrightarrow O + O$	$4.85\times10^{-7}\exp(-.46\ \tau_d(Z))$	Hudson (1971)

Table 2.2

Molecule formation on grains and ionisation by cosmic rays(CR)

	Reactions	Rates (sec^{-1})	References
1.	$H + (H + dust) \longrightarrow H_2 + dust + h\nu$	$3\times10^{-18}\, n_H T_e^{\frac{1}{2}}\, e^{-T_e/100}$	Elitzer & de Jong (1978)
2.	$C + (H + dust) \longrightarrow CH + dust + h\nu$	$\{3 + (20-T_e)\times 0.06\}\times10^{-17}\, n_H$, $10 < T_e < 50$ K	Solomon & Klemperer(1972)
		$3\times10^{-18} n_H$, $T_e \geq 100$ K	
3.	$C^+ + (H + dust) \longrightarrow CH^+ + dust + h\nu$	$7\times10^{-17} n_H$, $T_e < 50$ K	
		$3.5\times10^{-17} n_H$, $T_e = 100$ K	Solomon & Klemperer(1972)
		$2\times10^{-17} n_H$, $T_e \geq 200$ K	
4.	$O + (H + dust) \longrightarrow OH + dust + h\nu$	$8.7\times10^{-18} n_H\, T_e^{-.38}$	Smith & Sweibel (1976)
5.	$H + CR \longrightarrow H^+ + e + CR$	$6.8\times10^{-18} + 2\times10^{-15}\, e^{-N_H/1.5\times10^{20}}$	Spitzer & Tomasko (1968)
6.	$H_2 + CR \xrightarrow{95\%} H_2^+ + e + CR$	1.2×10^{-17}	Goldsmith & Langer (1978)
	$\xrightarrow{5\%} H + H^+ + e + CR$		

Table 2.2 (Continued)

	Reactions	Rates (sec^{-1})	References
7.	$He + CR \longrightarrow He^{+} + e + CR$	1.2×10^{-17}	Clavel et al.(1978)
8.	$C + CR \longrightarrow C^{+} + e + CR$	1.2×10^{-17}	de Jong et al.(1980)
9.	$O + CR \longrightarrow O^{+} + e + CR$	2×10^{-17}	de Jong et al.(1980)

Table 2.3

Ion-Molecule Reactions

	Reactions	Rates ($sec^{-1} cm^3$)	References
1.	$H^+ + O \longrightarrow O^+ + H$	$5 \times 10^{-10}\ e^{-232/T_e}$	de Jong et al. (1980)
2.	$H^+ + CH \longrightarrow CH^+ + H$	10^{-9}	Barsuhn (1977)
3.	$H^+ + OH \longrightarrow OH^+ + H$	10^{-9}	Herbst & Klemperer (1973)
4.	$H^+ + C_2 \longrightarrow C_2^+ + H$	10^{-9}	Langer (1976)
5.	$H^+ + O_2 \longrightarrow O_2^+ + H$	1.2×10^{-9}	Huntress (1977)
6.	$H^+ + H_2O \longrightarrow OH_2^+ + H$	8.2×10^{-9}	Huntress (1977)
7.	$H^+ + HCO \longrightarrow HCO^+ + H$	10^{-9}	Black (1975)
8.	$H^+ + CH_2 \longrightarrow CH_2^+ + H$	10^{-9}	Barsuhn (1977)
9.	$H^+ + H_2CO \longrightarrow H_2CO^+ + H$	10^{-9}	Herbst & Klemperer (1973)
10.	$He^+ + H_2 \longrightarrow H^+ + H + He$	10^{-13}	Johnsen & Biondi (1974)
11.	$He^+ + CO \longrightarrow C^+ + O + He$	1.6×10^{-9}	deJong et al. (1980)
12.	$He^+ + O_2 \xrightarrow{38\%} O_2^+ + He$	10^{-9}	deJong et al. (1980)
	$\xrightarrow{62\%} O^+ + O + He$		

Table 2.3 (Contd.)

	Reactions	Rates ($sec^{-1} cm^3$)	References
13.	$He^+ + H_2O \longrightarrow OH^+ + H + He$	4.4×10^{-10}	deJong et al. (1980)
14.	$He^+ + H_2CO \longrightarrow CH_2^+ + O + He$	10^{-9}	deJong et al. (1980)
15.	$C^+ + H_2 \longrightarrow CH_2^+ + h\nu$	10^{-16}	Clavel et al. (1978)
16.	$C^+ + CH \longrightarrow C_2^+ + H$	10^{-9}	deJong et al. (1980)
	$\longrightarrow CH^+ + C$	10^{-9}	deJong et al. (1980)
17.	$C^+ + OH \longrightarrow CO^+ + H$	8×10^{-10}	deJong et al. (1980)
	$\longrightarrow CO + H^+$	8×10^{-10}	deJong et al. (1980)
18.	$C^+ + O_2 \longrightarrow CO^+ + O$	7.8×10^{-10}	Huntress (1977)
	$\longrightarrow CO + O^+$	4.4×10^{-10}	Huntress (1977)
19.	$C^+ + CH_2 \longrightarrow C_2H^+ + H$	2×10^{-9}	Herbst & Klemperer (1973)
20.	$C^+ + HCO \longrightarrow HCO^+ + C$	10^{-9}	deJong et al. (1980)
	$\longrightarrow CH^+ + CO$	10^{-9}	deJong et al. (1980)

Table 2.3 (contd.)

	Reactions	Rates ($sec^{-1}cm^3$)	References
21.	$C^+ + H_2O \longrightarrow HCO^+ + H$	2.7×10^{-9}	deJong et al.(1980)
22.	$C^+ + H_2CO \longrightarrow CH_2^+ + CO$	2.1×10^{-9}	Huntress(1977)
	$\longrightarrow HCO^+ + CH$	9.2×10^{-10}	Huntress(1977)
	$\longrightarrow H_2CO^+ + C$	1.4×10^{-9}	Huntress (1977)
23.	$O^+ + H \longrightarrow H^+ + O$	5×10^{-10}	Black & Dalgarno(1977)
24.	$O^+ + H_2 \longrightarrow OH^+ + H$	1.58×10^{-9}	Huntress(1977)
25.	$S^+ + O_2 \longrightarrow SO^+ + O$	2×10^{-11}	Fehsenfeld & Ferguson(1973)
26.	$Cl^+ + H_2 \longrightarrow HCl^+ + H$	$10^{-9}(80/T_e)^{-1}$	Smith & Adams(1981) Raouf et al.(1980)
27.	$H_2^+ + H \longrightarrow H^+ + H_2$	5.8×10^{-10}	de Jong (1972)
28.	$H_2^+ + H_2 \longrightarrow H_3^+ + H$	2×10^{-9}	Clavel et al.(1978)
29.	$HCl^+ + H_2 \longrightarrow H_2Cl^+ + H$	1.3×10^{-9}	Smith & Adam (1981)
30.	$CH^+ + H \longrightarrow C^+ + H_2$	$7.5\times10^{-15}\ T_e^{1.25}$	Solomon & Klemperer(1972)

Table 2.3(Contd.)

	Reactions	Rates (sec^{-1} cm^{-3})	References
31.	$CH^+ + C \longrightarrow C_2^+ + H$	10^{-9}	Solomon & Klemperer(1972)
			Solomon & Klemperer(1972)
32.	$CH^+ + O \longrightarrow H^+ + CO$	10^{-9}	Clavel et al.(1978)
33.	$CH^+ + H_2 \longrightarrow CH_2^+ + H$	10^{-9}	Kim et al.(1975)
34.	$CO^+ + H \longrightarrow H^+ + CO$	10^{-9}	Oppenheimer (1975)
35.	$CO^+ + H_2 \longrightarrow HCO^+ + H$	1.4×10^{-9}	Kim et al.(1975)
36.	$OH^+ + H_2 \longrightarrow OH_2^+ + H$	1.1×10^{-9}	Kim et al.(1975)
37.	$O_2^+ + C \longrightarrow C^+ + O_2$	10^{-9}	Herbst & Klemperer (1973)
38.	$O_2^+ + Mg \longrightarrow Mg^+ + O_2$	10^{-10}	Oppenheimer & Dalgarno (1974)
39.	$O_2^+ + Si \longrightarrow Si^+ + O_2$	10^{-10}	Oppenheimer & Dalgarno (1974)
40.	$O_2^+ + S \longrightarrow S^+ + O_2$	10^{-10}	Oppenheimer & Dalgarno (1974)
41.	$O_2^+ + Fe \longrightarrow Fe^+ + O_2$	10^{-10}	Oppenheimer & Dalgarno (1974)
42.	$H_3^+ + C \longrightarrow CH^+ + H_2$	2×10^{-9}	Herbst & Klemperer (1973)
	$\longrightarrow CH_2^+ + H$	10^{-9}	Barsuhn (1977)

Table 2.3 (Contd.)

	Reactions	Rates ($Sec^{-1}cm^3$)	References
43.	$H_3^+ + O \longrightarrow OH^+ + H_2$	$8x10^{-10}$	Fehsenfeld (1976)
44.	$H_3^+ + OH \longrightarrow OH_2^+ + H_2$	$2x10^{-9}$	Herbst & Klemperer(1973)
45.	$H_3^+ + CO \longrightarrow HCO^+ + H_2$	$1.4x10^{-9}$	Watson (1974)
46.	$H_3^+ + H_2O \longrightarrow OH_3^+ + H_2$	$5.9x10^{-9}$	Huntress (1977)
47.	$H_3^+ + HCO \longrightarrow H_2CO^+ + H_2$	10^{-9}	deJong et al.(1980)
48.	$H_3^+ + H_2CO \longrightarrow H_3CO^+ + H_2$	$2x10^{-9}$	Herbst & Klemperer(1973)
49.	$CH_2^+ + O \longrightarrow HCO^+ + H$	10^{-9}	deJong et al.(1980)
50.	$CH_2^+ + H_2 \longrightarrow CH_3^+ + H$	$7.2x10^{-10}$	Watson (1974)
51.	$OH_2^+ + H_2 \longrightarrow OH_3^+ + H$	$6x10^{-10}$	Huntress (1977)
52.	$HCO^+ + C \longrightarrow CH^+ + CO$	10^{-9}	Mitchell et al(1978)
53.	$HCO^+ + Mg \longrightarrow Mg^+ + CO + H$	10^{-10}	Oppenheimer & Dalgarno (1974)
54.	$HCO^+ + Si \longrightarrow Si^+ + CO + H$	10^{-10}	Oppenheimer & Dalgarno (1974)

Table 2.3 (Contd.)

	Reactions	Rates ($Sec^{-1}cm^3$)	References
55.	$HCO^+ + Fe \longrightarrow Fe^+ + CO + H$	10^{-10}	Oppenheimer & Dalgarno (1974)
56.	$HCO^+ + H_2 \longrightarrow H_3CO^+ + h\nu$	$5x10^{-19}$	Herbst (1976)
57.	$HCO^+ + CH \longrightarrow CH_2^+ + CO$	10^{-9}	Mitchell (1978)
58.	$HCO^+ + OH \longrightarrow HCO_2^+ + H$	10^{-9}	Herbst & Klemperer (1973)
59.	$HCO^+ + H_2O \longrightarrow OH_3^+ + CO$	$2.7x10^{-9}$	Huntress & Anicich (1976)
60.	$HCO^+ + CH_2 \longrightarrow CH_3^+ + CO$	10^{-9}	Mitchell (1978)
61.	$HCO^+ + H_2CO \longrightarrow H_3CO^+ + CO$	10^{-9}	Herbst & Klemperer (1973)
62.	$CH_3^+ + O \longrightarrow HCO^+ + H_2$	$4x10^{-10}$	Fehsenfeld (1976)
63.	$\longrightarrow H_2CO^+ + H$	$4x10^{-11}$	deJong et al.(1980)
63.	$CH_3^+ + Mg \longrightarrow Mg^+ + CH_3$	10^{-10}	Dalgarno et al.(1973)
64.	$CH_3^+ + Si \longrightarrow Si^+ + CH_3$	10^{-10}	Dalgarno et al.(1973)
65.	$CH_3^+ + S \longrightarrow S^+ + CH_3$	10^{-10}	Dalgarno et al.(1973)

Table 2.3 (Contd.)

	Reactions	Rates ($sec^{-1} cm^3$)	References
66	$CH_3^+ + Fe \longrightarrow Fe^+ + CH_3$	10^{-10}	Dalgarno et al.(1973)
67	$CH_3^+ + H_2 \longrightarrow CH_5^+ + h\nu$	$4x10^{-13} \left(\frac{50}{T_e}\right)^{3.8}$	Smith & Adams (1978)
68	$OH_3^+ + C \longrightarrow HCO^+ + H_2$	$2x10^{-9}$	Herbst & Klemperer (1973)
69	$OH_3^+ + CH_2 \longrightarrow CH_3^+ + H_2O$	10^{-9}	Huntress (1977)

Table 2.4

Neutral - Neutral Reactions

	Reactions	Rates (cm^3 sec^{-1})	References
1	$C + CH \longrightarrow C_2 + H$	$4x10^{-11}$	Solomon & Klemperer (1972)
2	$C + OH \longrightarrow CO + H$	$4x10^{-11}$	Herbst & Klemperer (1973)
3	$C + HCO \longrightarrow CO + CH$	10^{-11}	deJong et al.(1980)
4	$O + CH \longrightarrow CO + H$	$4x10^{-11}$	Herbst & Klemperer (1973)
	$\longrightarrow HCO^+ + e$	10^{-11}	Black (1975)
		$1.6x10^{-12}\ T_e^{.44}$	Gerola & Glassgold (1978)
5	$O + OH \longrightarrow O_2 + H$	$5x10^{-11}$	Herbst & Klemperer (1973)
6	$O + HCO \longrightarrow OH + CO$	$1.2x10^{-10}$	Prasad & Huntress (1979)
	$\longrightarrow CO_2 + H$	8.9×10^{-11}	Prasad & Huntress (1979)
7	$O + CH_2 \longrightarrow CH + OH$	$8x10^{-12}$	deJong et al.(1980)
	$\longrightarrow HCO + H$	10^{-11}	deJong et al.(1980)
8	$O + CH_3 \longrightarrow H_2CO + H$	$3x10^{-11}$	Gerola & Glassgold (1978)
9	$O + H_2CO \longrightarrow HCO + OH$	10^{-13}	Gerola & Glassgold (1978)
10	$OH + CO \longrightarrow CO_2 + H$	$2.1x10^{-13}\ e^{-80/T_e}$	Prasad & Huntress (1979)

Table 2.5

Ion-Electron Recombination

	Recombination	Rates (cm^3 sec^{-1})	References
1.	$H^+ + e \longrightarrow H + h\nu$	1.75×10^{-10} $T_e^{-0.7}$	Seaton (1959), deJong(1977)
2.	$He^+ + e \longrightarrow He + h\nu$	1.9×10^{-10} $T_e^{-0.7}$	Bates & Dalgarno (1962)
3.	$C^+ + e \longrightarrow C + h\nu$	1.4×10^{-10} $T_e^{-0.61}$	deJong (1977)
4.	$O^+ + e \longrightarrow O + h\nu$	1.2×10^{-10} $T_e^{-0.63}$	deJong et al.(1980)
5.	$Mg^+ + e \longrightarrow Mg + h\nu$	3.7×10^{-10} $T_e^{-0.86}$	deJong (1977)
6.	$Si^+ + e \longrightarrow Si + h\nu$	1.5×10^{-10} $T_e^{-0.60}$	deJong (1977)
7.	$S^+ + e \longrightarrow S + h\nu$	1.4×10^{-10} $T_e^{-0.63}$	deJong (1977)
8.	$Cl^+ + e \longrightarrow Cl + h\nu$	1.9×10^{-10} $T_e^{-.61}$	estimated by us
9.	$Fe^+ + e \longrightarrow Fe + h\nu$	1.5×10^{-10} $T_e^{-.65}$	deJong (1977)
10.	$H_2^+ + e \longrightarrow H + H$	4×10^{-8} $T_e^{-0.5}$	Dubrovskii & Ob'edkov (1967)
11.	$HCl^+ + e \longrightarrow Cl + H$	10^{-6} $T_e^{-0.5}$	Based upon McGown (1979) and Barsuhn(1977)

Table 2.5 (Contd.)

	Recombination	Rates ($cm^3 sec^{-1}$)	References
12.	$CH^+ + e \longrightarrow C + H$	$2 \times 10^{-6}\ T_e^{-0.5}$	Barsuhn (1977)
13.	$OH^+ + e \longrightarrow O + H$	$10^{-6}\ T_e^{-0.5}$	deJong et al. (1980)
14.	$CO^+ + e \longrightarrow O + C$	$10^{-6}\ T_e^{-0.5}$	deJong et al. (1980)
15.	$O_2^+ + e \longrightarrow O + O$	$4 \times 10^{-6}\ T_e^{-0.5}$	Biondi (1969)
16.	$H_3^+ + e \longrightarrow H_2 + H$	$2 \times 10^{-6}\ T_e^{-0.5}$	Leu et al (1973)
	$\longrightarrow 3\ H$	$2 \times 10^{-6}\ T_e^{-0.5}$	Leu et al (1973)
17.	$CH_2^+ + e \longrightarrow CH + H$	$10^{-5}\ T_e^{-0.5}$	McGown (1979)
		$4 \times 10^{-6}\ T_e^{-0.5}$	Barsuhn (1977)
18.	$H_2Cl^+ + e \longrightarrow HCl + H$	$4 \times 10^{-6}\ T_e^{-0.5}$	Based upon Barsuhn (1977) as quoted in de Jong et al. (1980)
19.	$OH_2^+ + e \longrightarrow OH + H$	$3 \times 10^{-6}\ T_e^{-0.5}$	deJong et al. (1980)
20.	$HCO^+ + e \longrightarrow CO + H$	$1.5 \times 10^{-5}\ T_e^{-0.5}$	Mul & McGown (1979)

Table 2.5 (Contd.)

	Recombination	Rates ($cm^3\ sec^{-1}$)	References
21.	$CH_3^+ + e \longrightarrow CH + H_2$	$1.3\times10^{-5}\ T_e^{-.5}$	McGowan (1979)
	$\longrightarrow CH_2 + H$	$2.1\times10^{-6}\ T_e^{-.5}$	McGowan (1979)
	$\longrightarrow CH_3 + h\nu$	$3.9\times10^{-9}\ T_e^{-0.5}$	McGowan (1979)
22.	$OH_3^+ + e \longrightarrow OH + H_2$	$10^{-5}\ T_e^{-0.5}$	Herbst (1978), McGowan (1979)
	$\longrightarrow H_2O + H$	$10^{-6}\ T_e^{-0.5}$	Herbst (1978), McGowan (1979)
23.	$H_2CO^+ + e \longrightarrow CO + H + H$	$6\times10^{-6}\ T_e^{-0.5}$	deJong et al. (1980)
24.	$HCO_2^+ + e \longrightarrow CO_2 + H$	$10^{-5}\ T_e^{-0.5}$	deJong et al. (1980)
	$\longrightarrow CO + O + H$	$10^{-5}\ T_e^{-0.5}$	deJong et al. (1980)
25.	$H_3CO^+ + e \longrightarrow CO + 3H$	$10^{-5}\ T_e^{-0.5}$	deJong et al. (1980)
	$\longrightarrow H_2CO + H$	$10^{-5}\ T_e^{-0.5}$	deJong et al. (1980)

Table 2.6

Dependence of emission measure (EM) and their ratios on hydrogen number density n_H for $R=10^{-17}(cm^3 Sec^{-1})$

Abundance	Density n_H (cm^{-3})	Emission measures							
		H II	C II	S II	Si II	Fe II	Mg II	$\frac{\sum_X EM(XII)}{EM\ CII}$	$\frac{EM(H\ II)}{EM(C\ II)}$
Solar	$5x10^3$	.5049	2.2640	.1199	.2701	.1880	.2666	.373	.22
	10^4	1.0798	4.4447	.2378	.5366	.3732	.5294	.377	.24
	$2x10^4$	1.8483	8.2739	.4514	1.0213	.7085	1.0060	.385	.22
	$5x10^4$	2.6586	17.5301	.9958	2.2623	1.5604	2.2200	.401	.15
Depleted	$5x10^3$	.1967	.2658	.0272	.0042	.0015	.0058	.146	.74
	10^4	.4220	.5324	.0545	.0083	.0032	.0116	.146	.79
	$2x10^4$	.7375	.9992	.1033	.0158	.0060	.0220	.147	.74
	$5x10^4$	1.1140	2.1017	.2223	.0341	.0130	.0474	.150	.61

Table 2.7

Values of emission measures and their ratios at $n_H = 10^4$ cm^{-3} for various reaction rates.

	Solar abundance			Depleted abundance		
R ($cm^3 Sec^{-1}$)	EM(HII)	EM(CII)	EM(HII)/EM(CII)	EM(HII)	EM(CII)	EM(HII)/EM(CII)
$5x10^{-18}$	.7067	4.2731	.17	.2837	.4946	.57
10^{-17}	1.0798	4.4447	.24	.4220	.5324	.79
$3x10^{-17}$	1.9669	4.7791	.41	.7493	.6014	1.25
$5x10^{-17}$	2.4952	4.9438	.50	.9443	.6341	1.49

Table 2.8

Computed column densities of our cloud models for $N_H = 5 \times 10^{22}$ cm^{-2}

Abundance	n_H (cm^{-3})	N(H)	N(CH)	N(OH)	N(CO)	N(O_2)	N(CH_2)	N(H_2O)	N(H_2CO)	N(CH^+)	N(CO^+)	N(HCO^+)
Solar	10^3	5.4(21) / 4.1(20)	9.2(15)	2.7(16)	1.1(19)	2.2(17)	9.0(13)	6.4(16)	1.1(15)	4.7(11)	2.4(10)	4.2(14)
	10^4	2.3(21) / 2.0(20)	3(15)	7.3(15)	1.4(19)	2.5(17)	2.7(13)	4.8(16)	1.0(15)	2.9(11)	2.5(9)	2.0(14)
	10^5	1.5(21) / 1.5(20)	3.8(14)	3.3(15)	1.6(19)	2.8(17)	2.1(13)	3.9(16)	5.1(14)	1.2(11)	4.1(8)	3.3(13)
	10^6	5.1(20) / 1.15(20)	1.9(14)	2.7(15)	1.7(19)	4.3(17)	2.0(13)	2.2(16)	2.2(14)	3.3(10)	1.2(8)	6.6(12)
Depleted	10^3	5.6(21) / 4.3(20)	1.1(15)	3.6(16)	2.5(18)	1.8(17)	2.1(14)	4.6(16)	6.2(13)	2.7(11)	1.6(10)	1.8(14)
	10^4	2.3(21) / 2.1(20)	5.0(14)	9.9(15)	3.5(18)	2.0(17)	7.0(13)	5.0(16)	4.2(13)	1.8(11)	2.1(9)	1.1(14)
	10^5	1.5(21) / 1.5(20)	3.0(14)	4.3(15)	4.1(18)	2.3(17)	4.6(13)	4.3(16)	3.2(13)	5.1(10)	3.5(8)	3.6(13)
	10^6	5.2(20) / 1.15(20)	2.8(14)	3.2(15)	4.6(18)	3.3(17)	3.8(13)	2.8(16)	2.0(13)	2.0(10)	1.3(8)	1.3(13)

Note: (i) The UV radiations are from the exciting star of associated HII regions plus general background radiations of Habing (1968).

(ii) The quantities in the bracket are the powers of 10.

Table 2.9

Observed column densities of the clouds adjacent to H II regions

Cloud	N(H)	N(CH)	N(OH)	N(CO)	$N(H_2CO)$
NGC 2024	3×10^{21} (a) 5.5×10^{20} (a) 2.9×10^{20} (a)	4×10^{13} (b)	$\sim 2\times10^{15}$ (d)	1.2×10^{19} (f) 8.2×10^{18} (g)	$\sim 2\times10^{13}$ (f) 1.8×10^{13} (b) 4×10^{13} (h)
Orion A	1.7×10^{21} (a) 6.2×10^{20} (a) 3.8×10^{20} (a)	$<5\times10^{13}$ (c)	$\sim 3\times10^{15}$ (c)	1.5×10^{19} (g)	$\sim 2.5\times10^{13}$ (c) $\sim 4\times10^{13}$ (h)
W3		4.9×10^{13} (b)	$\sim 5\times10^{15}$ (c)	6.0×10^{18} (g)	$\sim 2.2\times10^{13}$ (f) $\sim 1.1\times10^{13}$ (b) $\sim 2.8\times10^{13}$ (h)

(a) Radhakrishnan, V., Goss, W.M., Murray, J.D. & Brook, J.W. (1972) Astrophys. J. Suppl., 24, 49.

(b) Genzel, R., Downes, D., Pauls, T., Wilson, T.L. & Beiging, J. (1979) Astron.& Astrophys. 73, 253.

(c) Zukerman, B. & Turner, B.E. (1975), B.E.(1975), Ap. J., 197, 123.

(d) Goss, W.M. (1968) Ap. J. Suppl. No., 15 , 131.

(e) Crovisier, J., Fillit, R. & Kazes, I. (1975) Astron. & Astrophys., 45, 97.

(f) Hudson, H.S. & Soifer, B.T. (1976), Ap. J., 206, 100

(g) Wilson, W.J., Schwartz, P.R., Epstein, E.E., Johnson, W.A., Etcheverry, R.O., Mori, T.T., Berry, G.G. & Dyson, H.B. (1974), Ap.J., 191, 357.

(h) Evans, N.J., Zuckerman, B., Morris, G. & Sato, T. (1975), Ap.J. 196, 433.

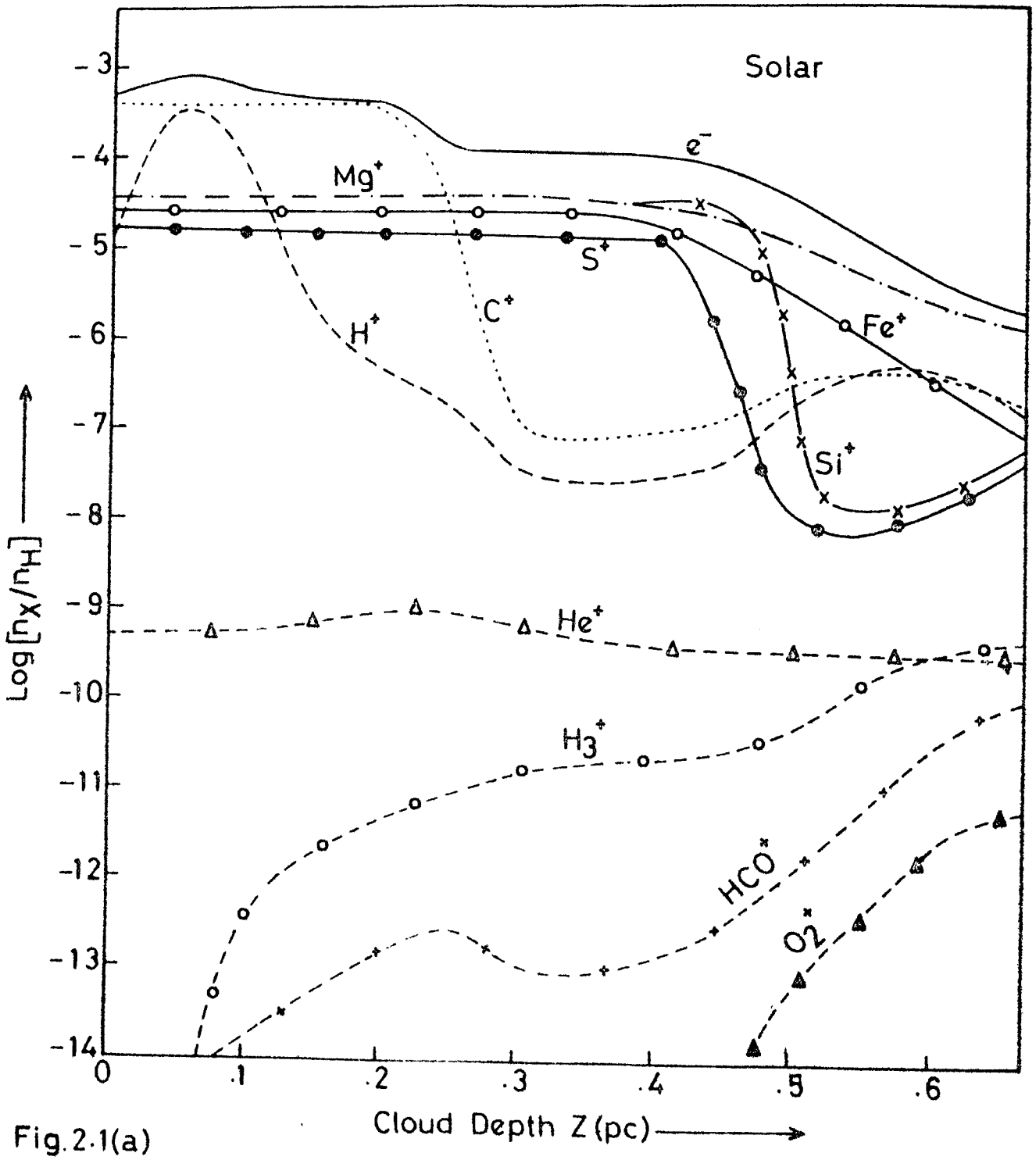
Solar
e^-
Mg^+
S^+
C^+
H^+
Fe^+
Si^+
He^+
H_3^+
HCO^+
O_2^+
Log [n_X/n_H]
-3
-4
-5
-6
-7
-8
-9
-10
-11
-12
-13
-14
0
.1
.2
.3
.4
.5
.6
Cloud Depth Z (pc)

Fig. 2·1(a)

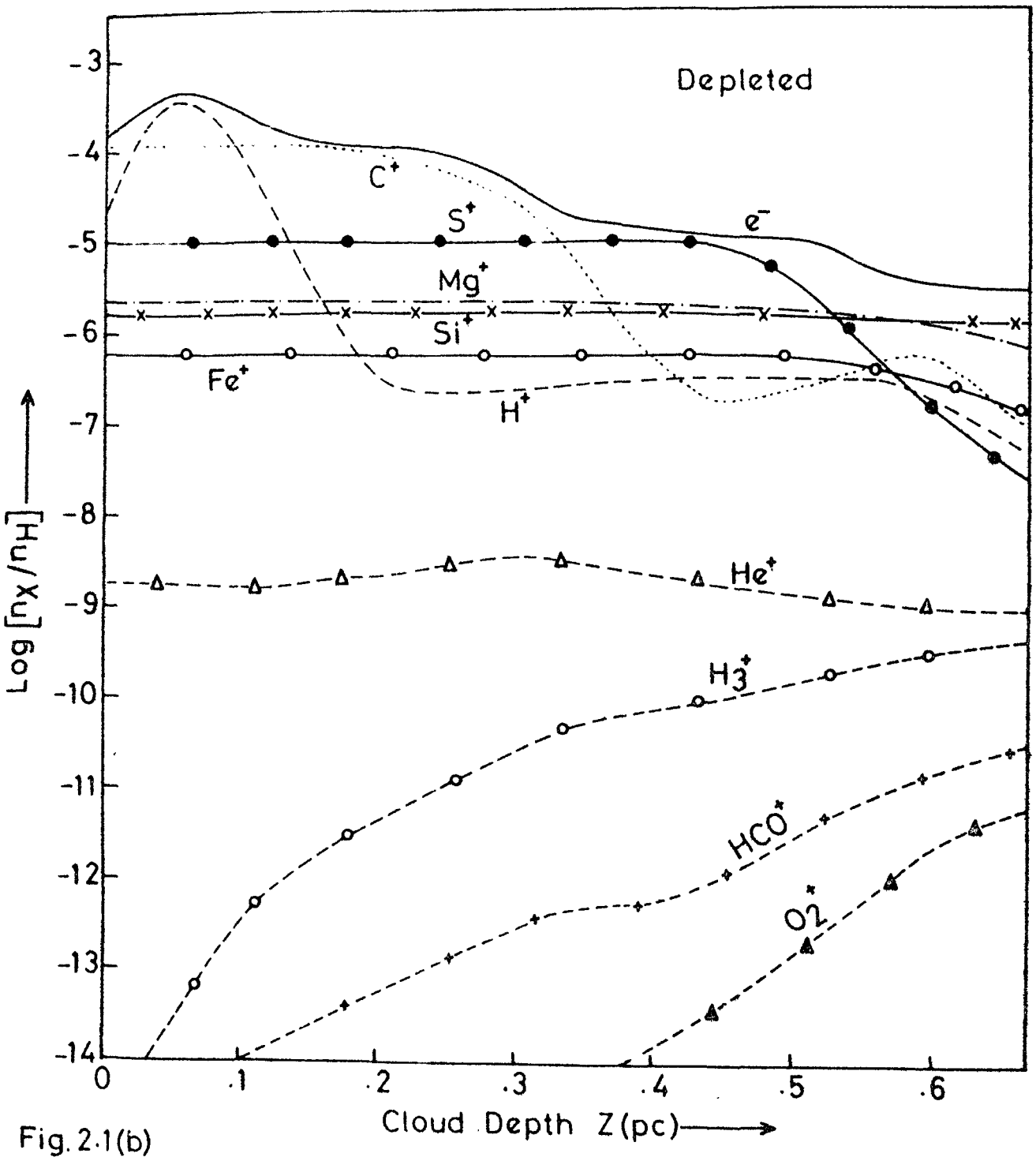
Depleted
C+
S+
e−
Mg+
Si+
Fe+
H+
He+
H3+
HCO+
O2+
-3
-4
-5
-6
-7
-8
-9
-10
-11
-12
-13
-14
0
.1
.2
.3
.4
.5
.6
Log [nx/nH]
Cloud Depth Z(pc)

Fig. 2.1(b)

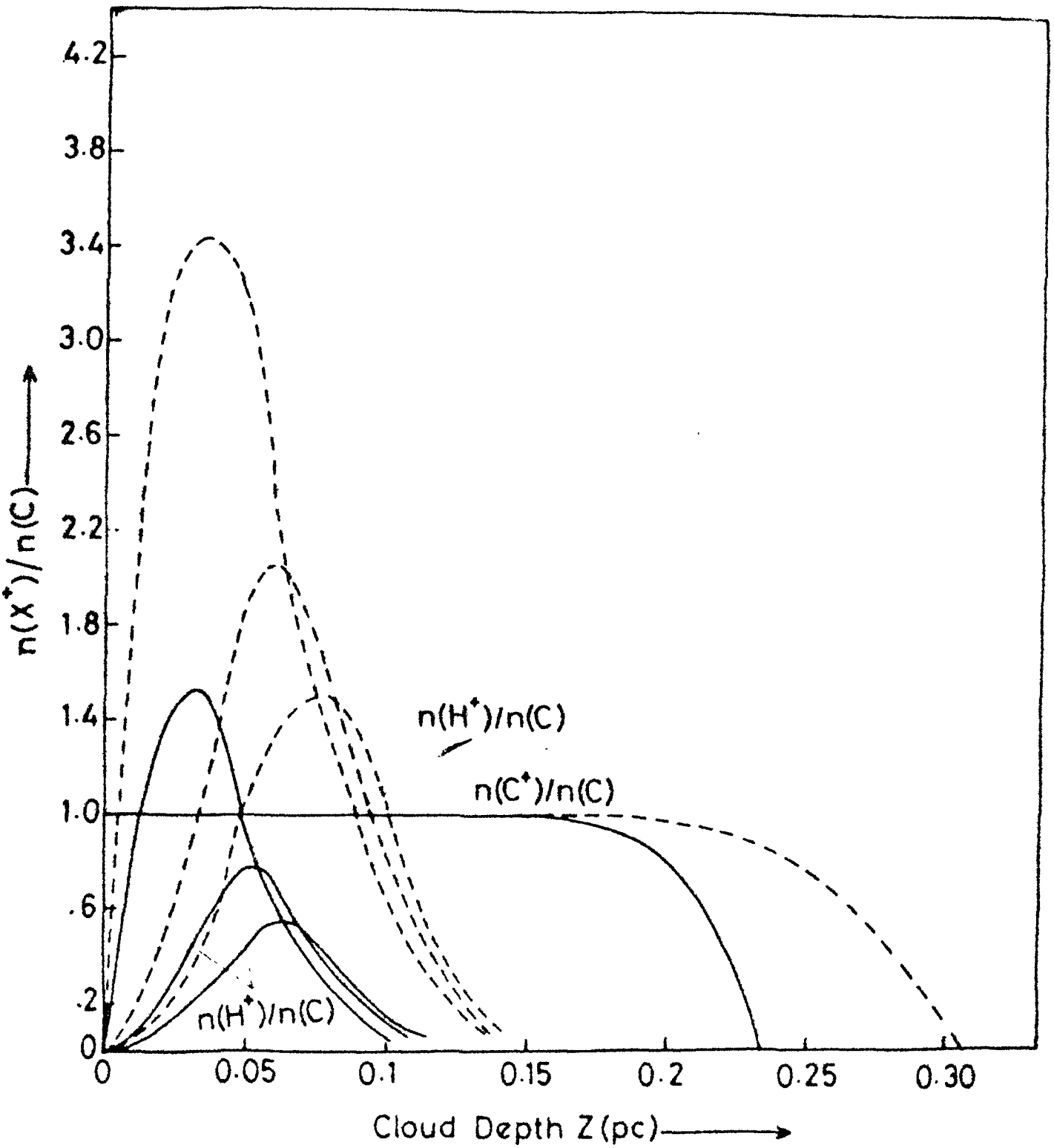
4.2
3.8
3.4
3.0
2.6
2.2
1.8
1.4
1.0
.6
.2
0
n(X⁺)/n(C)
n(H⁺)/n(C)
n(C⁺)/n(C)
n(H⁺)/n(C)
0
0.05
0.1
0.15
0.2
0.25
0.30
Cloud Depth Z (pc)

Fig. 2.2

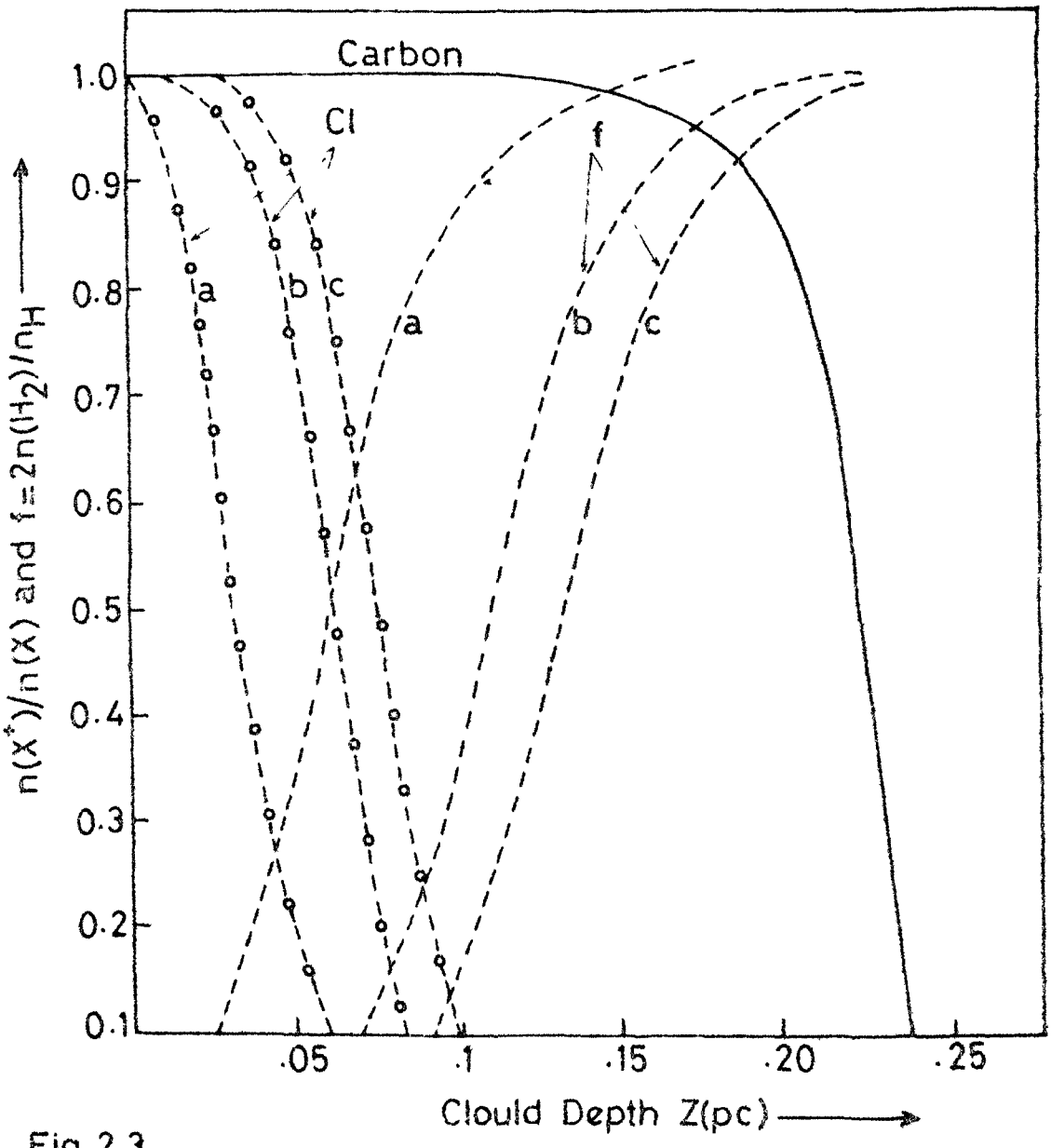
Carbon
Cl
a
b
c
f
1.0
0.9
0.8
0.7
0.6
0.5
0.4
0.3
0.2
0.1
.05
.1
.15
.20
.25
n(X+)/n(X) and f=2n(H2)/nH
Clould Depth Z(pc)

Fig. 2.3

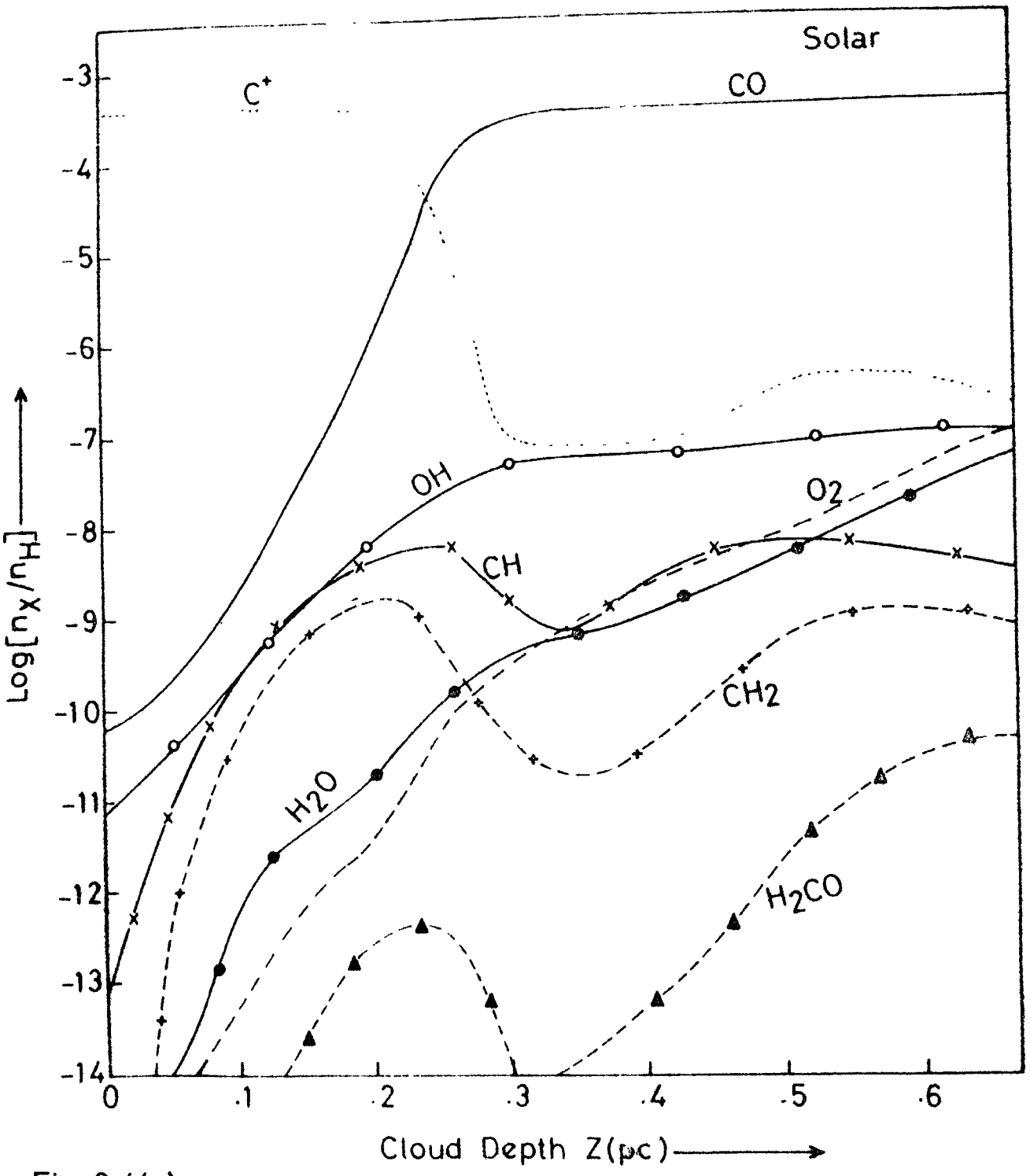
Solar
C+
CO
OH
O2
CH
CH2
H2O
H2CO
-3
-4
-5
-6
-7
-8
-9
-10
-11
-12
-13
-14
0
.1
.2
.3
.4
.5
.6
Log[nx/nH]
Cloud Depth Z(pc)

Fig. 2.4(a)

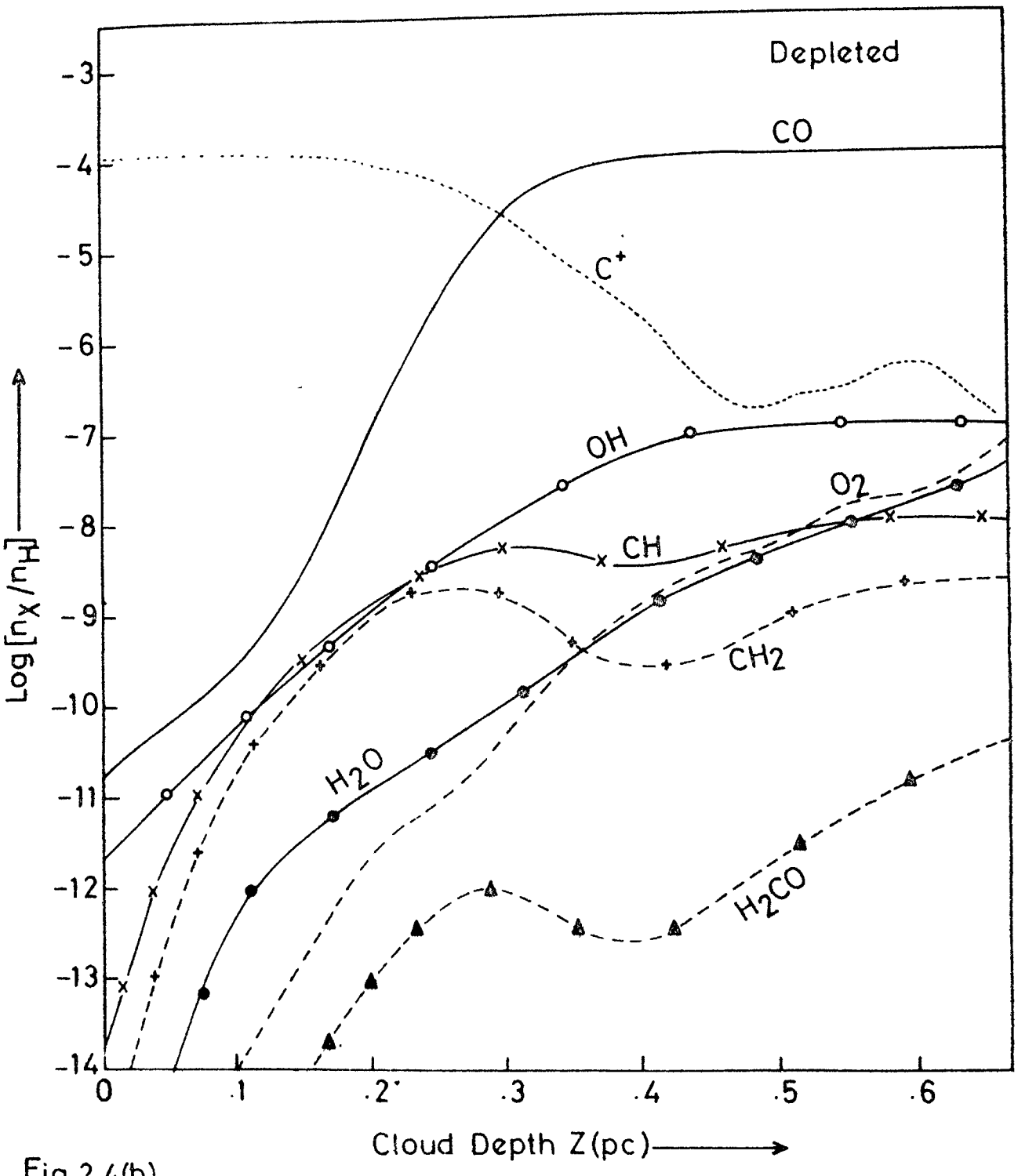
Depleted
CO
C+
OH
O2
CH
CH2
H2O
H2CO
-3
-4
-5
-6
-7
-8
-9
-10
-11
-12
-13
-14
0
.1
.2
.3
.4
.5
.6
Log [nX/nH]
Cloud Depth Z(pc)

Fig. 2.4(b)

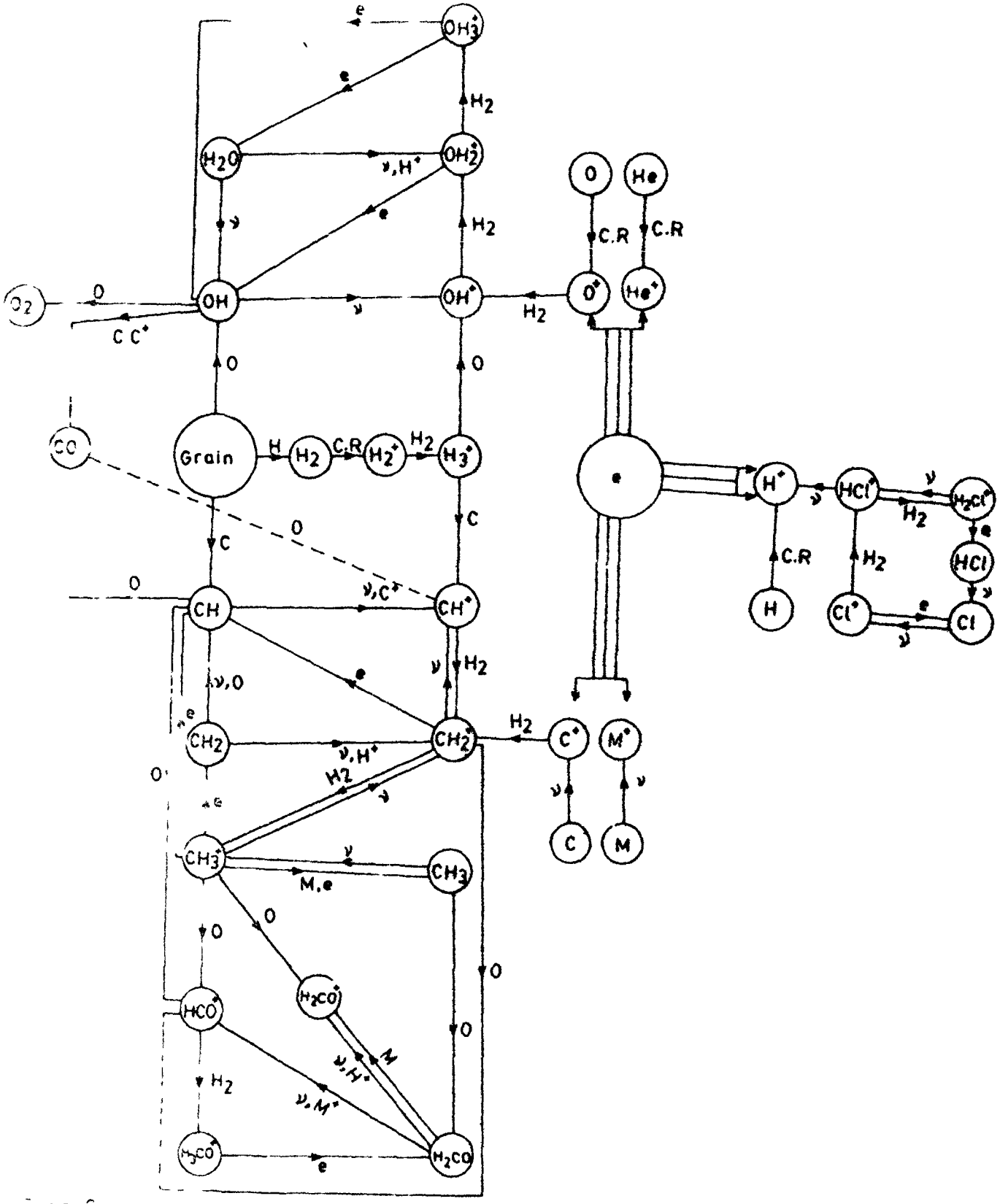
OH3+
H2O
OH2+
OH
OH+
O2
CO
Grain
H
H2
H2+
H3+
CH
CH+
CH2
CH2+
CH3+
CH3
HCO+
H2CO+
H3CO+
H2CO
O
He
O+
He+
C.R
H+
HCl+
H2Cl+
HCl
Cl+
Cl
C+
M+
C
M
e
ν
C
M.e
ν,H+
ν,C+
ν,M+

Drag 2

FIGURE CAPTIONS

Fig.2.1 Variation of abundances (relative to hydrogen) of electrons, atomic and molecular ions with the cloud depth for two different abundances;

(a) Solar and (b) Depleted.

Fig.2.2 Variation of ionised carbon and hydrogen as a function of cloud depth for the abundances : solar (——) and depleted (----).

Fig.2.3 Degree of ionisation of carbon (solid line) and chlorine (dotted line) as a function of cloud depth. The fraction of hydrogen in molecular form (f) is shown by dotted lines. Curves are drawn for three different values of R(a) 5×10^{-17} (b) 10^{-17} and (c) 5×10^{-18} cm^3 sec^{-1}.

Fig.2.4 Abundances (relative to hydrogen) of C^+ and molecules as a function of position in the cloud for two assumed abundances:

(a) Solar and (b) Depleted.

Diag.2 Schematic representation of chemical reaction scheme.

CHAPTER 3

THERMAL STRUCTURE

3.1. Introduction

The line radiations from atom, ions and molecules have greatly modified our ideas about the interstellar matter and have revealed a large variety of physical conditions in the interstellar medium. That is why the low temperature and high density interstellar medium have received considerable attention in the last decade. However, the identification of important processes responsible for the observed temperature of interstellar gas continues to be one of the major problems in the theory of interstellar medium, though several studies bearing on the thermal structure of the atomic and molecular clouds have been carried out (Clavel et al. 1978, Viala et al. 1979 and deJong et al.1980).

A number of heating mechanisms that have been proposed are: cosmic rays, photoionisation of carbon and other heavy elements by background radiation. Photo-emission of electrons from dust grains, formation of H_2 on grains and its dissociation, energy deposition during chemical reactions, and gravitational collapse. In the following section we consider each of these processes one by one.

The molecular line emissions are expected to play an important role in thermal balance of dense clouds, whereas

in diffuse clouds the cooling is predominantly by the ionic and atomic species, the fine structure (f.s.) of which have low excitation energy. The most important species are C,O,Si and F_e atoms and some of their ions.

The dust grains have also a significant role in the interstellar medium. They protect the atoms and molecules from ionisation and/or dissociation by absorbing the ultra-violet radiation from the galactic background or nearest hot stars of associated HII regions. The photo-electrons from dust grains are now supposed to be a potential heating agent in the interstellar medium. This is discussed in some detail in this chapter.

In calculating the thermal structure we include the far-infrared radiations from the dust grains in the associated HII regions and photon trapping. It is found that the latter and FIR are also important for determining the level populations of atoms, ions and molecules. As a result cooling from the available species is also modified.

In the following we study: i) The relative importance of various heating and cooling mechanisms in different regions of the cloud. ii) The effect of FIR field from associated HII regions on level populations of CO molecules, its isotopes, carbon atom and its ion and resulting cooling from these species. iii) Variation of level populations and cooling rates over the

hydrogen density range 10 to 10^7 cm^{-3}, kinetic temperature 10 to 100 K and abundance between 10^{-3} to 10^{-6}. Thermal structure is solved using detailed balance between heating and cooling based upon the assumption that thermal and dynamical time scales are of the same order of magnitude and thermal equilibrium prevails. From the above study we are also able to draw some useful conclusions about the thermal structure in the cloud in the light of observations.

3.2 Heating Mechanism

3.2.1 Heating due to photo-electrons from dust grains

In recent years photo-electric emission from dust grains has received much attention as a potentially important heat source for the interstellar medium (Watson 1972, Glassgold & Langer 1974, Jura 1976, deJong 1977 and Draine 1978). None of the above authors have however accounted for the attenuation effect and also ultraviolet radiations from the hot stars of the associated HII regions. It may be mentioned that the heating of the gas by this process depends upon the electron and photon energy distribution and also upon the charge on the grains. The charge itself depends upon the electron density and temperature of the medium. Following the method of Draine (1978) we derive the expressions for the charge on the grain and heating of the gas.

i) Grain Potential

Before discussing the heating due to photo-electrons we must solve for electron and proton capture rates on the grains, R_e and R_P respectively, and rate of photo-electron emission ϵ_e from the surface of the grain to determine the potential U on the surface of grains. The capture and emission rates themselves depend upon the grain potential. The expressions for the capture of electrons and protons on the surfaces of grains are (Spitzer 1968)

$$R_e = n_e s_e v_e (1+\varphi) \quad \text{for } \varphi > 0 \qquad 3.1a$$

$$= n_e s_e v_e e^{\varphi} \quad \text{for } \varphi < 0 \qquad 3.1b$$

$$R_P = n(H^+) s_p v_p e^{-\varphi} \quad \text{for } \varphi > 0 \qquad 3.2a$$

$$= n(H^+) s_p v_p (1-\varphi) \quad \text{for } \varphi < 0 \qquad 3.2b$$

where $\varphi = U/kT_e$, n_e and $n(H^+)$ are the electron and proton densities, v_e and v_p are the respective thermal velocities, and s_e & s_p are the sticking coefficients respectively. The photo-electron emission rate ϵ_e from the grain surface is written, as:

$$\epsilon_e = \int_{E_{min}}^{E_{max}} J_e(E)\, dE \qquad 3.3$$

where

$$J_e(E) = \int_{\nu_{th}}^{\nu_o} h\, Q_{abs}(\nu)\, F_\nu\, Y(\nu) f(E,\nu)\, d\nu \qquad 3.4$$

Here ν_o is the Lyman limit and ν_{th} the threshold frequency for the ejection of electrons. E_{min} depends on the charge on the grain. It is zero for negatively charged grain and equal to potential U for positively charged grains. $E_{max} = h(\nu_o - \nu_{th})$. The coefficient of absorption $Q_{abs} = \sigma_{abs}/\sigma_g$ (geometrical) and is taken to be equal to 0.75 for $h\nu > 6$ev(Draine 1978). The flux of ultraviolet radiations F_ν around $1000A^o$, which causes the emission of electrons from the grains, is taken to be equal to the value defined by equation 2.2. $Y(\nu)$ is the yield of electrons and $f(E,\nu)$ the photo-electron kinetic energy distribution. Here we adopt after Draine (1978),

$$f(E,\nu) \cong \frac{1}{(h\nu - \beta)} \qquad 3.5$$

$$Y(\nu) \cong y_\infty \left(1 - \frac{\beta}{h\nu}\right) . \qquad 3.6$$

The parameter B is slightly greater than the threshold frequency ν_{th} and its value equal to 8 eV gives a representative form of the yield from combined grains of all types for $y_\infty = 0.5$ (see fig.1, Draine 1978). In the present case ν_{th} is also approximated by B.

Substituting 2.2, 3.5 and 3.6 in 3.4 and 3.4 in 3.3 the photo-electron emission rate may be approximated as:

$$\epsilon_e \simeq 1.5 \times 10^{10} Q_{abs} y_\infty \chi_F e^{-\tau_\lambda(Z)} / (0.5+Z)^2 \quad \text{for } U<0 \qquad 3.7a$$

$$\simeq 1.5\times10^{10} Q_{abs}\, y_\infty \chi_F e^{-\tau_\lambda(Z)} (1-U/5.6)^2/(0.5+Z)^2$$

$$\text{for } 0 \leq U < 5.6 \qquad 3.7b$$

$$\simeq 0 \qquad \text{for } U \geq 5.6 \qquad 3.7c$$

The typical value of $5.6 = 13.6-8 = h\nu_o - B$ depends evidently on the assumed value of B. The charge on the grain is determined using the balance between charges. This is equivalent to equating the capture and emission rates, namely,

$$\epsilon_e = R_e - R_P \simeq R_e \qquad 3.8$$

since $R_P \propto 1/\sqrt{m_P}$. A simplified expression for the grain potential $U \geq 0$ is obtained from 3.8 by substituting values from 3.7b and 3.1a as follows:

$$\psi(1 + \theta P) = (1-p)^2 \quad , \quad p = U/5.6$$

which gives

$$U \simeq 5.6\left[1 + \frac{\psi\theta}{2}\left\{1 - \left(1 + \frac{4}{\psi\theta}\right)^{\frac{1}{2}}\right\}\right] \qquad 3.9a$$

Here $\Psi = n_e\ s_e\ (\frac{2kT_e}{\pi m_e})^{\frac{1}{2}}\ (0.5+Z)^2\ e^{\tau_\lambda(Z)}/1.5\times10^{10}\ Q_{abs}\ y_\infty\ \chi_F$

< 1 (in our case)

and $\theta = \frac{5.6(eV)}{kT_e} = \frac{6.5\times10^4}{T_e(K)}$

The solution for $U < 0$ is rather simple

$$e^{-\varphi} = \Psi$$

$$U = -kT_e \ln\Psi \qquad 3.9b$$

Using these two simplified forms of expression for U we can calculate the potential on the grain.

ii) Heating

The heating of the gas depends upon the amount of energy carried by photo-electrons emitted from the dust grains. Averaging over the electron current distribution we get for the heating per unit volume.

$$H(\text{grain}) = n_H\ \sigma_g \int_{E_{min}}^{E_{max}} (E-U)\ J_e(E)\ dE \qquad 3.10$$

Where σ_g is the cross-section of the grain. Putting the various values in the above equation, the expression may be approximated as:

$$H(\text{grain}) \cong 4.5\times10^{-2}\ Q_{abs}\ y_\infty\ \chi_F\ e^{-\tau_\lambda(Z)}\ n_H\ \sigma_g(1-\frac{U}{5.6})^3/(0.5+Z)^2 \ldots$$

$$\text{erg cm}^{-3}\text{sec}^{-1} \text{ for } 0 \leq U < 5.6 \quad (3.11)$$

$$\simeq 4.5\times10^{-2}\, Q_{abs}\, y_{\infty}\, \chi_F\, e^{-\tau_\lambda(Z)}\, n_H\, \sigma_g\, (1-\tfrac{U}{1.4})/(0.5+Z)^2 \text{ erg cm}^{-3}\text{sec}^{-1}$$

for $U < 0$

$$= 0 \qquad \text{for } U > 5.6$$

It may be mentioned that numerical results obtained from the general expression 3.10 are not significantly different from those obtained from/the approximate expression 3.11.

3.2.2. Cosmic ray heating

The ionisation of atomic and molecular hydrogen as discussed in section (2.5) and the resulting heating rates are quite uncertain. It have been demonstrated by Cravens and Dalgarno (1978) that only protons of energy $\gtrsim$ 20 Mev can penetrate a hydrogen column density $\gtrsim 6\times10^{22}$ cm^{-2} which is the value adopted in the present work. O'Donnel and Watson(1974), Glassgold and Langer (1976) and Black & Dalgarno (1977) argued on the basis of observations of HD and OH in diffuse clouds that the ionisation rate of H_2 is $(1.5 - 3.0)\times10^{-17}$ sec^{-1} This may be achieved if the proton flux in the range $10 < E < 100$MeV is considered in addition to that of 2 MeV. The ionisation rate adopted here for ionisation of different elements by cosmic rays are listed in the Table 2.2.

The total heating rate due to ionisation of hydrogen, helium and hydrogen molecule by cosmic rays is

$$H(CR) = \zeta_{CR}(H)\, n(H)\, Q_{CR}(H) + \zeta_{CR} n(He) Q_{CR}(He) + \zeta_{CR}(H_2)\, n(H_2) Q_{CR}(H_2) \quad 3.12$$

Where $Q'_{CR}s$ are the energy supplied to the medium through the ionisation of mentioned species, it depend upon the energy of the cosmic ray protons and also on fractional abundance of electrons. According to Cravens & Dalgarno (1978) the amount of heat deposited for various species may be taken $Q_{CR}(He) \simeq Q_{CR}(H) = 7.0$ eV and $Q_{CR}(H_2) = 17$eV for 10 MeV protons, while 100 MeV protons gives 8 eV and 26 eV respectively. The average values adopted for $10 < E < 100$ MeV protons are ~ 7.5 ev for hydrogen and helium and ~ 20 ev for hydrogen molecule. Now using the relations $n_H = n(H) + 2n(H_2)$, $f_{He} = n(He)/n_H$, $f = 2\, n(H_2)/n_H$, $\zeta_{CR}(H_2) \simeq \zeta_{CR}(He) \simeq \frac{5}{3} \zeta_{CR}(H)$ (Table 2.2) and substituting the values of Q_{CR} we represent equation 3.12 as follows:

$H(CR) = (4.5 + 7.5\, f_{He})\, \zeta_{CR}(H_2)\, n_H + 5.5\, f\, \zeta_{CR}(H_2) n_H$ + term due to 2 Mev proton. Since $f_{He} \sim .1$, we can write $(4.5 + 7.5\, f_{He}) \simeq 5(1+f_{He})$ and also $5.5 \simeq 5\,(1 + f_{He})$

Therefore

$$H(CR) \simeq (1+f_{He})(5+5f)\, \zeta_{CR}(H_2)\, n_H + 2.25\times10^{-26}\, e^{-N_H/1.5\times10^{+20}} \quad \text{erg cm}^{-3}\text{sec}^{-1} \quad 3.13$$

This equation is similar to Clavel et al.(1978) but not exactly equal. The last term of the equation is arising due to 2 MeV protons. The maximum value for the ionisation by 2MeV proton is

adopted $\sim 2\times10^{-15}\,sec^{-1}$ (Spitzer and Tomasko 1968).

Heating due to H_2 formation and its dissociation

The H_2 molecules formed on the grains are ejected into the gas with energy equal to its binding energy 4.48 ev. A part of this energy is utilized to raise the internal energy of H_2 and also of grains which may be radiated away, while the rest of the energy goes into the gas as heat. The heating from this process is therefore

$$H(H_2 \text{ form}) = R\, n_H\, n(H)\, Q_{H_2} = R\,(1-f) n_H^2\, Q_{H_2} \text{ ergs cm}^{-3}\text{sec}^{-1} \qquad 3.14$$

where R is the molecular formation rate of H_2 and Q_{H_2} is the energy converted to heat. The total heating through this process is uncertain on two grounds. Firstly, the actual fraction of binding energy converted to heat is not known. Barlow & Silk (1976) have shown that the mean value of the heat input is 2.2 ev for graphite grain which could be the main site for H_2 formation. This value is adopted in the present work. Secondly, the value of (1-f) depend on the theory of molecular evolution. Goldsmith & Langer (1978) have discussed that time dependent theory will give a high value of (1-f) in comparison with the steady state theory. As a result net input will also be high. In the following we argue that the value of (1-f) obtained at $n_H \sim 10^4$ by both these theories will be approximately equal for the clouds considered here. According to

the time dependent evolution the value of $(1-f) \backsim 10^{-4}$ may be obtained for $n_H = 10^4$ cm^{-3} in a time scale of 2×10^6 years (Allen & Robinson 1976), the life time of the clouds mentioned here. However, the steady state theory also yields approximately same result $(1-f) \backsim 10^{-4}$ (Goldsmith & Langer 1978). Therefore heating in both the cases will be approximately same.

The photo-dissociation of H_2 molecules also give rise to heat energy = 0.42 ev $\backsim$ .094 of the binding energy per pair of H-atom formed. Therefore

$$H\ (H_2,\ \text{disso}) = 8\times10^{-13}\ \zeta_{uv}^{diss}\ n(H_2)\ \text{erg cm}^{-3}\text{sec}^{-1} \qquad 3.15$$

(Stephens & Dalgarno 1972).

3.2.4 Heating by Photo-ionisation of heavy elements:

A medium can also be heated by the ejected photo-electrons from heavy elements having ionisation potential less than Lyman limit, i.e. from C, Mg, Si, S and Fe. The electrons will carry an energy $(h\nu - h\ \nu_i)$, where ν is the frequency of radiation and ν_i is the ionisation limit of an element. The heat is produced after thermalization of electrons. The heating rate is given by

$$H(\text{Photo-ion}) = \sum_i n_i \int_{\nu_i}^{\nu_o} h\nu\,(1-\frac{\nu_i}{\nu})F_\nu(Z)\,\sigma_i(\nu)\,e^{-\tau_\nu(Z)}\,d\nu$$

$$\text{erg cm}^{-3}\text{sec}^{-1} \qquad 3.16$$

Here n_i is the density of specie i and $\sigma_i(\nu)$ the corresponding ionisation cross-section. In the present calculation the ionisation cross-sections and flux F_ν (Z) used are referred in Chapter 2.

3.2.5 Chemical heating

The molecules in the dense and cool clouds are mostly formed through the exothermic reactions. The energy released during the reaction is either converted into kinetic or internal energy of the system. The fraction of the energy liberated, that is deposited in the form of heat is quite uncertain. A part of the energy is certainly utilized to increase the internal energy of the gas. If Q_{ij} is the energy appearing as heat energy during the reaction (Clavel et al.1978) and R_{ij} are the reaction rates (see Tables 2.3 to 2.5) then the heating is given by

$$H(\text{Chem}) = \sum_{i,j} n_i n_j R_{ij} Q_{ij} \quad (\text{erg cm}^{-3} \text{ sec}^{-1}) \qquad 3.17$$

Where sum is taken over every pair of chemical reactions having the densities n_i and n_j. For simplicity we presume that the total energy released is deposited as a heat which is rather upper bound of the heating by this process.

3.2.6 Gravitational Contraction:

Gravitational collapse is one of the various dynamical

processes for the line broadening of CO molecules and accounts for the observed line width ranging from 5 to 10 km sec^{-1} in large clouds near HII regions (Leung & Liszt 1976). Therefore, this process could also be considered to contribute in the heating of the ISM, as discussed in detail by Goldsmith & Langer (1978). According to the latter, during the gravitational collapse the compressional work $P \frac{d}{dt} (\frac{1}{n_H})$ per particle against the internal pressure P will be converted into heat. The maximum value of this work is achieved by equating it to the gravitational potential per particle $\frac{1}{Vn_H} \frac{d\Omega}{dt}$ where V is the volume and Ω the gravitational potential. In the presence of the thermal pressure only Goldsmith & Langer(1978) obtain the following expression for heating by setting gravitational contraction equal to compression work, viz.,

$$H(comp) = \frac{3P}{t_{ff}} = 3.6 \times 10^{-31} T_e \; n(H_2)^{3/2} \text{ erg cm}^{-3}\text{sec}^{-1} \qquad 3.18$$

where t_{ff} is the free fall time $= (\frac{3\pi}{32 G \rho})^{\frac{1}{2}}$, ρ is the density. The temperature T_e can be determined using thermal equilibrium, which is set up in dense clouds within a time less than t_{ff}.

3.2.7 Gass - grain interaction

Scoville and Kwan (1976) have shown that there is no coupling between the dust and the gas. As a result, the energy exchange between gas-grain collision may be an important source

of heating or cooling depending upon the temperatures of the dust and the gas. The rate of the energy exchange in the gas through such collisions is (Spitzer 1949).

$$H(\text{Coll}) = \sum_p \frac{3k}{2(2m_p)^{\frac{1}{2}}} \left(\frac{8k}{\pi}\right)^{\frac{1}{2}} n_p\, n_g \sigma_g\, \xi_p\, T_e^{\frac{1}{2}} (T_g - T_e). \qquad 3.19$$

Here n_p is the density of particles of mass m_p, n_g is the grain density, σ_g is the geometric cross-section of a grain and T_g is the grain temperature. ξ_p is the accomodation coefficient of particle. Since the most abundant particles are either hydrogen or its molecule for which ξ_p is taken to be equal to 1. The equation 3.19 is simplified as:

$$H(\text{Coll}) = 1.45\times10^{-33} (1 - .65f)\, n_H^2\, T_e^{\frac{1}{2}} (T_g - T_e) \text{ erg cm}^{-3}\text{sec}^{-1} \qquad 3.20$$

If $T_g > T_e$, the heating of the gas will occur because of the energy transfer from the dust to the gas, while the cooling will occur for $T_g < T_e$.

3.3 Cooling

3.3.1 Level population and cooling rate:

To solve the level population of multilevel molecules and also of atoms and ions at a particular position Z in the cloud, all the populating and depopulating processes of a particular level i are considered. In general we can write.

$$n_i(X) \sum_j P_{ij}(X) = \sum_j n_j(X)\, P_{ji}(X) \qquad 3.21$$

Where n_i and n_j are the number densities of element X in levels i and j. P_{ij} is expressible in terms of radiative, induced and collisional transition probabilities A_{ij}, $\mathcal{B}_{ij}$ and C_{ij} respectively as follows:

$$P_{ij}(X) = A_{ij}(X) + \mathcal{B}_{ij}(X)\ \langle J_{ij}\rangle + C_{ij}(X) \qquad (i > j) \qquad 3.22$$

$$= \mathcal{B}_{ij}(X)\ \langle J_{ij}\rangle + C_{ij}(X) \qquad (i < j)$$

The mean radiation field $\langle J_{ij}\rangle$ includes the background radiation and local source function. With the assumption of the complete redistribution of frequencies for a spherical cloud, this mean radiation field $\langle J_{ij}\rangle$ may be written as (deJong et al.1975)

$$\langle J_{ij}\rangle = \left[1 - \beta_{ij}\right] S_{ij} + \beta_{ij}\ B_{ij}(\nu_{ij}, T_{2.7}, T_g) \qquad 3.23$$

Where B_{ij} is the Plank function at frequency ν_{ij}, $T_{2.7}$ is the temperature of the universal background radiation and T_g is the grain temperature. S_{ij} is the local source function, given by (deJong et al.1975),

$$S_{ij}(X) = 2h\nu_{ij}^3 / \left\{ c^2 \left[n_j(X)\ W_i(X) / n_i(X) W_j(X) - 1 \right] \right\} \qquad 3.24$$

Where W's are the statistical weights corresponding to level i and j. The escape probability for a spherical cloud (Goldsmith & Langer 1978).

$$\beta_{ij}(X) = \left(1 - e^{-\tau_{ij}(X)} \right) / \tau_{ij}(X) \qquad 3.25$$

Scoville and Solomon (1974) have explored a similar model of a plane parallel cloud with uniform density and obtain for escape probability.

$$\beta_{ij}(X) = (1 - e^{-3\,\tau_{ij}(X)}) / 3\,\tau_{ij}(X). \qquad 3.26$$

The numerical results at large values of τ_{ij} differ from those of the spherical clouds. The optical depth $\tau_{ij}(X)$ in the velocity gradient (dv/dr) model is

$$\tau_{ij}(X) = h\left[n_i(X)\,\beta_{ij}(X) - n_j(X)\,\beta_{ji}(X)\right] / (dv/dr). \qquad 3.27$$

Considering all the possible transitions from a particular species X, the total cooling rate (erg cm^{-3} sec^{-1}) is after Goldsmith & Langer (1978).

$$\Lambda(X) = \sum_j \sum_{i<j} \left\{n_j(X)\left[A_{ji} + \beta_{ji}\,U(\nu_{ij})\right] - n_i(X)\,\beta_{ij}\,U(\nu_{ij})\right\} \times \beta_{ij}\,(E_j - E_i) \qquad 3.28$$

Here $U(\nu_{ij})$ is the energy density of the background radiation in which we include beside the universal background 2.7k also FIR field.

3.3.2 Induced transition:

Level populations of atoms/molecules are very much governed by the induced transitions due to background radiation

combined with the local source function. It is customary to consider only the universal background radiation of 2.7k. It has however been observed that a number of cool and dense clouds are associated with HII regions, and in neighbour-hood of the HII regions a typical value of grain temperature is found to be 60 k with an optical depth of unity at 60 μ (Westbrook et al.1976). Following Ungerecht & Walmsley (1978), we attempt here to take into account also the FIR field from associated HII regional (Qaiyum & Ansari 1983 b). This field can be approximated as:

$$J(\nu)_{IR} = W B_{\nu} (T_g) (1 - e^{-\tau_g(\nu)}) \qquad 3.29$$

In this expression W is the dilution factor equal to 0.5-1.0 depending upon the proximity of the regions considered here. $B_{\nu} (T_g)$ is the Plank function at grain temperature T_g. τ_g is the dust optical depth, which is determined by using the observation that $\tau_g = 1$ at the turn-over frequency 60 μ but it may vary as $\frac{1}{\lambda}$. Hence the level population and the resulting cooling are calculated here using FIR field. We study the effect of grain temperature 40 k and 60 k on level population and cooling also.

3.3.3 Cooling by atoms, ions and molecules

The interstellar gas is cooled by the neutral, ionic and molecular species collisionally excited by electrons

hydrogen atoms or its molecules. The selection of a particular coolant, in a medium of temperature range 10-500 K, depends upon two main parameters that enter into the cooling rates, namely, the level spacing T_{ij} (^{o}K) = $\frac{1}{k} E_{ij}$ and the abundance of the species.

For a two level model, the cooling rates in the optically thin and thick limits are proportional to $T_{ij}\, e^{-T_{ij}/T_e}$ and $T_{ij}^{4}\, e^{-T_{ij}/T_e}$ respectively. So, we may argue that, in the temperature range mentioned above, the cooling from the species having very low and high level splitting, $T_{ij} \lesssim 1$ and $T_{ij} \gtrsim 600$K respectively, is therefore unimportant. Since the rotational level splitting T_{ij} in the molecule is inversely propotional to the moment of inertia, molecules with three or more heavy atoms (large moment of inertia) or with none (small moment of inertia) are unimportant for the cooling of the clouds in the range 10-500 K. Consequently, the important molecular species are H_2, HD, HCl, CO, O_2, CS, SiO, H_2O and HCN apart from the atoms of C, O, Si and Fe and some of their ions. Furthermore these molecules may have also an appreciable fractional abundance and have also a low excitation energy in the range 10-500 K.

Apart from the level spacing and the abundance of the coolant, the cooling is sensitive, in general, also to the parameters: kinetic temperature, density, velocity structure and optical depth. Besides these parameters the cooling depends

also on the collisional, induced and radiative rates and the resulting photon trapping.

The most abundant atomic specie CI and its ion CII, the fine structures of the latter are $^2P_{3/2}$ — $^2P_{1/2}$ (91.3°K) and of the former $^3P_2$ — $^3P_1$ (38.9°K), and $^3P_1$ — ^3P_o(23.6°K), have low excitation energy (level spacing) that can be collisionally excited. Other heavy elements Si, S and Fe are mostly in ionised form to a greater depth in the cloud. The analogous transitions of ionised atoms, namely, SiII $\left[^2P_{3/2} — ^2P_{\frac{1}{2}}\ (413°K)\right]$, FeII $\left[^6D_{9/2} — ^6D_{7/2}\ (554°K)\right]$. and also of OI $\left[^3P_o — ^3P_1\ (97.9°K),\ ^3P_1 — ^3P_2\ (228°K)\right]$ will be suppressed by the Boltzman factors in the collisional excitation rates at very low temperature, thereby negligibly contributing to the cooling. Since in the present calculations the temperature in the outer regions of the clouds (i.e. in the neighbourhood of HII regions) may be about 100 K therefore, the cooling from these species is also considered. However ions of SII and MgII are ineffective, because of their too high excitation energies, e.g. for SII T_{ij} = 21400°K.

The cooling due to the fine structure transitions of CI excited by electrons and H-atoms has been studied by Penston (1970), Dalgarno and McCray (1972), and Launay and Roueff(1977a). Since the collisional excitation of CI by H_2 has yet to be studied in detail, its rate is taken presently as 10 times

smaller than the rate of collisional excitation by H-atom (Goldsmith and Langer 1978). We take the rates of excitation of CII by electrons from Saraph et al. (1969), by H from Launay and Roueff (1977b), and by H_2 from Chu & Dalgarno(1975) and Flower and Launay (1977a,b).

The cooling due to OI, SiII and FeII by electron and H-atoms is reviewed by Dalgarno and McCray (1972). The electron impact excitation rates for SiII and FeII are taken from Seaton (1955) and Seaton (1958) respectively. The rate of collisional excitation of these species by H_2 has not been studied. These rates are taken to be equal to the collisional excitation rate by H-atom after Gerola and Glassgold (1978).

The formation of molecules has important implications for the cooling of the interstellar gas. The most abundant molecule is H_2 but its level spacing (509K) of $2 \longrightarrow 0$ transition is too large to compete, in general, with many atomic and molecular coolants even after the complete conversion of H to H_2. The temperature range considered in the present work is rather high. Therefore the contribution from this molecule is also considered.

The second most abundant molecule is CO and its level spacing for J rotational quantum numbers are 5.53J (^{o}K). From this value we see that levels upto J=20 may contribute appreciably to the cooling. Actually CO is found to be the main cooling agent in the interstellar medium.

The cooling due to HD is not significant here because of its low excitation rates and abundance. Further, the Boltzman factor suppresses here also the cooling for the level spacing J= 1→ 0 transition at 131K (Goldsmith & Langer 1978). Goldreich and Kwan (1974) have studied the cooling due to CS and SiO and found it to be negligibly small as compared to that due to CO because of low abundance.

The cooling due to HCl is studied by Glassgold and Langer (1976) for $HCl/n_H \lesssim 10^{-7}$. It was found that the contribution of HCl can not compete with other coolants even at this abundance. It should be mentioned here that the calculated abundance of HCl/n_H is $\sim 10^{-8}$ (Qaiyum & Ansari 1979). Therefore HCl is not considered here as a coolant.

It has also been shown that at high density H_2O and O_2 will be contributing to the cooling, in particular the contribution of H_2O is large (Goldsmith and Langer 1978). Our abundance calculations of H_2O and O_2 presented in the Figures 2.4 (a) and (b) show that the abundance of these molecules are smaller by an order of magnitude than those assumed by (Goldsmith and Langer 1978). Therefore again these molecules do not contribute to the cooling as compared to CO molecule and its isotopes.

3.4 Numerical results and discussion

3.4.1 Effect of density and UV radiation on Photo-electron heating

Here we would like to study the variation of photo-electron heating with densities and UV radiation along with the charge U.

Fig.3.1: We have plotted the grain potential U(ev) as well as heating rates as a function of the number density n_H, for two different ultraviolet radiation fields and two abundances: Solar (continuous lines) and depleted (dotted). Apart from many parameters U depends explicitly on two main factors. Firstly, it depends upon the number density (n_e) of electrons in the medium which recombine on the surface of grain to make it negatively charged; $n_e \propto n_H$. Secondly, the rate of photo-electron emission that leaves the grain positively charged. The detail balance between these two processes determines the magnitude of the potential on the surface of grains. With the increase of n_e the recombination increases resulting in a decrease in the positive potential on the surface. This is evident from the figure and it can also be deduced from the equation 3.9. Similarly with the increase of radiation the photo-emission of electrons causes the deficiency of electrons on the grain surface thereby increasing the positive charge on the grain. It is also clear from the same figure that grains are more positively charged for depleted abundance that for solar abundance, n_H remaining the same. Evidently less electrons are available to neutralize

the grain in the case of depleted abundance.

From the same figure the following conclusions(explained in the sequel) may be drawn about the heating efficiency:

(i) The photo-electron heating does not depend as strongly on the ultraviolet radiation as on the number density of hydrogen. In fact the enhancement in χ_F increases U that in turn reduces H(grain) by the factor $(1-U/5.6)^3$. At large densities $n_H > 10^5 cm^{-3}$ the heating is propotional to n_H.

ii) For the low density $n_H < 2x10^4$, an increase in the amount of radiation results in reduced heating while for $n_H > 2x10^4$ the heating increases with increasing radiation. For $n_H > 10^6$ cm^{-3} the heating is directly propotional to χ_F as expected from equation 3.11, also U being substantially reduced.

iii) Although no number density other than that of hydrogen is involved explicitly in the expression 3.11, yet heating depends implicitly upon n_e and through it on the assumed abundance of elements, see equation 2.10.

iv) The variations in the heating for depleted abundance is not significant for the two assumed values of χ_F in the range $10^4 < n_H < 10^5$ cm^{-3}. These conclusions may be explained as follows:

Again, for the low electron density and high radiation the grain becomes highly positively charged, and as a result

the heating is tremendously reduced inspite of the increase in the radiation density, i.e. χ_F = 1 to 10. We can see this from the figure that at $n_H = 10^4$ cm^{-3} and for χ_F = 10.0 the potential U on the grain is $\sim$ 5 ev that makes the threshold limit $\lesssim$ 13 ev for B = 8ev. Therefore only very small fraction of the energy is available for heating. For high density, U is small. Therefore enhancement in the radiation increases the heating and it becomes almost linearly dependent on χ_F for very high density. However in the cloud of interest, $10^4 < n_H < 10^5$ cm^{-3}, the uncertainty in the amount of UV radiation from hot stars (assumed values of χ_F) would not affect the thermal structure significantly.

3.4.2 Effect of Far Infra-red Radiations on Cooling

As mentioned earlier, the aim of this section is to demonstrate that cooling efficiency in the low temperature region, $T_e < 100$K, is greatly modified in the presence of FIR from the nearest associated HII regions. We present here our calculation of the cooling rates of C, C^+, CO and brightness temperature of CO. The calculations have been carried out for the density n_H = 10 to 10^7 cm^{-3} and abundances (denoted by X (element)) ranging between 10^{-6} to 10^{-3}. The grain temperatures considered are T_g = 40 and 60K.

Fig 3.2 : The cooling rates $\Lambda(X)/n(X)$ are plotted against the hydrogen molecule density $n(H_2)$ cm^{-3}. The cooling rates for carbon atoms are shown in Figures 3.2(a) to 3.2(c) at kinetic temperatures 10, 20 and 100 K respectively. At T_e = 10 K (Figure 3.2(a)) the colling rates with FIR from T_g = 40 K are compared with those without FIR. At low temperature and low $n(H_2)$ the cooling is reduced by a factor about 5 in the presence of FIR. This factor increases further with increasing $n(H_2)$. In the regime where photon-trapping becomes important, there is discontinuity in the dash curve. This is due to the fact that after a particular density of H_2 the absorption of radiation takes place instead of the emission from the fine structure transitions of the atom. It may be added that this discontinuity is a special feature of such low temperature as T_e = 10K.

At T_e = 20 K (Fig.3.2(b)) the cooling rates with FIR from T_g = 40 and 60 K are compared with those FIR. At this particular temperature the factor, by which cooling rates in the two cases are reduced, is almost constant over the whole range of density $n(H_2)$. The increase of the grain temperature decreases further the rate of cooling. At T_e = 100 K(Fig.3.2(c)) the effect of FIR is negligibly small. In general, increase in the temperature T_e decreases the effect of FIR.

Fig.3.3: The cooling from carbon ion CII is shown in Figures 3.3(a) & 3.3(b). T_e = 10 K is not considered here, because

collisional rates at this temperature contribute negligibly small due to high splitting of fine structure ~ 92 K. At this low temperature the heating of the medium instead of the cooling will result by the absorption radiation. At T_e = 40 K (Fig.3.3(a)), the effect of various parameters on the cooling is considered. It should be noted here that cooling from carbon ion is largely modified at this temperature as compared with the cooling from other species even at lower temperature, e.g., T_e = 20 K; compare Fig.3.3(a) with 3.2(b) and 3.4(c). The high reduction in the cooling is due to the large level splitting and high rate of induced emission. The increase of kinetic temperature T_e decreases the contribution of the background radiation. At T_e = 100 K (Fig.3.3(b)) the contribution of FIR is again small.

Fig.3.4: The reduced cooling rates of various transitions of CO molecule are plotted against $n(H_2)$ in Fig.3.4(a). It is significant that the cooling from higher transitions dominates at high $n(H_2)$ and thus total cooling remains propotional to $n(H_2)$ long after the lower levels are thermalized. From the same figure it can be seen that the cooling from the lower transitions are affected more in the presence of FIR at low $n(H_2)$ than at high molecular hydrogen density. For higher transitions the situation is quite reversed because of high induced rates. On the other hand,

for higher transitions and low $n(H_2)$ the cooling is enhanced in the presence of FIR by several factors. As $n(H_2)$ increases, the cooling with and without FIR approaches the same value. With further increase in $n(H_2)$ for the same transitions the cooling with FIR reduces by several factors. Moreover, it can also be inferred that cooling with FIR from higher levels having high transition rates is much affected as compared with that from lower levels.

The total cooling (summed over all transitions) at low $n(H_2)$ predominantly from the lower transitions while at high density it is mainly due to the higher transitions. Therefore the total cooling from CO molecule is less affected at low $n(H_2)$ in the presence of FIR field as compared to that at high density where it is reduced by several factors (see Figs.3.4(b)to 3.4(d)).

It can be seen from Figures 3.4(b) to 3.4(d) that there exist a low hydrogen density regime in which the to cooling per coolant $\Lambda(CO)/n(CO)$ is independent of abundance and is propotional to $n(H_2)$, whereas in the high density region the cooling $\Lambda(CO)/n(CO)$ is propotional to abundance. In the case of molecules also, the cooling rate with FIR is much affected at low temperature 10 and 20 K (Figs.3.4(b) & 3.4(c)), and the FIR effect is negligibly small at T_e = 100 K (Fig.3.4(d)).

Figure 3.5 illustrates $n(H_2)$ versus the calculated ratio of the brightness temperature T_B of $2 \longrightarrow 1$ and $1 \longrightarrow 0$ lines of ^{12}CO for the velocity gradient $\frac{dv}{dr}$ = 10 km Sec^{-1} Pc^{-1}, kinetic

temperature T_e= 20, 100 K and T_g = 60 K. This ratio increases with density and becomes greater than 1 for T_e = 100K in the range of hydrogen density 10^3 — 10^5 cm^{-3}. This increase is because the 2 → 1 transition is thermalized at lower density as compared to the 1→ 0 transition, as a result of enhanced collision rate coefficient for J = 2→ 0 transition. Further it is seen from the same figure that ratio with FIR is larger (or smaller) than that without FIR for lower (or higher) $n(H_2)$. This is due to the reason that as we move towards the higher transitions the cooling reduces in the presence of FIR for high density of $n(H_2)$.

It may be reiterated that the cooling due to the fine-structure transitions of atom and ions of carbon, of other heavy elements and also due to rotational transitions of CO molecule and its isotopes are greatly modified in the presence of FIR from the dust in the adjacent HII regions. Therefore in the future, infra-red spectroscopy offers exciting prospects for direct and correct measurement of the abundance of the principal coolants.

3.4.3 Relative importance of various heating and cooling mechanisms and temperature distribution:

The thermal balance equation,

$$H(n_X(Z), T_e(Z)) = \Lambda(n_X(Z), T_e(Z)) \qquad 3.30$$

is solved numerically in a self-consistent way till convergence

is achieved. The thermal structure of the cloud depends, of course, on some parameters involved in the various heating and cooling mechanisms, as we have discussed in the previous sections. The results of the calculations are summarised in Figures 3.6(a) to 3.8. The heating and cooling rates are plotted on Figures 3.6(a) and 3.7(a) for A_0 and on 3.6(b) and 3.7(b) for A_D. The temperature distribution inside the cloud is given in Figure 3.8 for the two different abundances assumed here, for $\chi_F = 1.0$ and also for the UV background radiation field of Habing (1968).

The relative importance of the different physical processes depends upon the assumed abundances as seen from Figures 3.6(a) to 3.7(b). In the case of depleted abundance (Fig.3.7(a)) the contribution of the photo-electron heating from the dust grain increases initially upto a depth of 0.05 pc, then decreases because of the attenuation of UV radiation by dust itself, and becomes insignificant after a depth of about 0.3 pc. In the region <0.05 pc the presence of a high positive charge on the grain, caused by the high flux of radiation at the exposed surface and low electron density because of depletion, is responsible for the reduction in the heating. The heating in this region is mainly by the H_2 formation on the grain which remains significant throughout the cloud. The photo-ionisation of heavy elements, especially

that of carbon, contributes only to 10% of the total heating near 0.3 pc and is negligible before and after this depth.

In deeper layers of the cloud after 0.3 pc the heating is due to chemical reactions, H_2 formation on the grain, cosmic ray ionisation of H_2 and gravitational collapse. The last process is contributing negligibly while cosmic ray ionisation becomes dominant followed by chemical reactions which in turn is mainly due to the reaction $O+OH \rightarrow O_2 + H + h\nu$, O itself being produced mainly by photo-dissociation of O_2 in the interior of the cloud. It may be added that although sufficient energy is deposited through photo-dissociation of H_2 in the outer region as compared to various heating mechanism, yet its contribution to the total heating is very small at all depths of the cloud.

Figure 3.6(a) shows the different heating mechanisms for solar abundance. The nature of the various mechanisms remains almost the same as for A_D. A significant difference occurs in the outer region of the cloud where the cooling is only due to the photo-electron emission from the grain and at the intermediate depths ($0.25 < Z < .5$ pc) the cloud is heated almost solely by the photo-ionisation of heavy elements, especially that of carbon. In the deeper layers of the cloud cosmic ray ionisation of H_2 is the dominant process followed by the chemical reactions and H_2 formation as before. The contribution

to the heating due to gravitational collapse and photo-dissociation of H_2 over the whole region is negligibly small.

The carbon (IP = 11.256ev) and other heavy elements (IP $<$ 13.6 ev) are in ionised form in the region adjacent to HII because of the high ultraviolet flux from the central star of HII region while oxygen with IP = 13.614 ev is neutral. Therefore the cooling in the outer region (adjacent to HII) is due to the fine structure transitions of CII, SiII, FeII and OI (see section 3.3.3).

In the case of A_D, the contribution to the cooling due to SiII, FeII and OI is significant only upto the depth of 0.15 pc. Their contribution decreases because of the low temperature, the factor e^{-T_{ij}/T_e} suppresses the cooling. But according to the Figure 3.7(b) the cloud is predominantly cooled by CII upto a depth of 0.25 pc. At the intermediate depth around 0.3 pc, the contribution to the cooling due to neutral carbon is significant, otherwise at depths $<$ or $>$ 0.3 pc its contribution falls.

The $2 \rightarrow 0$ rotational transition of H_2 with level spacing 509 K may also contribute to the cooling at high temperature. It is shown here (Fig.3.7(a) & (b)) for A_D, when temperature is $\gtrsim$ 200 K, H_2 molecules contributes by 10% of the total cooling in a limited region around 0.1 pc. Before the depth $<$ 0.1 pc the contribution is small because of its low abundance and at $>$ 0.1 pc the cooling is suppressed by the Boltzman factor.

The cooling beyond 0.3 pc is mainly due to rotational excitation of ^{12}CO and to a less extent of ^{13}CO by collision with H_2, because of high abundance and low excitation temperature of CO molecule as compared to CI CII. In deeper regions of the cloud the ratio of the cooling rates $\Lambda(^{12}CO)/\Lambda(^{13}CO)$ is about 3.5 which is much lower than the adopted isotopic abundance of 40. This shows that photon trapping is important and opacity of high abundant molecule causes relatively less cooling than that due to the relatively low abundant molecule.

A comparison of the cooling rates for solar and depleted abundance (see Figs.3.7(a) and 3.7(b)) shows that the cooling from SiII, FeII and OI is dominant over others upto $Z \lesssim 0.2$pc for solar abundance in contrast to depleted one. However, at $Z \simeq 0.2 - 0.27$ pc the main contribution to the total cooling due to C ion occurs, while at larger depth its contribution falls. Neutral carbon is also contributing in the neighbourhood of this region and its cooling decreases while remaining significant upto a depth of 0.5 pc. Beyond 0.27 pc, ^{12}CO is the main coolant again for solar abundance and its isotope ^{13}CO contributes about 25% to the total cooling. The contribution of H_2 is negligibly small for $A_\odot$ because of the low temperature, $T_e < 150K$, that causes an exponential reduction by the factor e^{-509/T_e}.

The present calculation is an attempt to show that in the neighbourhood of HII region the electron temperature T_e is not constant over the whole region as assumed by Dupree (1974), Hoang-Binh & Walmsley (1974), Rickard et al.(1977) and Pankonin et al.(1977) but it is position-dependent inside the cloud. The temperature distribution for the cool and partially ionised hydrogen medium is shown in Figure 3.8 for $n_H = 10^4$ cm^{-3} as a function of cloud depth. Comparisons are made between the two assumed elemental abundances for ultraviolet background radiation from the nearest hot stars and radiation flux of Hobing (1968). The effect of far infra-red radiation from the dust grain at $T_g = 60$ K is also shown.

The following conclusions may be drawn from Figure 3.8 and be explained as follows:

i) The temperature at the exposed surface of the cloud (adjacent to HII region) are very much different for A_D and $A_\odot$ and hig as compared to those obtained from UV field of Habing (1968). The temperature variation for A_D is $\backsim$ 265 K to $\backsim$ 11 K, whereas for solar abundance it lies between $\backsim$ 140 K to $\backsim$ 10 K, when the high flux of radiation (equation 2.2) is used. The difference between the temperatures for two UV fields plotted here, in Figure 3.8 occurs evidently due to the difference in the amount of heating by the photo-electron emission from the surface of dust grains that dominates at the exposed surface. Although

less heating results for A_D than that for $A_\odot$, (see Fig.3.6(a) and 3.6(b)), yet the temperature derived for A_D is high due to the diminished cooling rates by an order of magnitude; the main coolant CII and other heavy elements being depleted. In the case of $A_\odot$ the cooling arises due to the fine structure transitions of highly abundant OI, SiII and FeII (see Fig.3.7(a)) thereby effectively decreasing the temperature.

ii) The temperatures for the two radiation fields considered here merge to the same value for respective abundances in the interior region of the cloud. This is due to the fact that the heating in the interior part of the cloud is independent of the radiation field (see Figs.3.6(a) and 3.6(b)).

iii) The temperature for A_D falls rapidly and become less than that for $A_\odot$ in the depth $0.2 < Z < 0.5$ pc. As a matter of fact in this range the cloud is predominantly heated by Photo-ionisation of heavy elements, other than carbon for the case of $A_\odot$. This high abundance increases the heating rate by an order of magnitude as compared to that for A_D. The cooling in this range is either due to neutral carbon or its ion and molecule. These species are not depleted by a factor > 3. Thus cooling for $A_\odot$ can be more at the most by a factor of 3. Therefore thermal balance gives a high temperature for $A_\odot$ in this range.

iv) In the deeper region of the cloud the temperature for A_D is $\sim$ 11 K, again a slightly greater value than $\sim$ 10 K for A_Θ. This can also be understood in terms of cooling and heating rates. The interior part of the cloud is predominantly heated by the cosmic ray ionisation of H_2, also significantly by H_2 formation on the grain and chemical reaction. The first two mechanisms are independent while the third depends on the assumed abundances. Therefore the total heating due to these three mechanisms will be very slightly dependent on the abundances. Here the cooling is due to the CO molecule and its isotope that are depleted by the same factor as the carbon. Although the cooling for the A_D will not be reduced by the factor of depletion because of photon-trapping but it will be slightly greater for A_Θ than that for A_D resulting in a slightly higher temperature for solar abundance.

v) From Figure 3.8 it is also clear that the temperature distribution in the deeper region (where the temperature is quite low) is very much affected by the presence of FIR field. The temperature obtained with the inclusion of FIR is greater by about 3 K, since the cooling is reduced by several factors in the presence of FIR field. This fact is discussed in detail earlier (section 3.4.2) and is also shown in Figures 3.2(a) to 3.4(d).

The temperature distributions in the cool clouds for $n_H = 10^4$ cm^{-3} are also discussed by Pankonin & Walmsley(1976) for solar and depleted abundances of C,O and Si and by Brown et al.(1978) for solar abundance only. The temperature distribution for the two assumed abundances as deduced by Pankonin & Walmsley (1976) are not significantly different from each other in contrast to our calculation as carried out in this work. Besides, these workers have not considered the FeII (26.2 μ) emission and infra-red radiation from dust grains. It may be noted here that for $T_e > 100$ K the transition of FeII $^6D_{9/2} - {}^6D_{7/2}$ (26.2 μ) for $A_\odot$ will also be contributing significantly to the cooling according to our calculation. At low temperature, as discussed earlier (Figure 3.8), the cooling is greatly modified in the presence of FIR field from dust grains.

It should be also emphasised here that temperature at the exposed surface, where carbon is mostly in ionic form, will be increased further with increase of n_H for solar and depleted abundances both. This can be seen from the comparison of the Figures 3.8 and those thermal structure given by Qaiyum and Ansari (1983a).

Table 3.1

Transitions for Cooling

Species	Transitions	Level spacing in term of temperature(K) (Wave length μ)	References for transition rate (A_{ij})	References for collision rates C_{ij}
CI	f.s. $^3P_1 - {}^3P_o$	23.6 (610)	Weise et al. (1966)	H - Launay & Roueff (1977a)
	$^3P_2 - {}^3P_1$	38.9 (369)		$H_2 = \frac{1}{10}$ of H Launay & Roueff (1977a)
OI	f.s. $^3P_o - {}^3P_1$	97.9 (147)	Weise et al. (1966)	e - Breig & Lin (1966) H - Launay & Roueff (1977a)
	$^3P_1 - {}^3P_2$	228 (63)		H_2 — same as for H
CII	f.s. $^2P_{3/2} - {}^2P_{1/2}$	91.3 (156)	Weise et al. (1966)	e - Saraph et al. (1969) H - Launay & Roueff (1977b) H_2 - Flower & Launay (1977)
SiII	f.s. $^2P_{3/2} - {}^2P_{1/2}$	413 (34.8)	Weise et al. (1966)	e - Seaton (1958) H - Penston(1970) H_2 - Same as H

Table 3.1 (Contd.)

Species	Transitions	Level spacing in term of temperature(K) (Wave length μ)	References for transition rate (A_{ij})	References for collision rates C_{ij}
Fe II	f.s. $^6D_{9/2}$ — $^6D_{7/2}$	554 (26.2)	Weise et al. (1966)	e - Seaton (1955) H - Dalgarno & McCray (1972) H_2- same as H
H_2(Ortho)	rotational 2 — 0	509 (28.2)	Goldsmith & Langer(1978)	Goldsmith & Langer (1978)
CO	rotational J — J-1	5.53 J	Gerola & Glassgold(1978)	H - Chu & Dalgarno (1975) H_2- Green & Thaddeus (1976)

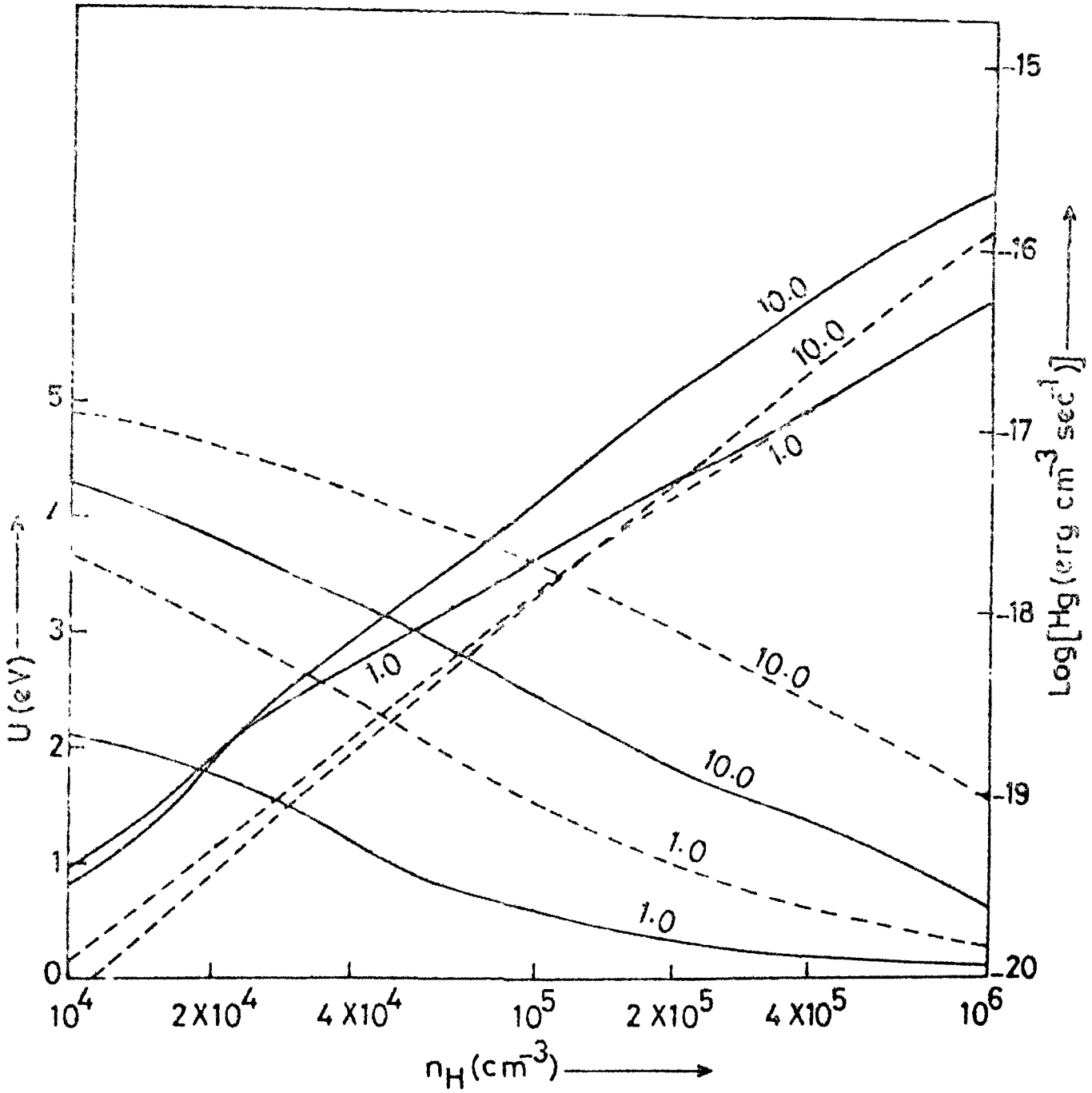
U (eV)
Log[Hg (erg cm^{-3} sec^{-1})]
n_H (cm^{-3})
10.0
10.0
1.0
1.0
10.0
10.0
1.0
1.0
0
1
2
3
5
-15
-16
-17
-18
-19
-20
10^4
$2X10^4$
$4X10^4$
10^5
$2X10^5$
$4X10^5$
10^6

Fig. 3.1

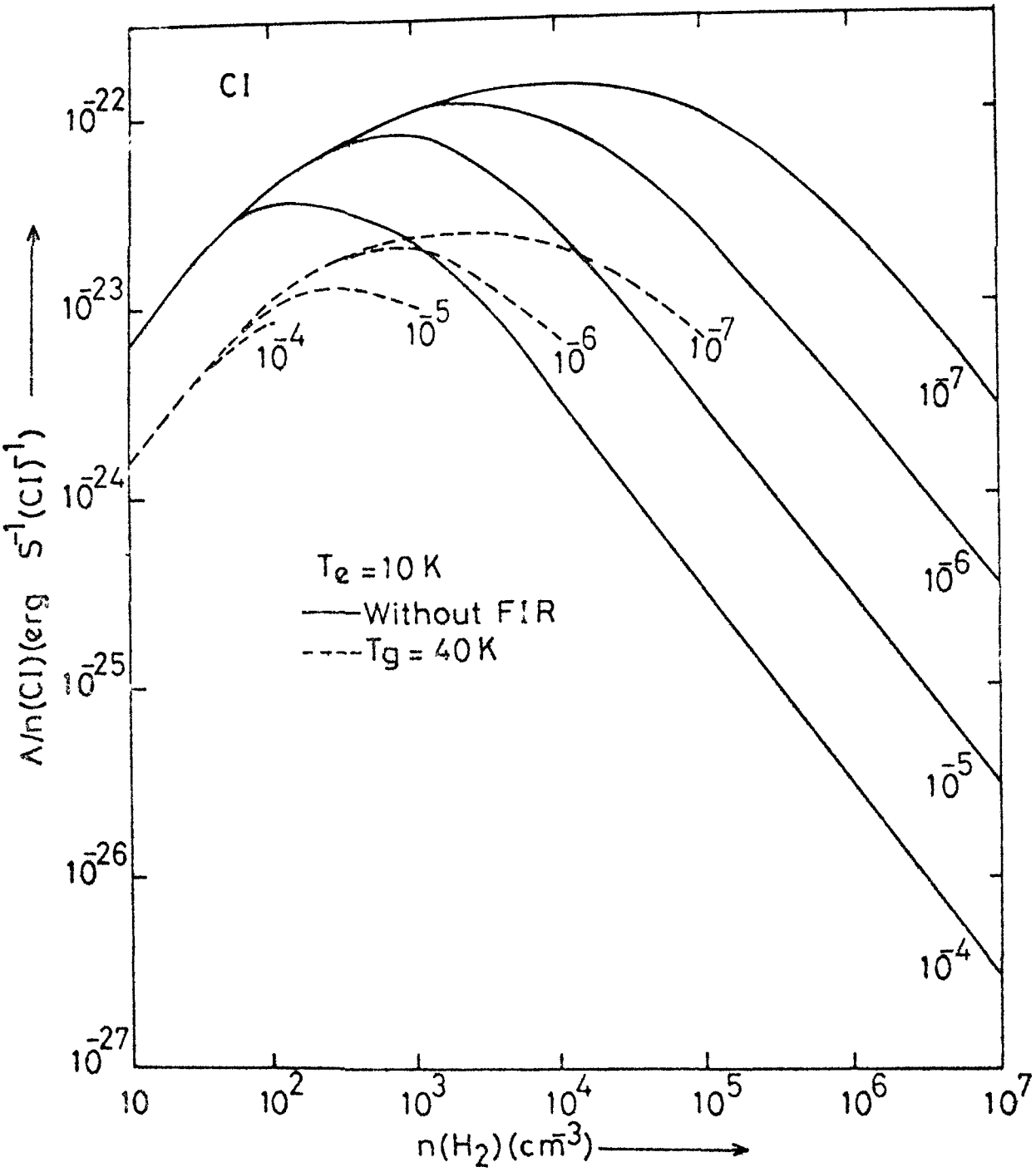
CI
10^{-22}
10^{-23}
10^{-24}
10^{-25}
10^{-26}
10^{-27}
$\Lambda/n(CI)(erg\ S^{-1}(CI)^{-1})$
10^{-4}
10^{-5}
10^{-6}
10^{-7}
$T_e = 10\ K$
——Without FIR
----Tg = 40 K
10^{-7}
10^{-6}
10^{-5}
10^{-4}
10
10^2
10^3
10^4
10^5
10^6
10^7
$n(H_2)(cm^{-3})$

Fig.3.2(a)

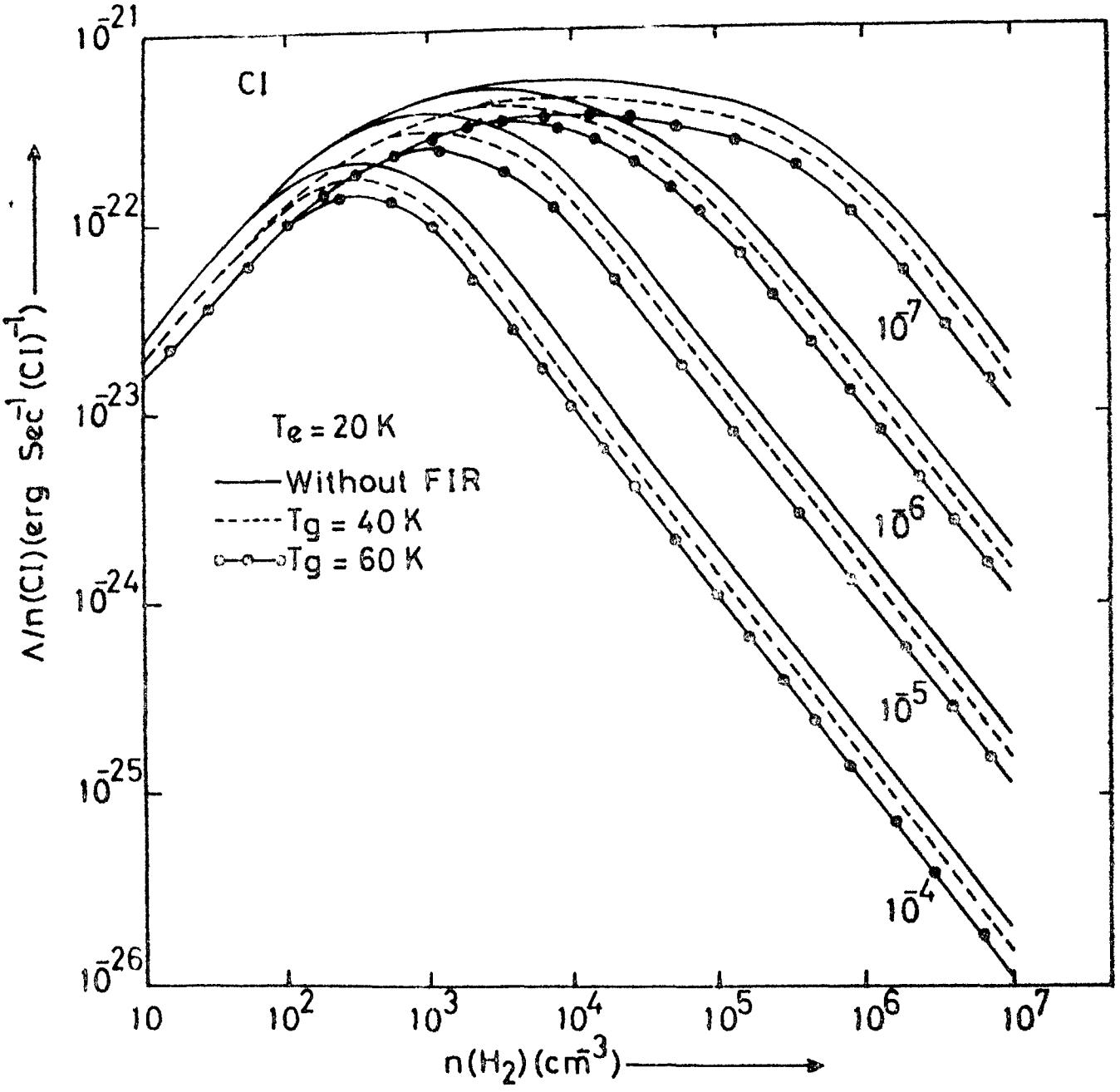
CI
Te = 20 K
Without FIR
Tg = 40 K
Tg = 60 K
10^{-7}
10^{-6}
10^{-5}
10^{-4}
10^{-21}
10^{-22}
10^{-23}
10^{-24}
10^{-25}
10^{-26}
10
10^{2}
10^{3}
10^{4}
10^{5}
10^{6}
10^{7}
$\Lambda/n(CI)(erg\ Sec^{-1}(CI)^{-1})$
$n(H_2)(cm^{-3})$

Fig.3.2(b)

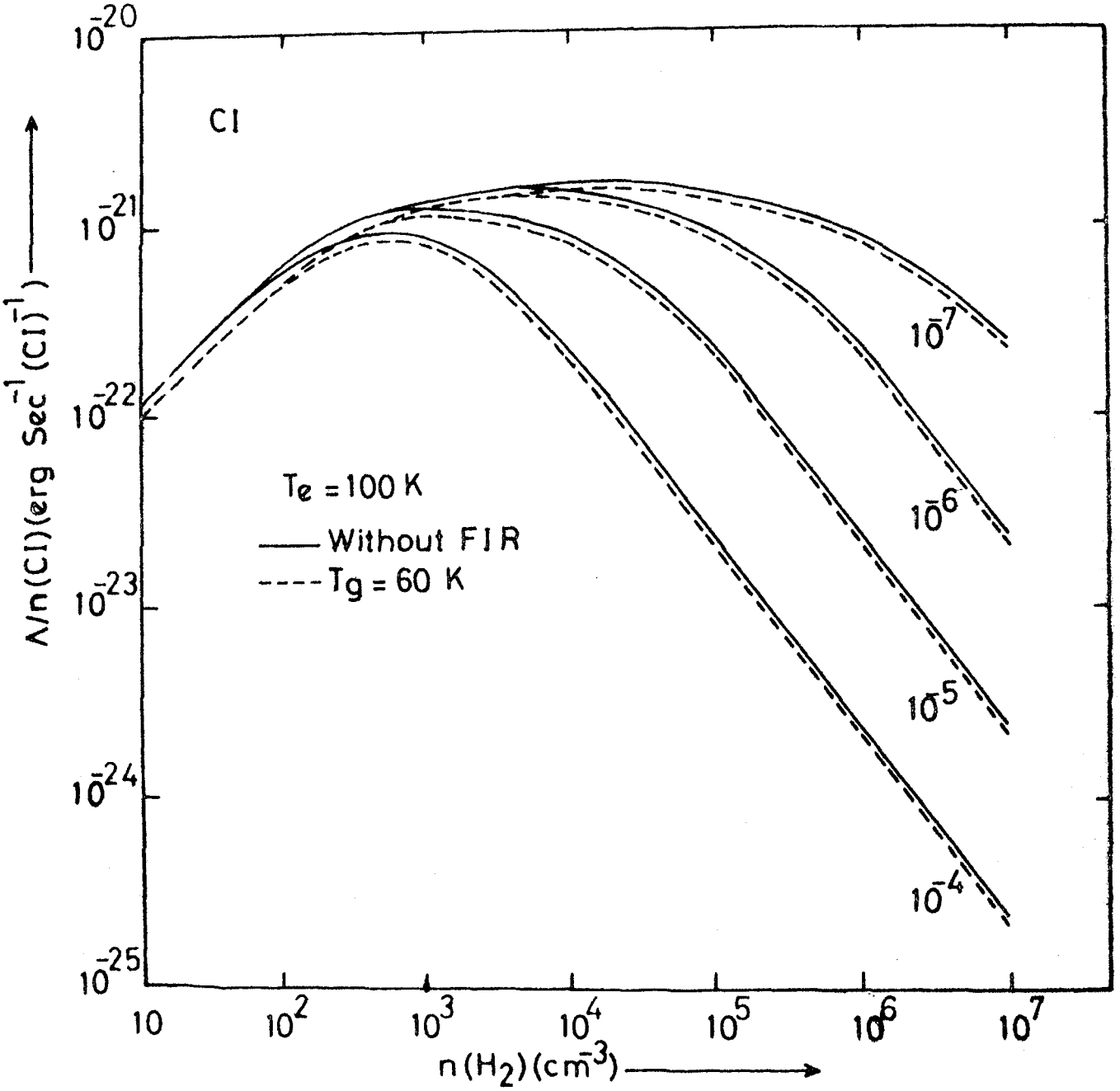
CI
10^{-20}
10^{-21}
10^{-22}
10^{-23}
10^{-24}
10^{-25}
$\Lambda/n(CI)(erg\ Sec^{-1}(CI)^{-1})$
$T_e = 100\ K$
Without FIR
$T_g = 60\ K$
10^{-7}
10^{-6}
10^{-5}
10^{-4}
10
10^2
10^3
10^4
10^5
10^6
10^7
$n(H_2)(cm^{-3})$

Fig. 3.2(c)

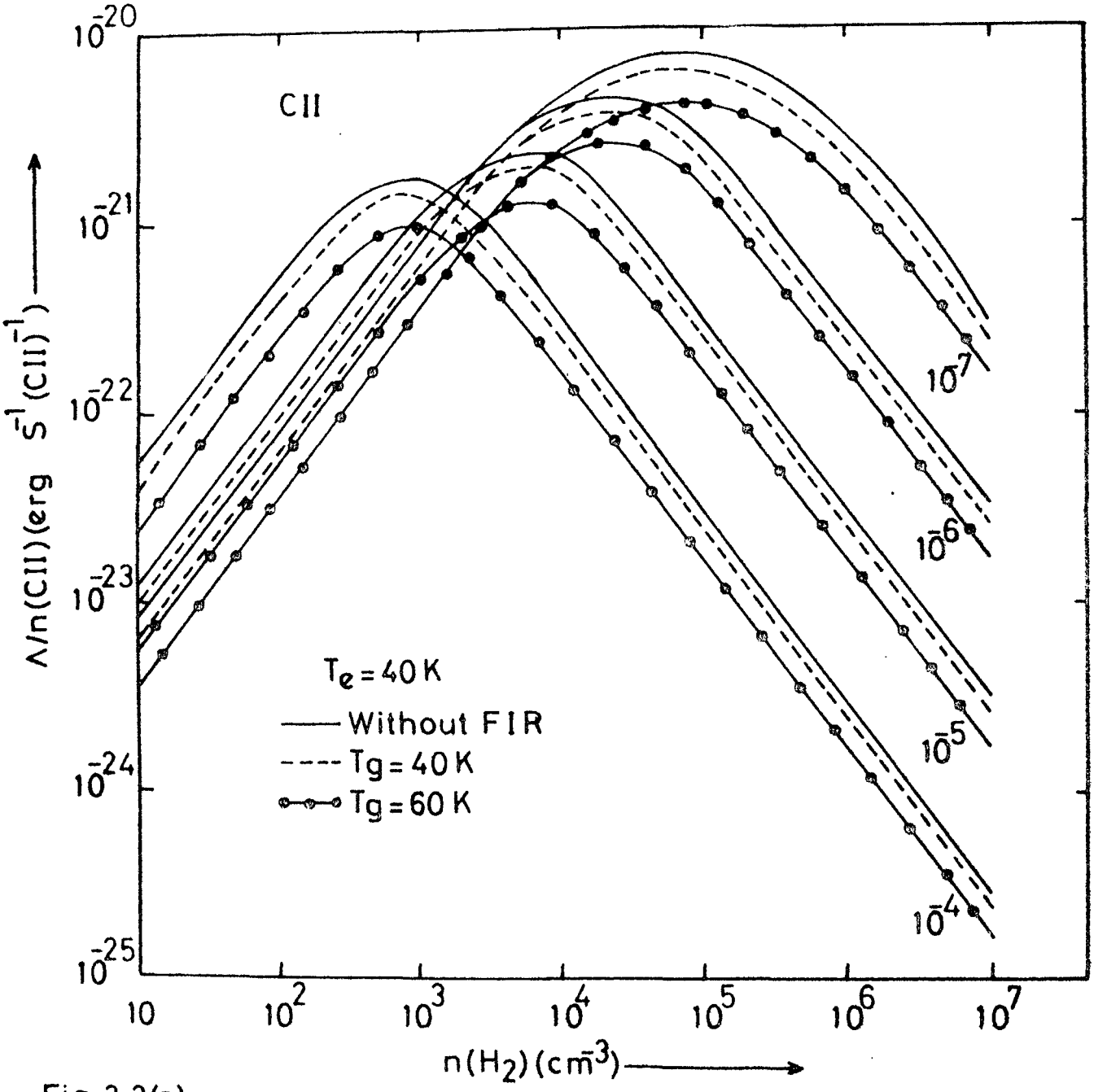
CII
10^{-20}
10^{-21}
10^{-22}
10^{-23}
10^{-24}
10^{-25}
$\Lambda/n(CII)(erg\ s^{-1}(CII)^{-1})$
$T_e = 40\,K$
Without FIR
Tg = 40 K
Tg = 60 K
10^{-7}
10^{-6}
10^{-5}
10^{-4}
10
10^2
10^3
10^4
10^5
10^6
10^7
$n(H_2)(cm^{-3})$

Fig.3.3(a)

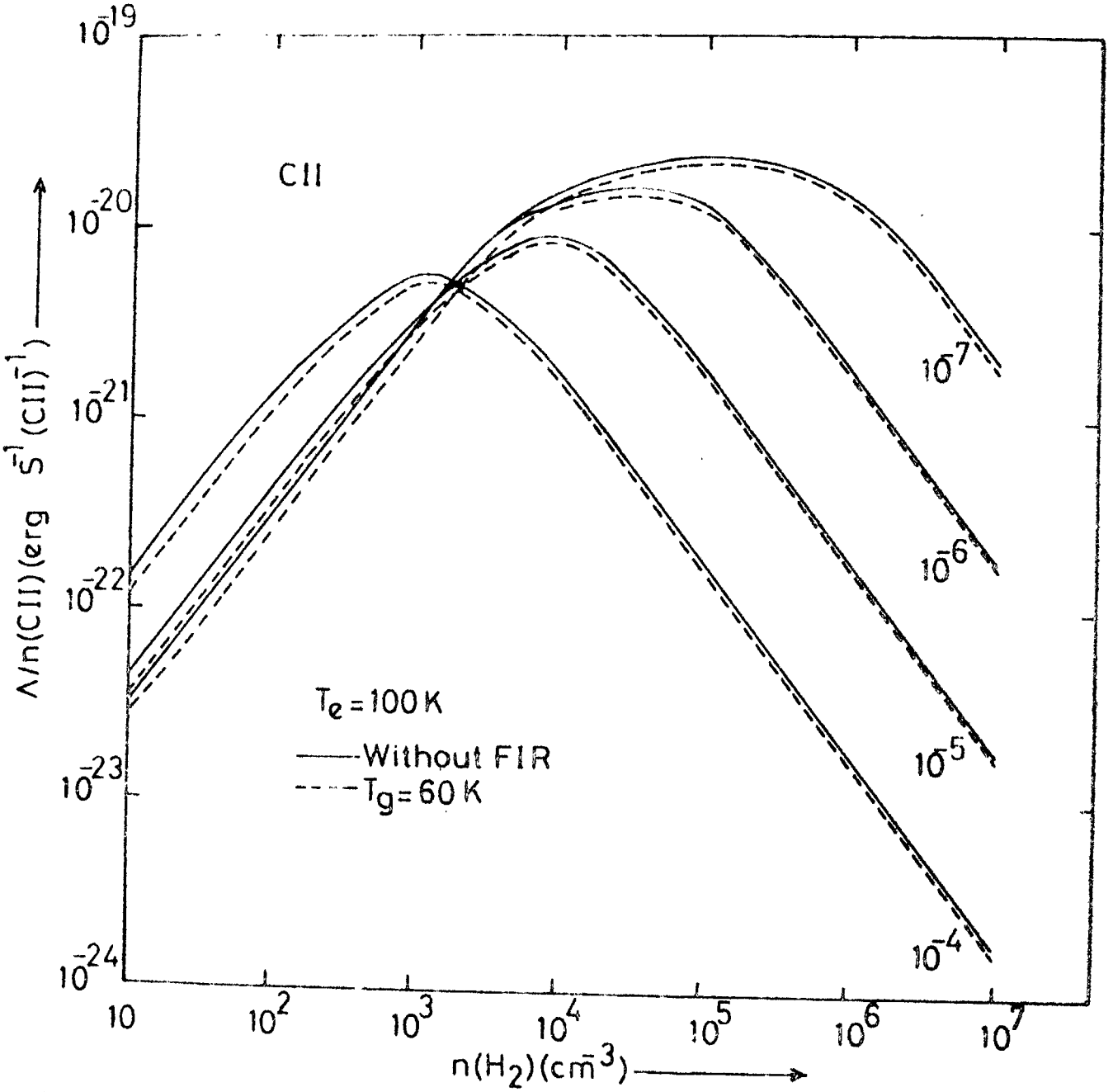
CII
10^{-19}
10^{-20}
10^{-21}
10^{-22}
10^{-23}
10^{-24}
$\Lambda/n(CII)(erg\ s^{-1}(CII)^{-1})$
$T_e = 100\,K$
——Without FIR
- - - $T_g = 60\,K$
10^{-7}
10^{-6}
10^{-5}
10^{-4}
10
10^2
10^3
10^4
10^5
10^6
10^7
$n(H_2)(cm^{-3})$

Fig 3 3(b)

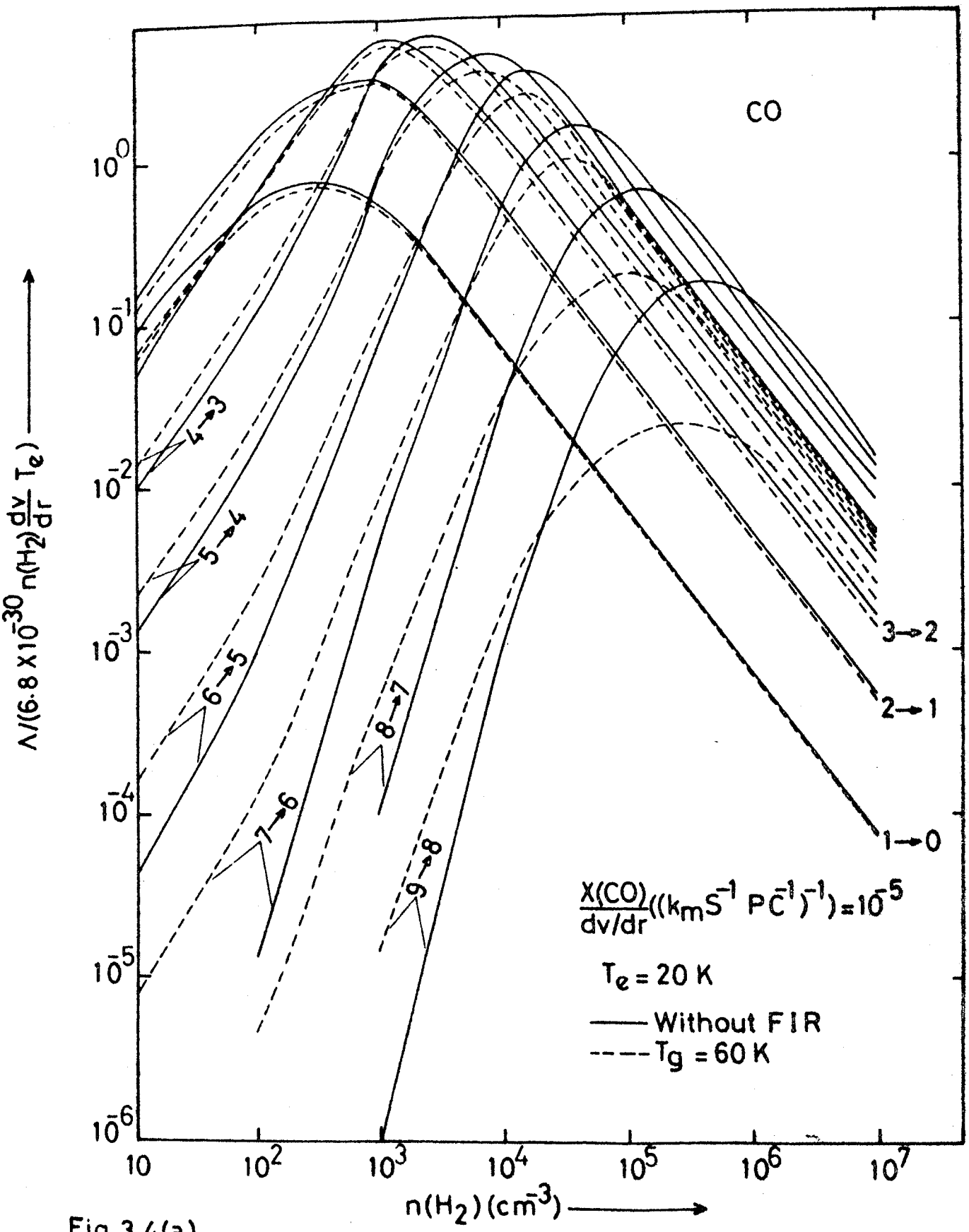
CO
10^0
10^{-1}
10^{-2}
10^{-3}
10^{-4}
10^{-5}
10^{-6}
$\Lambda/(6.8 \times 10^{-30} n(H_2) \frac{dv}{dr} T_e)$ ⟶
4→3
5→4
6→5
7→6
8→7
9→8
3→2
2→1
1→0
$\frac{X(CO)}{dv/dr}((k_m S^{-1} P\bar{C}^{1})^{-1}) = 10^{-5}$
$T_e = 20$ K
—— Without FIR
---- $T_g = 60$ K
10
10^2
10^3
10^4
10^5
10^6
10^7
$n(H_2)(cm^{-3})$ ⟶

Fig. 3.4(a)

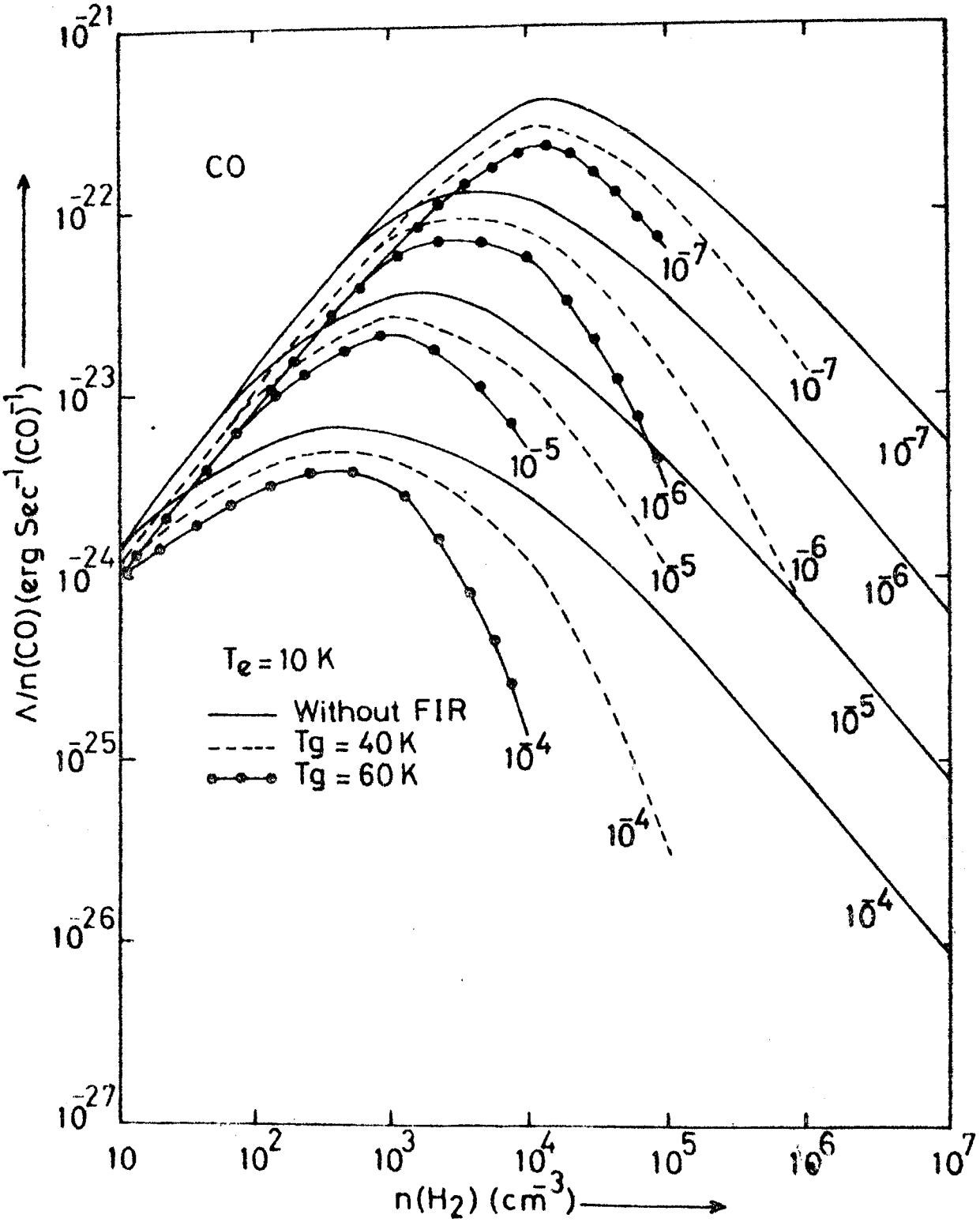
CO
$T_e = 10$ K
Without FIR
Tg = 40 K
Tg = 60 K
10^{-7}
10^{-7}
10^{-7}
10^{-5}
10^{-6}
10^{-5}
10^{-6}
10^{-6}
10^{-5}
10^{-4}
10^{-4}
10^{-4}
10^{-21}
10^{-22}
10^{-23}
10^{-24}
10^{-25}
10^{-26}
10^{-27}
$\Lambda/n(CO)$ (erg $Sec^{-1}(CO)^{-1}$)
10
10^2
10^3
10^4
10^5
10^6
10^7
$n(H_2)$ (cm^{-3})

Fig.3.4(b)

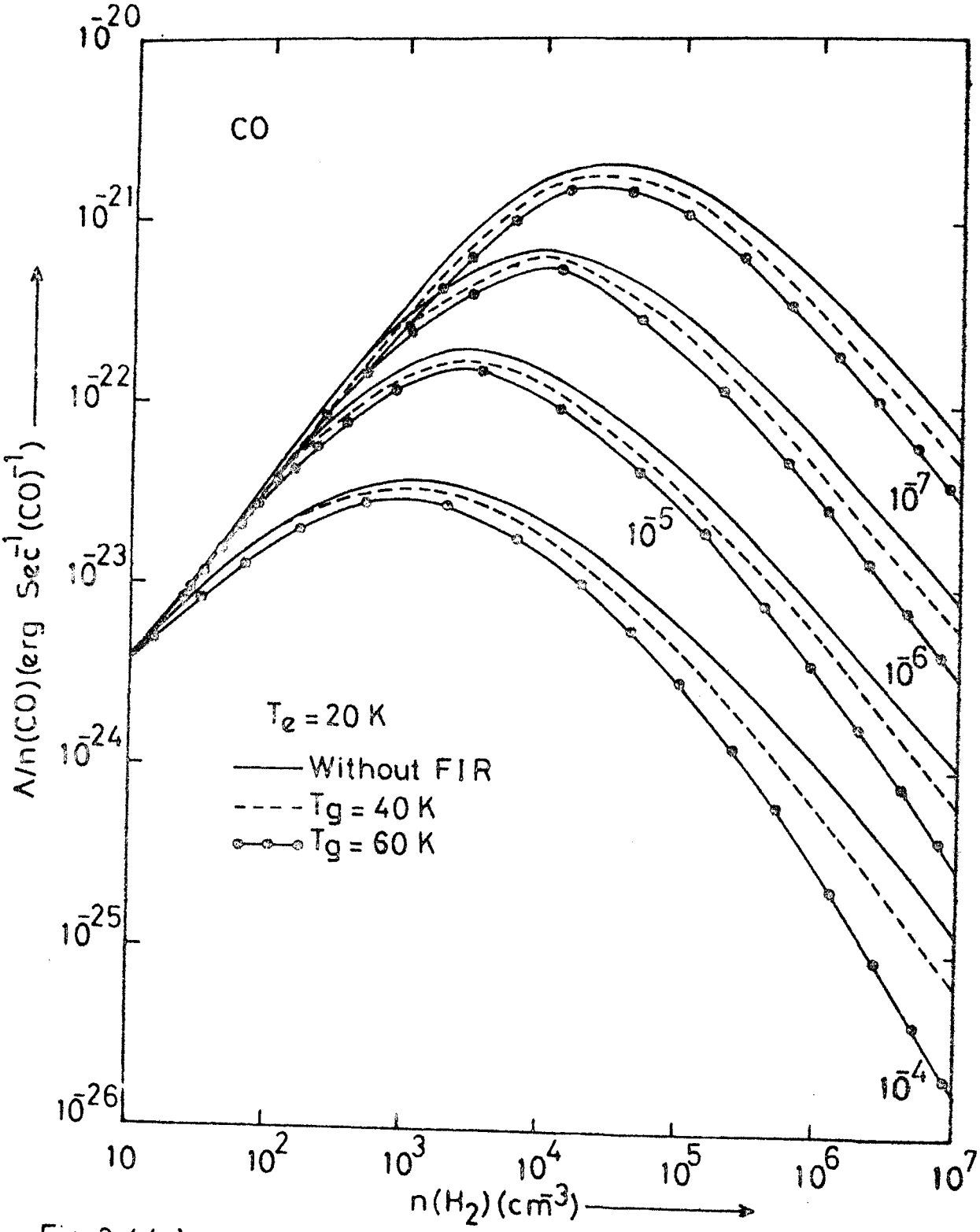
CO
10^{-20}
10^{-21}
10^{-22}
10^{-23}
10^{-24}
10^{-25}
10^{-26}
$\Lambda/n(CO)$(erg $Sec^{-1}(CO)^{-1}$)
10^{-7}
10^{-5}
10^{-6}
10^{-4}
T_e = 20 K
Without FIR
Tg = 40 K
Tg = 60 K
10
10^2
10^3
10^4
10^5
10^6
10^7
$n(H_2)(cm^{-3})$

Fig. 3.4 (c)

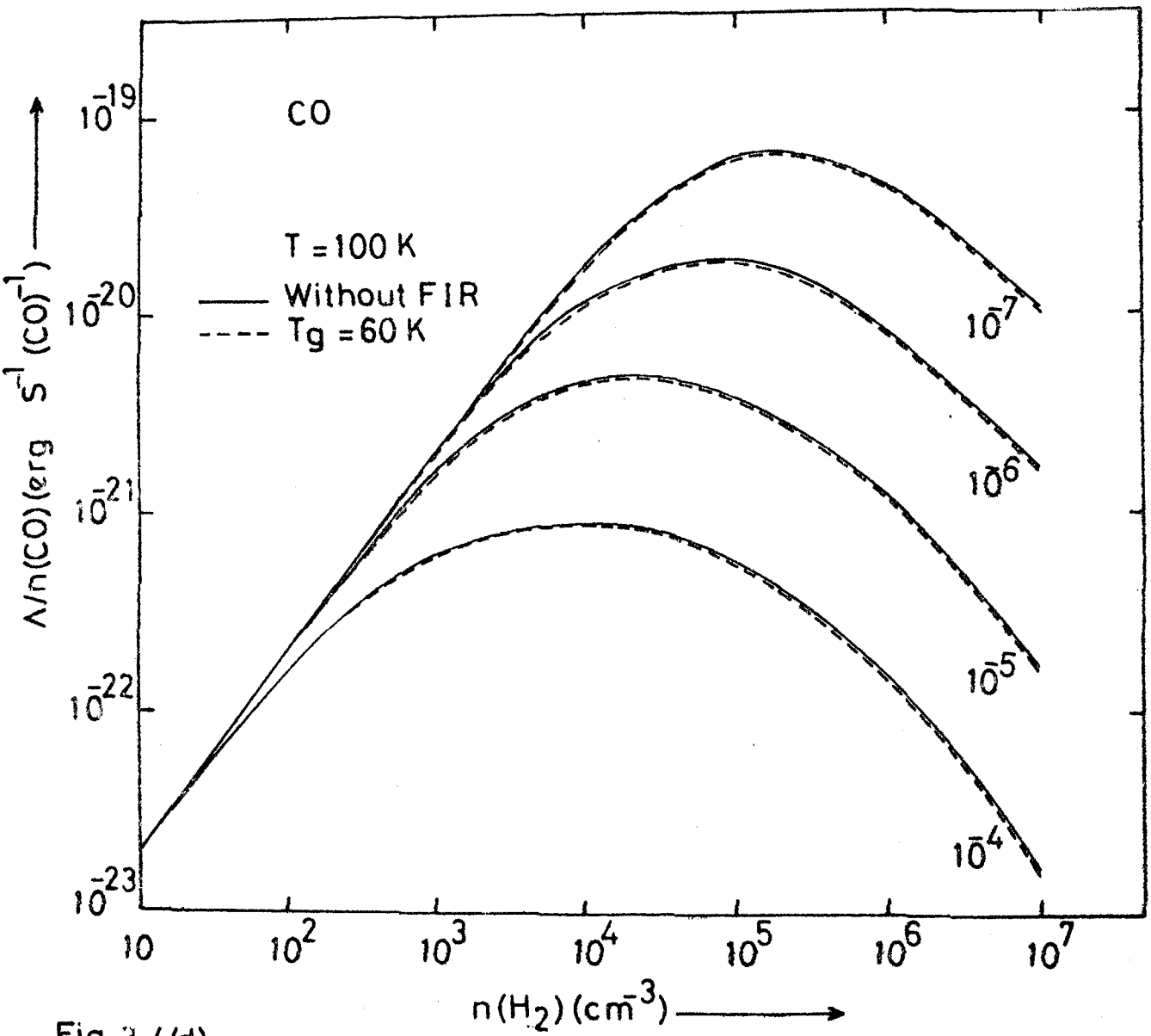
CO
T = 100 K
Without FIR
Tg = 60 K
10^{-7}
10^{-6}
10^{-5}
10^{-4}
10^{-19}
10^{-20}
10^{-21}
10^{-22}
10^{-23}
$\Lambda/n(CO)$ (erg s^{-1} $(CO)^{-1}$)
10
10^2
10^3
10^4
10^5
10^6
10^7
$n(H_2)$ (cm^{-3})

Fig. 3.4(d)

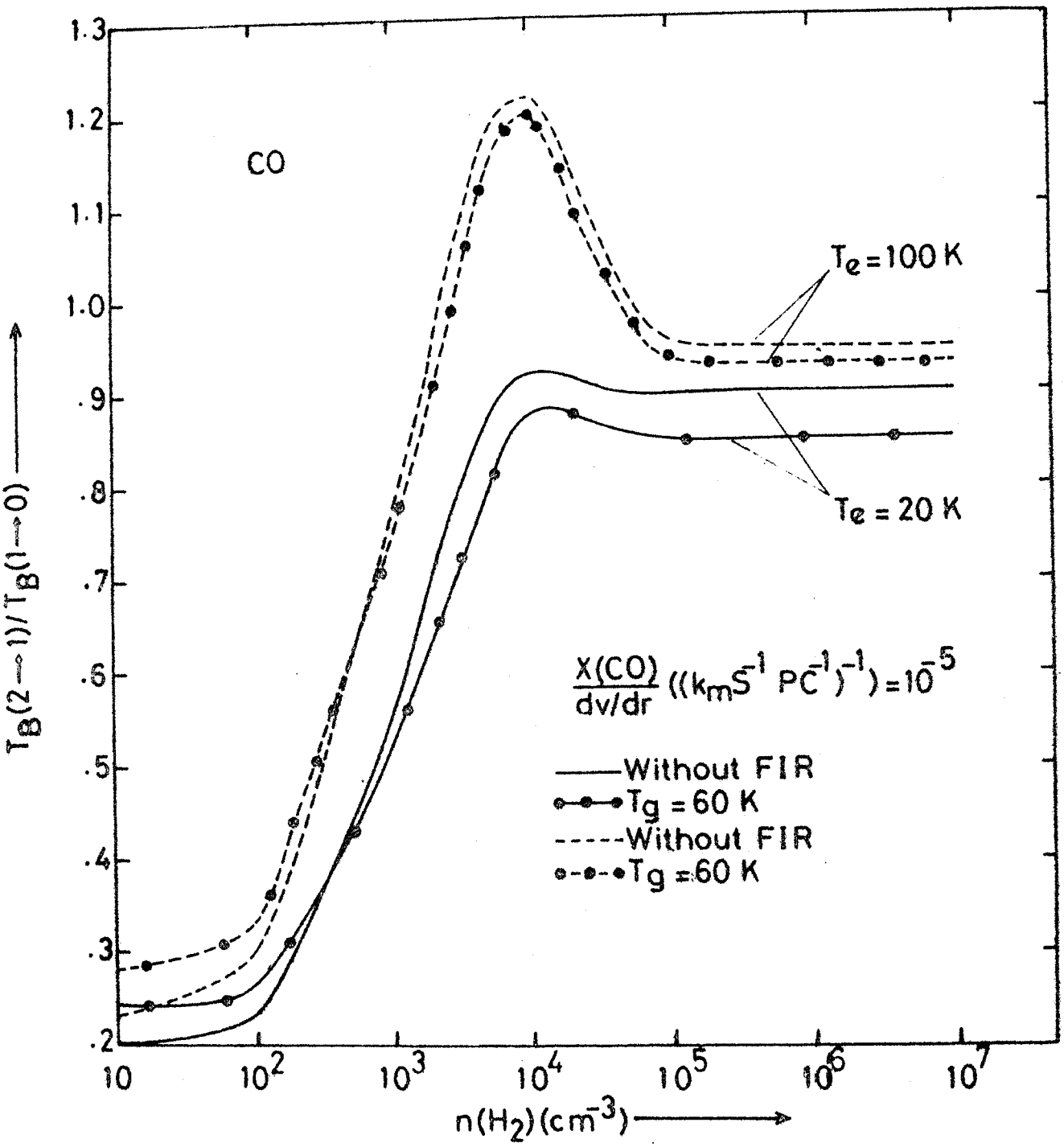
CO
T_e = 100 K
T_e = 20 K
$\frac{X(CO)}{dv/dr}((k_m S^{-1} PC^{-1})^{-1}) = 10^{-5}$
Without FIR
T_g = 60 K
Without FIR
T_g = 60 K
$T_B(2\rightarrow1)/T_B(1\rightarrow0)$
$n(H_2)(cm^{-3})$
1.3
1.2
1.1
1.0
.9
.8
.7
.6
.5
.4
.3
.2
10
10^2
10^3
10^4
10^5
10^6
10^7

Fig.3.5

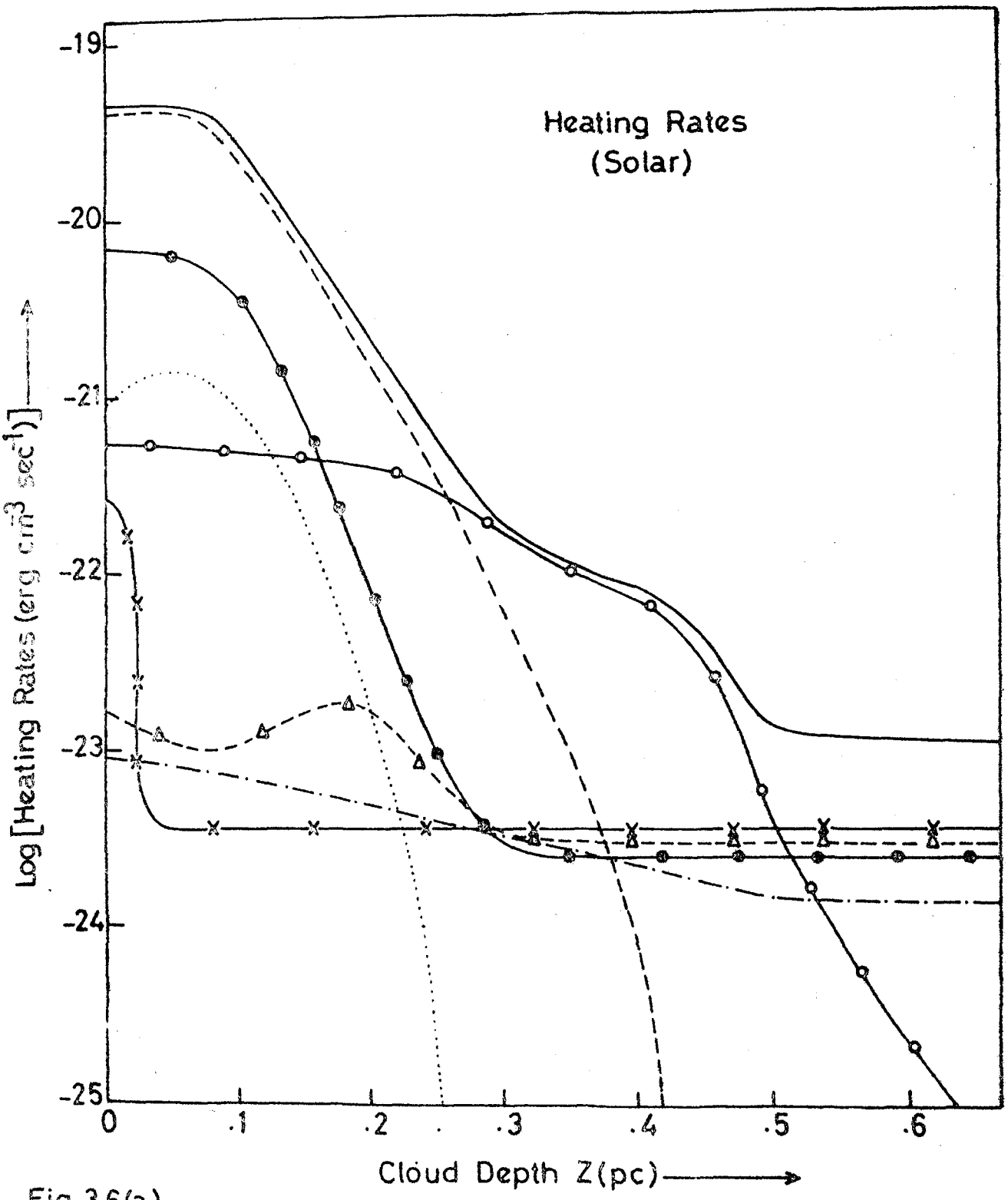
Heating Rates
(Solar)
-19
-20
-21
-22
-23
-24
-25
0
.1
.2
.3
.4
.5
.6
Log [Heating Rates (erg cm^{-3} sec^{-1})]
Cloud Depth Z(pc)

Fig.3.6(a)

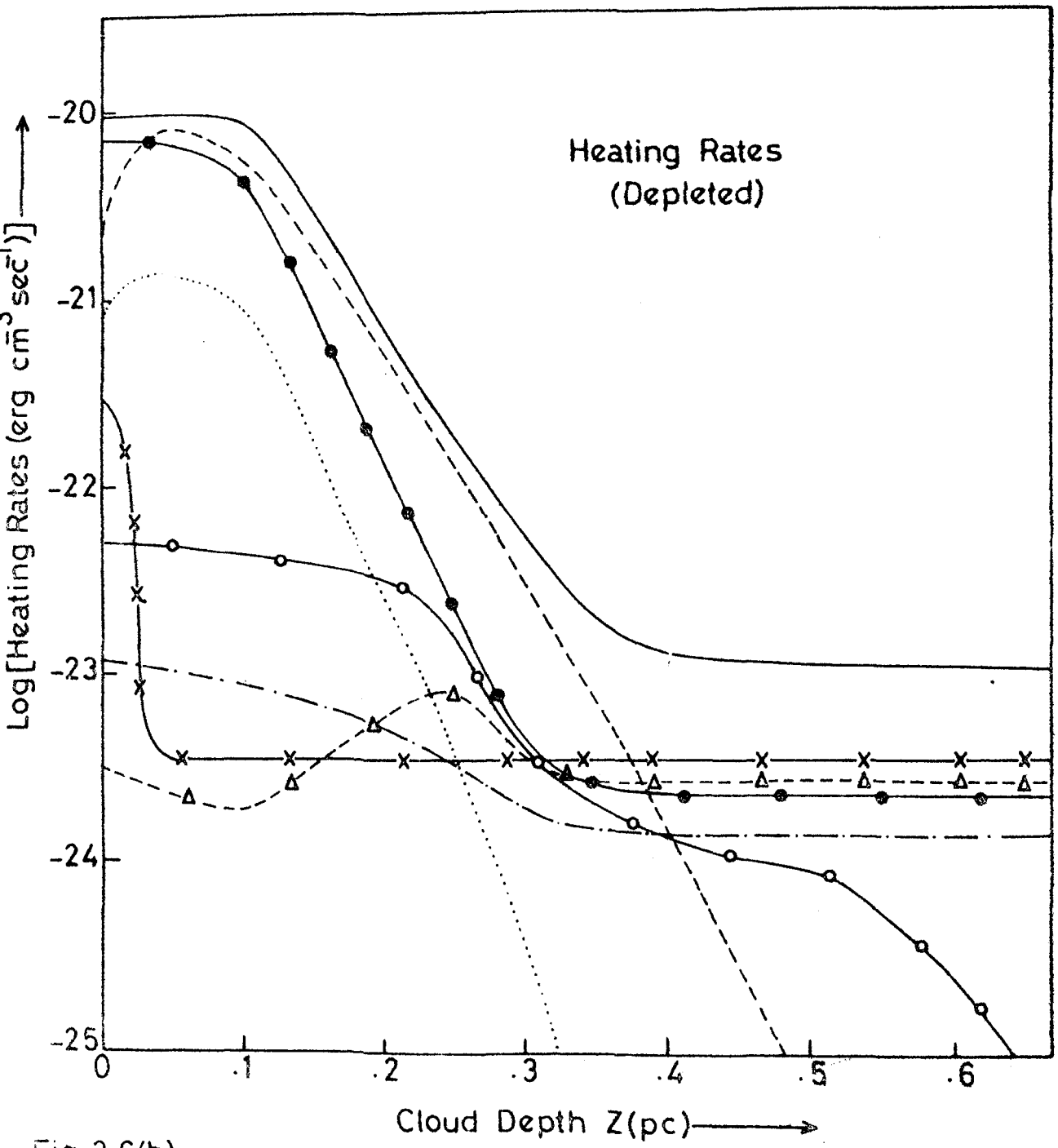
Heating Rates
(Depleted)
Log[Heating Rates (erg cm^{-3} sec^{-1})]
-20
-21
-22
-23
-24
-25
0
.1
.2
.3
.4
.5
.6
Cloud Depth Z(pc)

Fig.3·6(b)

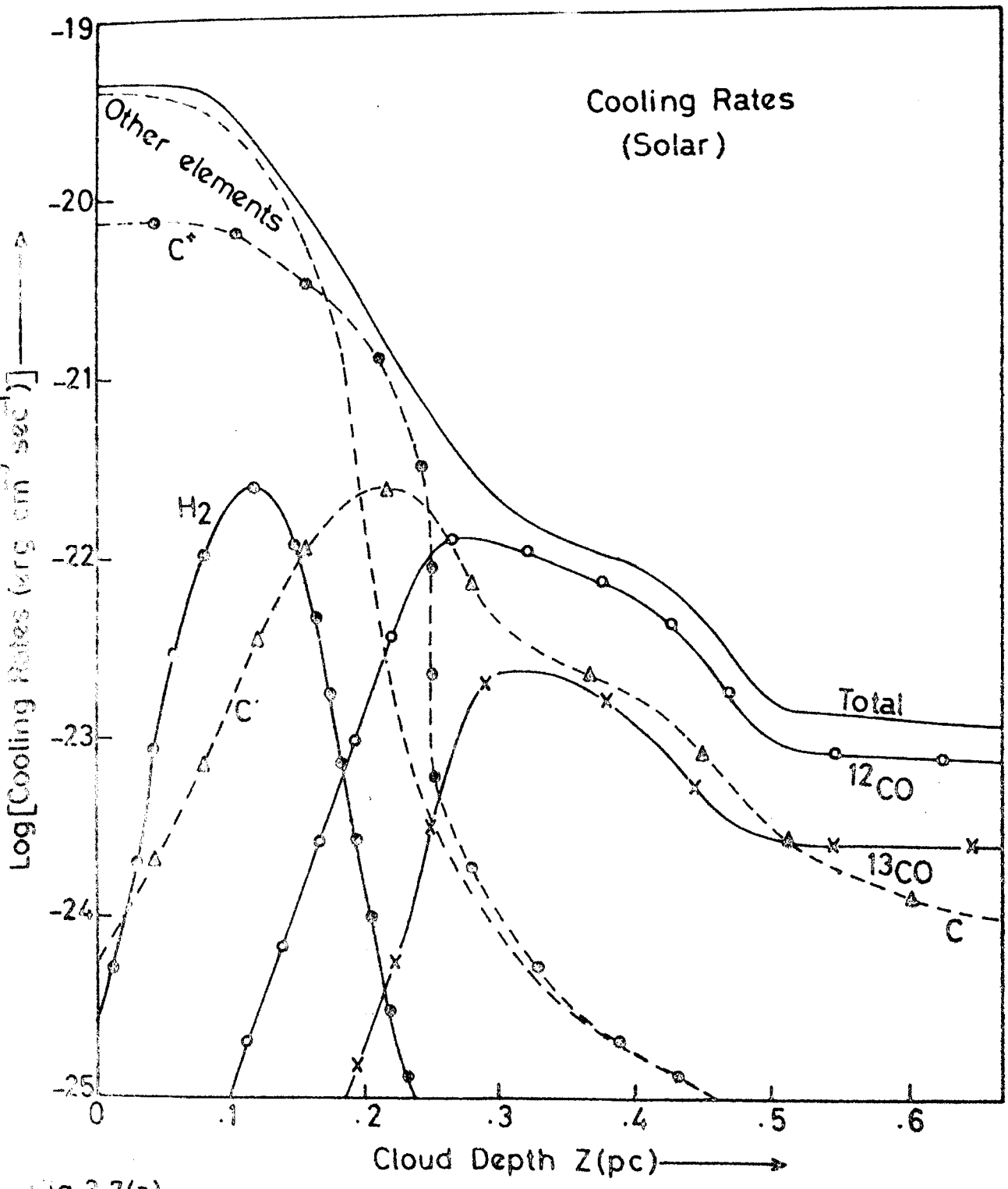
Cooling Rates
(Solar)
Other elements
C+
H2
C
Total
12CO
13CO
C
-19
-20
-21
-22
-23
-24
-25
0
.1
.2
.3
.4
.5
.6
Log [Cooling Rates (ergs cm-3 sec-1)]
Cloud Depth Z(pc)

Fig.3.7(a)

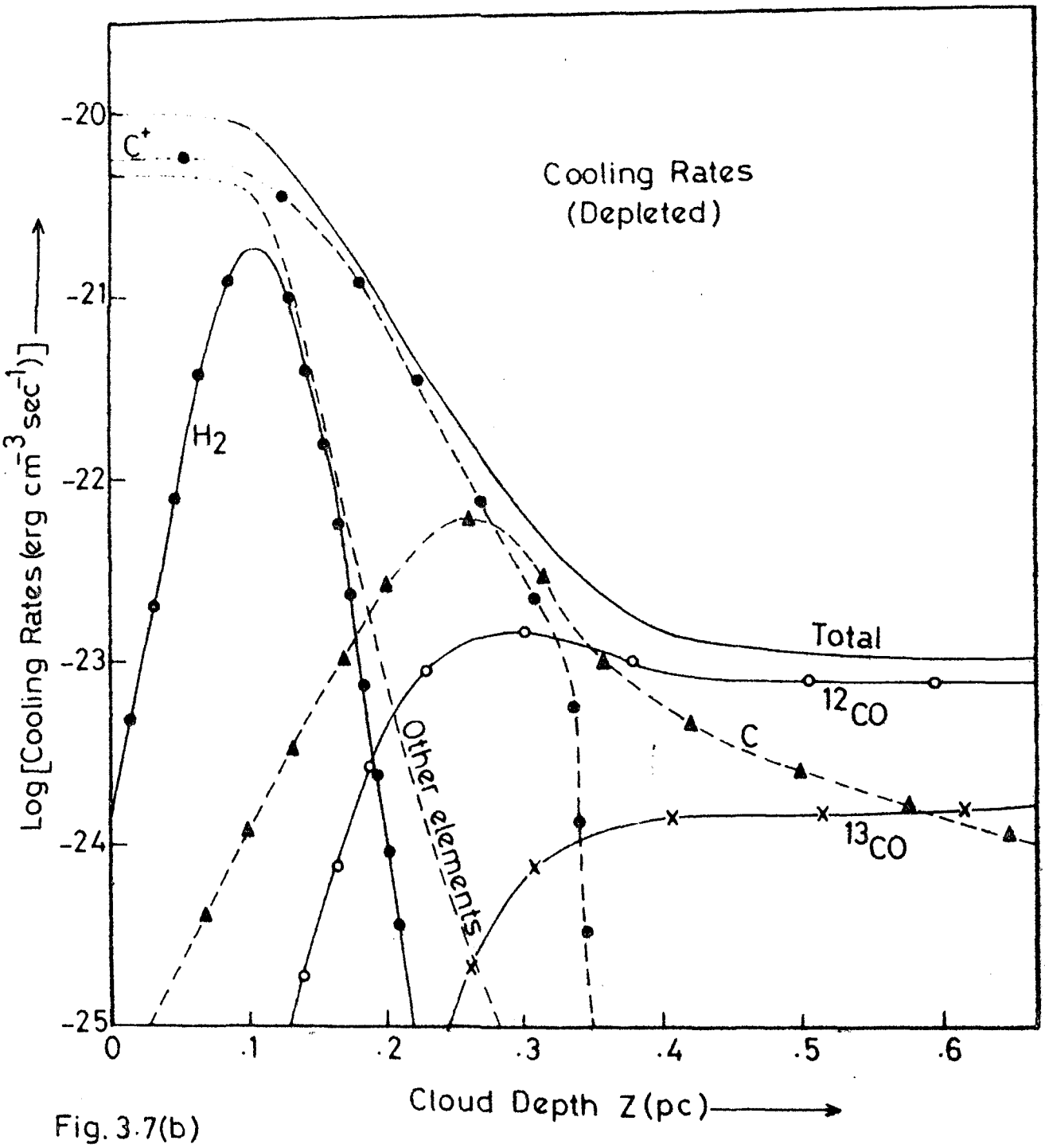
Cooling Rates
(Depleted)
C+
H2
Total
12CO
C
13CO
Other elements
-20
-21
-22
-23
-24
-25
0
.1
.2
.3
.4
.5
.6
Log [Cooling Rates (erg cm-3 sec-1)]
Cloud Depth Z (pc)

Fig. 3.7(b)

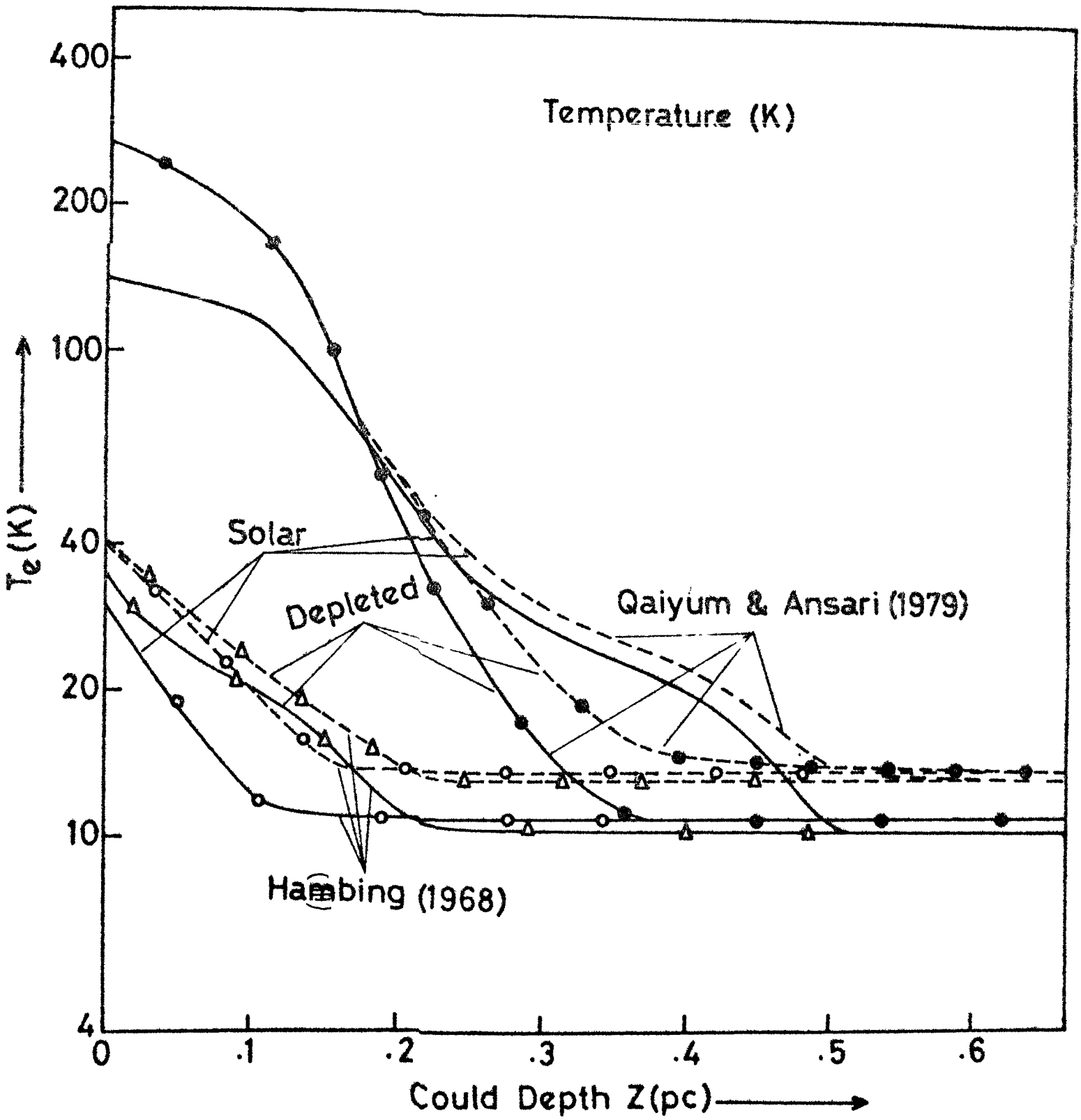
Temperature (K)
400
200
100
40
20
10
4
T_e (K)
Solar
Depleted
Qaiyum & Ansari (1979)
Hamabing (1968)
0
.1
.2
.3
.4
.5
.6
Could Depth Z(pc)

Fig.3.8

FIGURE CAPTIONS

Fig.3.1 The grain potential(U) and heating rate for grain (H_g) as a function of hydrogen number density n_H at two values of χ_F = 1.0 and 10.0 for Solar(——) and depleted (----) abundances.

Fig.3.2 Total cooling per atom from the fine structure transitions of the neutral carbon for X(CI)/dv/dr=10^{-4}, 10^{-5}, 10^{-6} and 10^{-7}($(kmS^{-1}\ Pc^{-1})^{-1}$) at kinetic temperatures ,
(a) 10 K, (b) 20 K, (c) 100 K.

Fig.2.3 Cooling per ion from the fine structure transition of carnon ion for X(CII)/dv/dr = 10^{-4}, 10^{-5}, 10^{-6} and 10^{-7} ($(km\ S^{-1}Pc^{-1})^{-1}$) at kinetic temperatures.
(a) 40 K, (b) 100 K.

Fig.3.4 Cooling from rotational transitions of CO
(a) Reduced cooling rates for individual transitions at T_e = 20 K; Total cooling per CO for X(CO)/dv/dr = 10^{-4}, 10^{-5}, 10^{-6} and 10^{-7} ($(km\ S^{-1}\ Pc^{-1})^{-1}$) at
(b) 10K, (c) 20 K, (d) 100K.

Fig.3.5 Calculated ratio of brightness temperatures of $2 \rightarrow 1$ and $1 \rightarrow 0$ transitions of ^{12}CO at T_e = 20 K and 100 K.

Fig.3.6. Variation of heating rates with cloud depth: Total heating (——), Photo-electron from grain(----), H_2 formation (—•—), H_2 dissociation (.....), Photo-ionisation of heavy elements (—O—), Chemical heating (—Δ—), Gravitational collapse (—·—), Cosmic ray ionisation (—X—) for abundances, (a) Solar, (b) Depleted.

Fig.3.7. Variation of cooling rates for main cooling agents and their total as a function of cloud depth.

Fig.3.8. Gass temperature distribution in the cloud for UV field of Habing (1968) and Qaiyum & Ansari (1979) and also the solar and depleted abundances. Without FIR (solid line) and with FIR (dotted lines).

******

CHAPTER - 4

Interpretation of Radio-Recombination Lines from Partially Ionized Medium Adjacent to HII Regions

4.1 Introduction

The thermal properties and physical conditions inside dense interstellar clouds are known to be of fundamental importance, since these objects are beleived to be the actual site of proto-star formation and chemical evolution of complex molecules. Radio recombination lines from ionised species offer a direct method for investigation of the structure and physical conditions within various components of interstellar medium. Radio-frequency emission from partially ionised dense interstellar media have been detected towards approximately fifteen galactic HII regions. Detailed observational studies of carbon line emission have been carried out mainly from NGC 2024 (W12), Orion A (W10) and W3 (IC 1795). These are also the sources which display recombination line feature attributed to an element(s) heavier than carbon. The data are available over the frequency range 15GHz(n=75) to 0.6 GHz(n=220) (Dupree 1974, Rickard et al.1977, Pankonin et al.1977, Jaffe and Pankonin 1978, and Pankonin 1980).

Since the original detection of carbon recombination line (Palmer 1967), various mechanisms and models have been

proposed to explain the line intensities of carbon, hydrogen and of other heavier elements, in order to characterize the emitting region. Dupree (1974) and Qaiyum (1976) interpreted the observations of NGC2024 and W3 as a stimulated emission by continuum radiation from the nearest HII region. Hoang-Binh and Walmsley (1974) preferred the spontaneous emission model to explain the line intensities. Taking into account details of the observation of Orion A, Zuckerman and Ball (1974) suggested the possibility of the existence of both these mechanisms to some extent in most sources. Ahmad (1976*b*) discussed in length two component model of Orion A. Rickard et al. (1977), Pankonin et al. (1977), Jaffe and Pankonin(1978), Pankonin (1980) and Qaiyum and Ansari (1983a) set up two or more component models of NGC 2024, W3 and Orion A, to explain the observed intensities over the range of frequencies (0.6 GHz to 15 GHz).

The present study is also an attempt to explain the line intensities of carbon and other anomalous recombination lines using two component model (Diagram 1). The basic difference from the earlier attempts of other than us lies in the following :

i) Thermal, chemical and charge balance equations are solved numerically and iterated to deduce the thermal and ionisation structure in a self-consistent way, till convergence

is achieved.

ii) As discussed in the previous chapters, the cloud considered are not electrically homogeneous and isothermal. Consequently, the line intensities are calculated by dividing the cloud(s) into equally thick isothermal and homogeneous thin slabs.

iii) The statistical equilibrium is set up to deduce the departure coefficient (b_n) for a particular electron density n_e and temperature T_e at each position. A best fit of observed intensity of recombination lines of carbon is carried out by taking, as free and independent parameters, the hydrogen density, emission measure (EM) of the associated HII region(s) and the cloud size.

iv) The continuum radiation from the HII regions, $3^{o}K$ radiation and radiations from dust grains are taken to be the background radiation.

4.2 Statistical Equilibrium

The line strength and absorption coefficient of the gas depend critically on the relative populations of the atomic energy levels. In order to determine the population N_n of the excited state n, we work with the equation of statistical equilibrium in a time independent form. The most important processes affecting the level populations are :

1. spontaneous transition to lower levels ($N_n \sum_{m<n} A_{n,m}$),

2. cascade from higher levels ($\sum_{m>n} N_m A_{m,n}$),

3. Induced transitions by continuum radiation

($N_n B_{n,n\pm n'} I_\nu$, $N_{n\pm n'} B_{n\pm n',n} I_\nu$),

4. collisional transitions ($N_n C_{n,n\pm n'}$, $N_{n\pm n'} C_{n\pm n',n}$),

5. collisional ionisation and three body recombination

($N_n C_{n,i}$, $n_e N_i C_{i,n}$),

6. radiative recombination ($n_e N_i \alpha_{i,n}$)

7. redistribution of angular momentum by collisions

($H^+ + H(n,l) \longrightarrow H(n,l \pm 1) + H^+$).

We expect here the collision frequency high enough so that substantial redistribution of population among l states will occur. The validity of this particular assumption has been discussed by Pengelly and Seaton (1964), Brocklehurst(1971), and Seaton (1980). Hence it is reasonable to assume that N_{nl}, the population of states nl, will be related to the level population N_n by its statistical factor:

$$N_{nl} = \frac{(2l+1)}{n^2} N_n \quad \text{where } N_n = \sum_l N_{nl} , \qquad 4.1$$

which makes it possible to solve for level population of level n. With the above assumptions, the equation of statistical equilibrium for the population of level n, $N_n(cm^{-3})$ is written as

$$N_n \left[\sum_{m<n} A_{n,m} + \sum_{n'} (B_{n,n\pm n'} I_\nu + C_{n,n\pm n'}) + C_{n,i} \right] =$$

$$\sum_{m>n} N_m A_{m,n} + \sum_{n'} N_{n\pm n'} (B_{n\pm n',n} I_\nu + C_{n\pm n',n}) + n_e N_i (\alpha_{i,n} + C_{i,n}). \qquad 4.2$$

The left hand side represents the depopulation and the right hand side the population of level n.

It is convenient to introduce the departure coefficient b_n, defined as the ratio of the actual population N_n to its value in local thermodynamic equilibrium N_n^* :

$$b_n = \frac{N_n}{N_n^*}$$

$$\text{where } N_n^* = n_e N_i \frac{W_n}{2} \frac{h^3}{(2\pi mk\, T_e)^{3/2}} e^{\chi_n} \qquad 4.3$$

N_i is the ion density and n_e the electron density, $\chi_n = I_n/kT_e$.

Introducing b_n factor we find

$$\sum_{K=1}^{3} R_n(K) = S_n \qquad 4.4$$

where

$$R_{n(1)} = - \sum_{n'} b_{n-n'} \frac{W_{n-n'}}{W_n} e^{\chi_{n-n'} - \chi_n} (B_{n-n',n} I_\nu + C_{n-n',n}) \qquad 4.5$$

Table 2.1 (continued)

	Photo reactions	Rates (sec^{-1}) $\chi_F/(0.5+Z)^2$	References
17.	$H_2O + h\nu \longrightarrow OH_2^+ + e$	$3.1\times10^{-8}\exp(-\tau_d(Z) - {}^{at}\tau_\lambda(Z))$	Katayama et al. (1973)
	$\longrightarrow OH + e$	$4.8\times10^{-7}\exp(-0.56\ \tau_d(Z))$	Katayama et al. (1973)
18.	$H_2Cl^+ + h\nu \longrightarrow H + HCl^+$	$4.8\times10^{-7}\exp(-0.64\ \tau_d(Z) - {}^{at}\tau_\lambda(Z))$	Jura (1974)
19.	$CH_2 + h\nu \longrightarrow CH_2^+ + e$	$1.5\times10^{-6}\exp(-0.76\ \tau_d(Z) - {}^{at}\tau_\lambda(Z))$	Barsuhn (1977)
	$\longrightarrow CH + H$	$7.5\times10^{-8}\exp(-0.6\ \tau_d(Z))$	deJong et al. (1980)
20.	$H_2CO + h\nu \longrightarrow H_2 + CO$		
	$\longrightarrow 2H + CO$	$1.8\times10^{-6}\exp(-0.8\ \tau_d(Z) - {}^{at}\tau_\lambda(Z))$	
	$\longrightarrow H + HCO$		deJong et al. (1980)
	$\longrightarrow H + HCO^+ + e$	$1.2\times10^{-9}\exp(-0.5\ \tau_d(Z))$	
	$\longrightarrow H_2CO^+ + e$		

Note: i) Whereever ${}^{at}\tau_\lambda(Z)$ contributes negligibly, it is omitted from the rates

ii) $\tau_d(Z)$ is the dust optical depth at $1000A^\circ$.

$$R_n(2) = b_n\left[\sum_{m<n} A_{n,m} + \sum_{n'} (B_{n,n\pm n'} I_\nu + C_{n,n\pm n'}) + C_{n,i}\right] \quad 4.6$$

$$R_n(3) = -\sum_{n'} b_{n+n'} \frac{W_{n+n'}}{W_n} e^{\chi_{n+n'} - \chi_n} (B_{n+n',n} I_\nu + C_{n+n',n} + A_{n+n',n}) \quad 4.7$$

$$S_n = \sum_{m>n+n'}^{\infty} b_m \frac{W_m}{W_n} e^{\chi_m - \chi_n} A_{m,n} + \left(\frac{2\pi m k T_e}{h^3}\right)^{3/2} \frac{2}{n^2} \alpha_{i,n} e^{-\chi_n} + C_{n,i} \quad 4.8$$

In the above equation $A_{m,n}$ is the Einstein coefficient for spontaneous transition between upper and lower level n respectively.

$$A_{m,n} = \frac{16 \alpha^4 C}{3\sqrt{3}\pi a_o} \frac{Z^4 g_{m,n}}{m^3 n(m^2-n^2)} \cong 1.57 \times 10^{10} \frac{Z^4 g_{m,n}}{m^3 n(m^2-n^2)} \text{ sec}^{-1} \quad 4.9$$

where $g_{m,n}$ is the Kramer Gaunt factor given by Summers(1969) as

$$g_{m,n} = 1.0 - T_4 (T_1 G_1 + T_2 G_2 + T_3 G_3) \quad 4.10$$

where

$$G_1 = \left(0.203 + \frac{0.256}{m^2} + \frac{0.257}{m^4}\right)$$

$$G_2 = 0.170\, m + 0.18$$

$$G_3 = \left(0.2214 + \frac{0.1554}{m^2} + \frac{0.370}{m^4}\right) m$$

$$T_1 = (2n-m)\ (n-m+1)$$

$$T_2 = 4.0\ (n-1)\ (m-n-1)$$

$$T_3 = (2n-m-0.001)\ (n-0.999)$$

$$T_4 = \frac{1}{(m-1.999)^2} \cdot \frac{1}{m\ n^{2/3}} \left(\frac{m-1}{m-n} \right)^{2/3}$$

The Einstein coefficient B is

$$B_{m,n} = A_{m,n} \left(\frac{8 \pi h \nu_{m,n}^3}{c^3} \right)^{-1}$$

The frequency of transition $m \longrightarrow n$, $\nu_{m,n} = \frac{Z^2 I_H}{h} \left(\frac{1}{n^2} - \frac{1}{m^2} \right)$

For $n >> 1$ and $|m-n| << n$ it is approximated as

$$\nu_{m,n} = 6.58 \ \Delta n \left(\frac{100}{n} \right)^3 GH_Z \quad , \quad \Delta n = |m-n| \qquad 4.12$$

The lines are referred as n_α, n_β and n_γ .... for $\Delta n = 1, 2, 3$ ----

For the clouds in question the radiation density I_ν for thermal radiation field at frequency ν is obtained from equation of transfer, to give

$$I_\nu = W_\nu \frac{8 \pi h \nu^3}{c^3} \left(e^{h\nu/kTr} - 1 \right) \left(1 - e^{-\tau_\nu (HII)} \right) \qquad 4.13$$

W_ν is the dilution factor taken to be equal to 0.5, since the medium in question is very close to HII region, $\tau_\nu (HII)$ is the optical depth of the thermal radiation source HII at temperature T_r,

$$\tau_\nu = \int_0^S K_\nu \ ds' \qquad 4.14$$

where S is the path length through the medium. The optical depth τ_ν is determined from the temperature T_r and emission measure E_r (pc cm^{-6}) of the HII region, where the radiation is originated. It is taken as (Salem 1975):

$$\tau_\nu = 4.646\, E_r\, \nu^{-7/3}\, T_r^{-3/2} \left[e^{.047993\,\nu/T_r} - 1 \right] I(v) \qquad 4.15$$

where ν is in GH_Z and

$$v = 0.6529 + \frac{2}{3}\log\nu - \log T_r$$

$$\log I(v) = \begin{cases} -1.1249v + 0.3788 & \text{for } v \leq -2.6 \\ -1.2326v + 0.0987 & \text{for } -2.6 < v \leq -0.25 \\ -1.0842v + 0.1359 & \text{for } v > -0.25 \end{cases}$$

The collisional ionisation rate is taken from Seaton (1964)

$$C_{n,i} = 3.45\times10^{-5}\, n_e\, \frac{n^2}{T_e^{1/2}}\, e^{-\chi_n}, \qquad 4.16$$

and this rate is related to three body recombination rate $C_{i,n}$ by detailed balance as

$$n_e\, N_i\, C_{i,n} = N_n^*\, C_{n,i} \qquad 4.17$$

The radiative recombination coefficient $\alpha_{i,n}$ is given by Seaton (1959)

$$\alpha_{i,n} = 2.06\times10^{11} \left(\frac{Z^2}{n\, T_e^{1/2}}\right) \chi_n\, S_n(\lambda), \qquad 4.18$$

where $\lambda = n^2 \chi_n$, and function $\chi_n S_n(\lambda)$ has been calculated and tabulated by Seaton (1959).

We use de-excitation rates of Gee et al.(1976) which are accurate over a wide range of energies, including particularly the difficult low-energy region. The cascade term $\sum_{m>n+n'}^{\infty} b_m \frac{W_m}{W_n} e^{\chi_m - \chi_n} A_{m,n}$ is evaluated for $A_{m,n}$ upto m = high N.

Above N we use $b_m = 1$ and use the relation obtained by integral (Seaton 1964), viz.,

$$\sum_{m=N+1}^{\infty} b_m \frac{W_m}{W_n} e^{\chi_m - \chi_n} A_{m,n} = \frac{7.87\times10^9\, \bar{g}}{n^3\, e^{\chi_n}} \left[\frac{1}{(N+1)^3\left(1-\frac{n^2}{(N+1)^2}\right)} - \frac{1}{n^2} \ln\left(1-\frac{n^2}{(N+1)^2}\right)\right], \qquad 4.19$$

$$\bar{g} = \tfrac{1}{2}\left(g_{n+1,n} + g_{\infty,n}\right) \qquad 4.20$$

To find b_n factor for a particular level n, we calculate

contributions from $n' = 40$ i.e. $n \pm 40$ levels. We use the formalism of Brocklehurst and Salem (1977), that is of matrix condensation method with little modification to include the effect of infra-red radiations from dust grains of associated HII regions.

Departing from Rickard et al.(1977) and Pankonin et al. (1977), the electron density n_e, and temperature T_e, as discussed in earlier two chapters, are used as a function of the position Z and n_e is taken as the sum of all ionised species of atoms and molecules; $n_e(Z) = \sum_X n_X^+(Z) + \sum_{X \text{ molecules}} n^+(Z)$. Further b_n factor is calculated at each position Z of the cloud.

4.3 Brightness Temperature

The intensity of radiation along a line of sight through the medium is governed by the equation of transfer

$$\frac{d}{dZ} I_\nu = - K_\nu I_\nu + J_\nu \quad , \qquad 4.21$$

where J_ν and K_ν are the emission and absorption coefficients for the line and the continuum. The emergent intensity in the absence of background radiation along a particular line of sight can be written as (Brocklehurst and Seaton 1972):

$$I_\nu^c = \int_o^S J_\nu^c \; e^{-\left[\tau_\nu^c - t_\nu^c (Z)\right]} dZ \quad \text{(for the continuum)} \qquad 4.22$$

and

$$I_\nu^L + I_\nu^C = \int_0^S (J_\nu^L + J_\nu^C)\, e^{-\zeta_\nu + t_\nu^L(Z) + t_\nu^C(Z)}\, dZ$$

(for the line plus continuum) 4.23

where S is the distance along the line of sight measured from the farthest part of the cloud to the observer. Here, J_ν^C and J_ν^L are the continuum and line emissivities, $t_\nu^C(Z)$ and $t_\nu^L(Z)$ are the continuum and line optical depths, ζ_ν is the total continuum and line optical depth over the whole cloud. ζ_ν^C is the total continuum optical depth.

In the presence of background radiation, the line plus continuum intensity may be written as :

$$I_\nu^L + I_\nu^C = \int_0^S (J_\nu^L + J_\nu^C)\, e^{-\zeta_\nu + t_\nu^L(Z) + t_\nu^C(Z)}\, dZ - I_o \int_0^S e^{-(t_\nu^L + t_\nu^C)} K_\nu(Z)\, dZ$$

4.24

Here I_o is the background intensity. A similar term of attenuated background radiation will appear in I_ν^C.

The line intensity along a particular line of sight in the presence of background radiation may be written in the form.

$$I_\nu^L = \int_0^S (J_\nu^L + J_\nu^C) e^{-\zeta_\nu + t_\nu^L + t_\nu^C}\, dZ + I_o \int_0^S e^{-t_\nu^C} K_\nu^C\, dZ - \int_0^S e^{-\zeta_\nu^C + t_\nu^C} J_\nu^C\, dZ$$

$$- I_o \int_0^S e^{-t_\nu^L - t_\nu^C} K_\nu\, dZ \qquad 4.25$$

Here K_ν^C is the continuum absorption coefficient and K_ν is the total continuum plus line absorption coefficient. For the transition m $\longrightarrow$ n the line coefficients are given by (Brocklehurst and Seaton 1972).

$$J_\nu^L = h\nu N_m \frac{A_{m,n}}{4\pi} \varphi_{n,m} \qquad 4.26$$

and

$$K_\nu^L = \frac{c^2}{8\pi\nu^2}\left[\frac{N_n}{W_n} - \frac{N_m}{W_m}\right] W_m A_{m,n} \varphi_{n,m} \qquad 4.27$$

Where $\varphi_{n,m}$ is the line profile.

These equations may be written as

$$J_\nu^L = h\nu b_m N_m^* \frac{A_{m,n}}{4\pi} \varphi_{n,m} = b_m J_\nu^{*L} \qquad 4.28$$

and

$$K_\nu^L = \frac{c^2}{8\pi\nu^2} N_n^* \left[1 - \frac{b_m}{b_n} e^{-h\nu/kT_e}\right] \frac{W_m}{W_n} A_{m,n} \varphi_{n,m} = b_n \beta K_\nu^{*L} \qquad 4.29$$

$$\text{Here } \beta = \frac{(1 - \frac{b_m}{b_n} e^{-h\nu/kT_e})}{(1 - e^{-h\nu/kT_e})} \qquad 4.30$$

$$\text{whence } K_\nu^{*L} = n_e N_i \frac{\pi e^2}{mc} \left(\frac{h^2}{2\pi m kT_e}\right)^{3/2} n^2 e^{\chi_{n/kT_e}} \times (1 - e^{-h\nu/kT_e}) f_{n,m} \varphi_{n,m} \qquad 4.31$$

The oscillator strength $f_{n,m}$ for $n \gg 1$ and $\Delta n = /m-n/ \ll n$ is given by (Menzel 1968) as:

$$\frac{f_{n,m}}{n} = K(\Delta n)\left[1 + \frac{3}{2}\frac{\Delta n}{n} + \ldots\ldots\right] \qquad 4.32$$

Where $K(1) = 0.1908$, $K(2) = 0.02633$, $K(3) = 0.00810$.

Here the line profile is determined by Doppler broadening only and expression 4.31 is simplified to

$$K_\nu^{*L} = 1.01\times10^{4}\, Z^2\, \Delta n \left(\frac{f_{n,m}}{n}\right) T_e^{-5/2}\, \Delta\nu_L^{-1}\, e^{\chi_n}\, n_e\, N_i \qquad 4.33$$

$\Delta\nu_L$(in KH_z) is the line width at half maximum intensity.

The expression for continuum absorption coefficient is the same as defined in equation 4.14 and 4.15. The emissivities are related to the absorption coefficient as:

$$J_\nu^{*L} = B\, K_\nu^{*L} \qquad 4.34$$

$$J_\nu^{C} = B\, K_\nu^{C}$$

where the Plank-function $B = \frac{2h\nu^3}{c^2}\left(e^{h\nu/kT_e} - 1\right)^{-1}$

Substituting for the various line coefficients as given above and applying Rayleigh-Jeans approximation under non-LTE condition, we obtain for the line brightness temperature from 4.25.

$$T_{L_b} = e^{-\zeta_\nu} \int_o^S \left[\eta T_e \left(b_m \beta \overset{*}{K}{}_\nu^L + K_\nu^C \right) \right] e^{t_\nu^L + t_\nu^C} dZ + T_o \int_o^S e^{-t_\nu^C} K_\nu^C \, dZ$$

4.35

$$- T_o \int_o^S \left(b_m \beta \overset{*}{K}{}_\nu^L + K_\nu^C \right) e^{-t_\nu^L - t_\nu^C} dZ - e^{-\zeta_\nu^C} \int_o^S T_e K_\nu^C e^{t_\nu^C} dZ$$

Here $$\eta = \frac{1 + b_m \overset{*}{K}{}_\nu^L / K_\nu^C}{1 + b_m \beta \overset{*}{K}{}_\nu^L / K_\nu^C} \qquad 4.36$$

and T_o is the background continuum temperature.

If the distance is measured along the line of sight from the closest part of the cloud to the observer then

$$T_{L_b} = \int_o^S \left[\eta T_e \left(b_m \beta \overset{*}{K}{}_\nu^L + K_\nu^C \right) \right] e^{-t_\nu^L - t_\nu^C} dZ + T_o e^{-\zeta_\nu^C} \int_o^S K_\nu^C e^{t_\nu^C} dZ$$

4.37

$$- T_o e^{-\zeta_\nu} \int_o^S \left(b_m \beta \overset{*}{K}{}_\nu^L + K_\nu^C \right) e^{t_\nu^L + t_\nu^C} dZ - \int_o^S T_e K_\nu^C e^{-t_\nu^C} dZ$$

For $\frac{h\nu}{kT_e} \ll 1$, 4.30 goes into

$$\beta = \frac{b_m}{b_n} \left[1 - \frac{k T_e}{h \nu} \left(1 - \frac{b_n}{b_m} \right) \right] \qquad 4.38$$

The expressions 4.35 and 4.37 reduces to the same form as given by Dupree (1974), Hoang-Binh and Walmsley (1974), and Rickard et al. (1977), for isothermal, homogeneous and optically thin cloud. For the foreground part of the cloud the continuum temperature is that of HII while for background part it is taken to be 2.7 K.

The theoretically predicted brightness temperatures discussed so far are true only to for an infinitely small solid angle $d\Omega$. However owing to the finite angular resolution of a radio telescope, an integrated value of line temperature over the antenna solid angle is always observed. Therefore, in order to use the theoretical relations developed above, we must relate T_{Lb} to the observed line temperature T_{AL}. If we define η_B the main beam efficiency, $f(\Omega)$ the main beam power pattern, $T_L(\Omega)$ the actual brightness temperature distribution of the line emission, and Ω_B the main beam solid angle then : (Churchwell 1970, Qaiyum 1976)

$$T_{Lb} = \frac{T_{AL}}{\eta_\beta} = \frac{1}{\Omega_B} \int_{\Omega_\beta} T_L(\Omega)\, f(\Omega)\, d\Omega \qquad 4.39$$

The main beam solid angle is definedby

$$\Omega_B = \int_{\substack{\text{main}\\ \text{beam}}} f(\Omega)\, d\Omega \qquad 4.40$$

This Ω_B is propotional to the product of half power width (HPW) θ_E and θ_H of the electric and magnetic planes of the main beam respectively. The actual source solid angle can be given by :

$$\Omega_S = \frac{1}{T_L} \int_{\text{Source}} T_L (\Omega) \, d\Omega \qquad 4.41$$

Where T_L is the maximum value of the brightness temperature distribution $T_L (\Omega)$. The effective source solid angle is

$$\Omega_S' = \frac{1}{T_L} \int_{\text{source}} T_L (\Omega) \, f (\Omega) \, d\Omega \qquad 4.42$$

Combining the expressions 4.39 and 4.42 we get

$$T_{Lb} = \frac{T_{AL}}{\eta_B} = \frac{\Omega_S'}{\Omega_B} T_L \qquad 4.43$$

As discussed earlier the value of Ω_S' / Ω_B depends upon the type of beam used.

For $\Omega_S >> \Omega_B$

$$T_{Lb} = T_L \qquad 4.44$$

and $\Omega_S << \Omega_B$

$$T_{Lb} = T_L \frac{\Omega_S}{\Omega_B} \qquad 4.45$$

The ratio of beam width and angular diameter is considered here as the function of beam width after Panagia and Walmsley (1978). In the calculation of line intensities the angular diameter of the cloud is varied to fit the observations.

4.4 Characteristics of the carbon emitting region

It is particularly difficult to deduce accurate physical parameters of the CII region from the line observations, because the line emission depends upon a number of factors, several of which are external to the CII region itself. Not only the geometry and the distribution of CII is important, but its location relative to the HII region and the spectral type of the exciting star also play important roles in the ionisation structure and thermal equilibrium in CII region.

The data of variable quality are available over the frequency range 0.6GH_Z (n=220) to 15 GH_Z (n=75) for NGC2024, W3 and Orion A. We believe that data are not presently complete enough to support a very detailed model of CII region. Dupree (1974) and Hoang Binh (1974) have tried to fit the observations by considering a single component cloud. On the contrary the observations have shown that CII regions appear to be rather complex structure and a single model with a single set of physical parameters and a simple geometry is not sufficient

to interpret the CII-lines. Ahmad (1976b), Rickard et al.(1977) and Pankonin et al.(1977) have argued, on the basis of systematic difference in the velocities of C-lines between high frequency (> 2.7 GH_Z) and low frequency (< 1.7 GH_Z), that emitting regions for these two ranges of frequencies are different. According to them velocity shift ΔV_{LSR} in the case of NGC 2024 is 1.0 to 1.5 km/sec. For W3, where scatter in the measured value is larger than that of NGC 2024, the shift is 0.5 to 1.5 km/sec. The velocity shift for Orion A is the largest, about 3 km/sec. The frequency dependence of the velocity of carbon lines is probably the most straight forward argument that different volumes of gas dominate the emission at different frequencies.

Inspite of the insufficient data available presently the following information can be extracted from the recombination lines data.

i) We establish for the CII clouds the range of hydrogen density that in turn gives the range of electron temperature and electron density.

ii) We determine the dominant processes for the line formation — stimulated or spontaneous emission.

iii) We determine the spatial extent of CII regions and distribution line intensities therein, relative to the HII regions.

In this work we have tried to fit the observations over the whole range of observed frequency spectrum 0.6 GH_Z to 15 GH_Z, using two component model: one behind and the other in front of HII region, see diagram 1. Each component of the model is characterized by three parameters, namely; (1) angular size θ_S, (2) hydrogen density n_H that gives the range of *electron temperature and electron density after solving for* thermal and ionization equilibrium as mentioned in chapter 2 and 3, and (3) emission measure E_C of the continuum of the associated HII region that determines the location of CII regions relative to HII regions. The parameters deduced from the best fit for each component differ for different abundances.

Having obtained several sets of values (θ_S, n_H, E_C) for each source model and also for each abundance, we calculate $\Omega_S \Delta V(n_\alpha) T_{L_b}(n_\alpha)$ in ^oK Sterad km/sec, for each observed n_α transition in order to compare with observations. We varied independently the model parameters to obtain a best fit to the observed lines. The observational values are converted to the above assumed form, using the telescope beam width and effeciency (discussed in the previous section). The observed results include the data from the telescopes of NRAO (140ft), Hystack observatory (120ft), Jodrell Bank Mark I (250ft) and MPIfR(100 m)*. The observational errors considered are mostly

of 3σ limits. The observed values for different transitions are given in Tables (4.1a - 4.1c).

The calculated and observed values for each source and also for both the abundances are plotted separately, Figures 4.1(a) to 4.3(b). It is clear from these figures that over the whole observed frequency spectrum the agreement between theory and observations is quite good for NGC 2024 but not so good for W3 and Orion A. There are some scattered points for W3 and Orion A. But majority of the observational values are close to the theoretical values within the error-range. The best fit obtained for depleted and solar abundances have approximately the same degree of agreement. Therefore on the basis of these calculations we can not conclude in favour of either abundance.

Our calculation shows also that high frequency (> 2.7 GH_Z) radiations are predominantly emitted through spontaneous transitions from the component behind the HII regions, see also Rickard et al.(1977). The background component of the model contributes, for instance $\backsim 90\%$ to the total intensity for C76α and C 85α lines. Its share decreases with frequency and for $\nu \lesssim 2.7$ GH_Z the foreground component dominates over the component behind the HII region. For low frequencies, the emission is due to stimulation from background radiation and is from the foreground volume of the gas.

---

* NRAO = National Radio Astronomy Observatery, U.S.A.
MPIfR = Max-Plank-Institut fur Radioastronomie, West Germany
Hystack Observatory, U.S.A.
Jodrell Bank Mark I, U.K.

The set of parameters, that characterizes best fits for each source model, are given in Table 4.5. The source sizes obtained from the observations belong mostly to high frequency group. At low frequency, the cloud size may not be accurately determined due to dominance of stimulated emission from background radiation. The observed source size at higher frequencies for NGC 2024 are 3.3' (Macleod et al.1975, C85α), 3.'6 (Wilson et al. 1975, C 134α), 3.'6 (Rickard et al.C76α) and $\gtrsim$1.5 (Chaisson 1973, C 94α). Thus, apparent observed source size ($\sim$ 3.'4) is very close to the fitted source size (3.'2 and 2.'4), of the background component, obtained by us for solar and depleted abundances respectively.

The angular extension reported for W3 are $\lesssim$ 4.'4 (cited by Rickard et al. 1977 for C 85α) and 3' $\pm$2' (Wilson et al.1975 for C 134α). These values are very close to the size (3.'5) deduced for depleted abundance. A detailed mapping of Orion A by Balick et al. (1974) gives a source size~8.' This is also close to our theoretically derived value (7.'3).

The hydrogen density n_H obtained for all the clouds of interest lies in the range $2x10^4$ — $4x10^5$ cm^{-3} for solar and $5x10^4$ — $2x10^6$ cm^{-3} for depleted abundance. For background component n_H is in general greater than that of the foreground component. For background sources, the most suitable dilution factor is found to be the same as for continuum of HII region,

which is approximately unity. This shows that background components are aligned with the peak emission of HII regions. The dilution factor for foreground component is approximately unity for NGC 2024, <0.1 for Orion A and in between these two values for W3. This is probably due to the reason that the foreground component is slightly shifted off the peak emission of HII region. This fact is observed for Orion A (Balick et al. 1974).

The cloud considered here are non-isothermal and electrically inhomogeneous. The temperature structure is shown in Figure 3.8 for $n_H = 10^4$ cm^{-3} and, see also, Qaiyum and Ansari(1983a). The temperature variations are $\backsim$ 150 K to $\backsim$ 10 K and $\backsim$ 250 K to $\backsim$ 11 K for solar and depleted abundances respectively. See Figures 2.1(a) and 2.1(b) for n_e variation: $\backsim$ 5.5 to $\backsim$ 2.0 cm^{-3} and $\backsim$ 2.0 to $\backsim$ 0.5 cm^{-3} for the two abundances respectively.

A more straight forward method of distinguishing between stimulated and spontaneous emission is to observe n_α and n'_β transitions which occur at nearly the same frequency. This has the observational advantage of carrying a large range of quantum levels with a telescope of constant beam size; the line ratio becomes also independent of the source size. The observational disadvantage is that n'_β lines are weak as compared to n_α lines. Since they are emitted at nearly the same frequency, they originate from the same volume of the gas thus the line intensity ratio

$I(n_\alpha)/I(n'_\beta)$ is independent of the source size and the beam width of the telescope, and therefore it is easy to calculate the ratio and to compare with the observations. We have listed in Table 4.2 the observed and calculated ratios of $C(n_\alpha)/C(n'_\beta)$ for NGC 2024, W3 and Orion A. The calculated α and β line intensities come out to be in good agreement with the observed values.

As discussed earlier the lines at high frequency are due to background component. Therefore, the intensity ratio of α and β lines at the same frequency, for high frequency group are, independent of the continuum of HII regions. However, the large ratio at low frequency can not be explained without stimulated emission from the continuum of HII regions. Moreover, for the low ratio at high frequency, no stimulated emission is required for agreement with the observed values. Thus line ratios also favour evidently two component model. We have also found that the background clouds (emitting high frequency lines of carbon) are denser than the foreground component from where low frequency of carbon are observed. This conclusion is also corraborated by the following:

The column densities of OH and H_2CO are found to be smaller for high density as compared to low density clouds (Table 2.8). Therefore, molecular line intensities from low density component will dominate over that of high density. This in turn supports

the fact that lines of OH and H_2CO are emitted from the low density component (i.e. foreground), the velocity V_{LSR} also correlating with the low frequency carbon emissions. Another significant fact is that the observed frequencies of OH and H_2CO are in the range 1 — 10 GH_Z in which the continuum radiation of HII region is significant and may alter the line temperatures of these molecules. Further, the calculated column densities of CO molecule is approximately independent of n_H. Therefore, both the components (low and high density) may contribute equally to the observed results, if not well resolved. Thus it is clear that the radial velocity may lie in between the low and high frequency group which is borne out by observations (Pankonin et al.1977). We may add that according to Zuckerman and Ball (1974) HCN abd CS may be abundant enough in high density region and therefore the radial velocities are close to that of high frequency emission of carbon. Thus we see that radial velocities of molecular line emitting regions also favour two or more component model and also show that molecular, carbon, neutral hydrogen and heavy line emitting regions are associated with each other.

4.5 SII-Region

The most extensively studied carbon line emitting regions are NGC 2024, W3 and Orion A. Lines from some heavy element

other than carbon are also observed from these sources. The following facts have been observed for line of an unknown heavy element(s). First, the observed line width for the element X is less than the carbon line width. Second, the velocity separation ΔV_{LSR} (C-X) lies between 8 and 9 in most of the cases (Chaisson et al.1972, Chaisson 1974, Pedlar and Hart 1974, Wilson et al.1975 and Pankonin et al.1977).

The most abundant elements other than carbon having ionisation potential less than 13.6 ev are Mg, Si, S and Fe. These elements may be singly ionised by the radiation $\lambda \gtrsim 912\text{A}^{\circ}$. Theoretically a blend emission from the elements would result in a broader line that that of carbon. The velocity separation Mg, Si, S and Fe with carbon are 6.94, 7.78, 8.58 and 10.77 km sec^{-1} respectively. On the basis of these theoretical values and above mentioned observations Pankonin et al. (1977) argued that X-line is not a blend emission from all the above-mentioned elements but it appears to be from a single element that may be identified as S.

Further, the assumption that carbon and heavy element line emitting regions are identical leads to the temperature of the emitting region $\backsim$ 4000 K (Pankonin et al. 1977). However, the theoretically deduced temperature from thermal balance for the density range obtained from the best fit of the carbon lines are at least smaller by an order of magnitude than that

mentioned above. (Qaiyum and Ansari 1983a). It should be emphasized further that temperature ~ 4000 K can not be explained with the known heating and cooling mechanisms. Besides, the Strömgren radius of carbon is less than that of other heavy elements (Figures 2.1a and 2.1b). As a consequence, assumption of co-spatiality does not hold.

The normalized brightness temperature T_{Lb} are plotted against the cloud depth (Z) for carbon and sulfur at 1 and 10.5 GH_Z in Figure 4.4. From this figure we infer the following:

i) The line intensity is not equally distributed over the whole region.

ii) The structure of line temperature for 1 and 10.5 GH_Z vary. Thus, derived values of ΔV_{LSR}(C-S) may also be slightly different for different lines. This has been observed by Pankonin et al.(1977).

iii) There is only a slight difference in intensity distribution for solar and depleted abundances. This small change is occuring due to the difference in the electron density structure obtained by the ionisation of heavy elements and temperature structure for these two abundances.

iv) C- and S-regions are not completely co-spatial.

v) The contribution to the C-lines comes mainly from the hot regions of the cloud especially from the inner edge of the Strömgren sphere of carbon.

vi) The line temperature of S is well spread over the depth of 0.5 Pc. But the main contribution to the intensity is from the regions slightly away from the boundary of the Strömgren sphere of carbon. Therefore, the properties deduced from the S-lines will be closer to that obtained from molecular lines.

vii) Three different regions are apparently contributing to the line intensity of S. Firstly, the outer most region (close to HII region) where ionisation of hydrogen is contributing significantly to the total electron density. Secondly, the inner edge of the carbon region where carbon is sufficiently ionised to yield enough n_e, but in which the temperature falls rapidly and consequently the line intensity increases by a factor $\propto T_e^{-1.5}$. Thirdly, the inner cool region where the temperature is rather low $\backsim$ 20 K (Qaiyum and Ansari 1983a).

viii) The intensity ratio of C and S lines can not be equated with the emission measure (EM) or abundance ratio. They will be equal only when the line emitting regions are identically the same. When the EM is equated with the line ratio, it turns out that the intensity ratio is underestimated by a factor 2-3.

The ratio of line-intensities of C and S for n_α transitions are also plotted in Figure 4.5 as a function of principal quantum number n for EM=10^5 and 10^6 (PC cm^{-6}) of the associated HII region. It is evident from the figure that the ratio

$I(S_{n_\alpha})$ / $I(C_{n_\alpha})$ depends upon the frequency of the n_α transition. For high frequency i.e. low n_α the ratio is small and it increases with the increase of n (decrease of frequency). From this figure it can be argued that low frequency transitions of S should have enough intensity to be observed, while high frequency transitions because of their low intensity may or may not be observed. Though most of the observed lines belong to low frequency group, yet some lines from high frequency group have also been observed. We think that detailed observational studies are needed to establish the frequency dependence of the line intensities of heavy elements especially of low frequency group. It should be further mentioned here that the ratio in question depends also upon the emission measure of the continuum of HII region. The ratio may increase or decrease as EM is increased. This dependance actually comes through the β factor (equation 4.38) that is sensitive to the electron density.

A detailed calculation for the line intensity C, Mg, Si, S and Fe have been carried out by us and their ratios are compared with the observations in Table 4.3. One may note:

i) The tabulated ratio $T_L(X)\ \Delta\nu_L(X)/\ T_L(C)\ \Delta\nu_L(C)$ for any element X and for any line is greater than the abundance ratio of Mg, Si, S and Fe to C for either abundance.

ii) The blend emission $\sum X$ gives a ratio greater than the observed value by different factors for different lines.

iii) The ratio increases with the decrease of frequency, because of the importance of background radiation, that enters through β factor, in the low temperature and low electron density region from where the heavy elements are contributing to the line intensities.

iv) Whereas in the case of NGC 2024 the ratio I(S)/I(C) for solar abundance is closer to the observed one than that for depleted abundance, the opposite is the case for Orion A and W3. However this is also possible that element S and C are both depleted by the same factor in the case of NGC 2024, and therefore the calculated ratio for the solar abundance will be closer to the observed one.

The identification of S as the heavy element emitter is consistent with the general feature of heavy element depletion obtained for ζ Oph and λ SCO. These observations show also that elements other than carbon and sulfur are depleted by an order of magnitude (Morton 1974, York 1975) due to which other elements are not contributing to the total line intensity.

4.6 H^o — Region

The narrow hydrogen recombination lines from cool and partially ionised medium (hereafter denoted as H^o) are observed

towards NGC 2024, W3 and Orion A (Ball et al.1970, Chaisson 1972, Chaisson and Goad 1972, Chaisson and Lada 1974 and Pankonin et al.1977). These lines have been found blended with the emission from HII region. The two gaussian decomposition of the observed profile yield consistent data for NGC 2024 and W3 but not for Orion A. Therefore, the latter is not included in Table 4.4. Further, angular size of H^{o} regions are not available, because the observations have generally been confined to low frequency measurements, where stimulated emission from the background radiation dominates.

The narrow hydrogen recombination lines have generally been studied towards NGC 2024. The data for α and β lines at the same frequency are available, and the ratio H 157α /H 197β > 7 is close to the observed ratio $\sim$.9 for carbon line at the same frequency. This observation indicates that physical condition of H^{o} and CII region are approximately same. The velocity difference ΔV_{LSR} (C-H) $\sim$ 0.5 are also observed for both the clouds W3 and NGC 2024. It can therefore be concluded that spatial extent of CII and H^{o} region are slightly different (Pankonin et al.1977). This conclusion is corroborated by the following consideration.

The ionisation of hydrogen through chlorine chemistry in the presence of UV flux from embedded hot star is discussed in detail in Chapter 2(see also Qaiyum and Ansari 1979,1983a).

It is clear from the Figure 2.2 and Diagram 1 that H^{o} and CII region do not coincide exactly but they have some region in common and the former is slightly shifted towards the HII region. Thus theoretically also it turns out that the physical conditions of H^{o} and CII regions are nearly the same.

The observed and our calculated intensity ratios of hydrogen and carbon at the same frequencies are given in Table 4.4 for NGC 2024 and W3. All the lines under consideration belong almost to the low frequency group ($\lesssim$ 2.7 GH_{Z}), which arises due to the stimulated emission from the foreground cloud. It is found that observed ratios fairly agree with the theoretical ratios for depleted abundance. It may be mentioned here that if observed H^{o} lines remain blended even after two gaussian decomposition, then their actual ratio will be probably closer to the theoretical results for solar abundance than the depleted one. Therefore one can not conclude from this table specifically that depleted abundance is the more favoured one. The detailed observational studies are required for H^{o} lines to derive the physical conditions and abundances of heavy elements.

Table 4.1a

NGC 2024 (W12) ; G 206.6 − 16.4

n_α	Frequency (GH_Z)	θ_{HPW} (arc min)	η_B beam efficiency	$T_L \Delta V \pm 3\sigma$ (K KH_Z)	References
76	14.7	2.3	.5	18.59 ± 8.32	Rickard et al.(1977)
85	10.5	3.2	.7	13.2 ± 1.4	MaCleod et al.(1975)
		3	.76	14.3 ± 2.24	Cited by Rickard et al.(1977)
		3	.76	19.93± 3.84	A.K. Dupree (1974)
92	8.3	4.0	.53	6.35± 2.48	Chaisson (1974)
94	7.8	4.2	.53	5.49± 2.45	Chaisson (1971)
109	5.0	6.45x6.3	.81	7.04± 1.68	Palmer (1968)
		6.45x6.3	.81	9.16± 1.68	Dupree (1974)
134	2.7	11	.76	8.68± 3.96	Dupree (1974)
		4.8	.65	15.86± 5.4	Wilson et al.(1975)
		11	.76	11.7 ± 1.8	Churchwell (1970)
137	2.56	11	.76	6.14± 2.3	Cesarsky (1971)
157	1.68	7.8	.65	18.32± 1.12	Pankonin et al.(1977)
		18	.7	3.75± 1.31	Ball et al.(1970)

Table 4.1a (Contd.)

n_α	Frequency (GH_Z)	θ_{HPW} (arc min)	η_B beam efficiency	$T_L \Delta V \pm 3\sigma$ (K KH_Z)	References
158	1.65	18	.7	4.27 ± .45	Chaisson et al.(1972)
166	1.425	21	.7	3.04 ± .9	Dupree (1974)
		8.5	.7	12.85 ± 1.5	Pankonin et al.(1977)
		13.0	.55	5.91	Pedlar & Hart (1974)
183	1.064	28	.66	2.03 ± 1.67	Dupree (1974)
198	.841	36	.67	1.008± 1.00	Zuckerman & Ball (1974)
210	.695	42	.77	1.4 ± 1.98	Dupree (1974)
220	.614	31	.49	.542± .19	Pedlar & Davis (1972)

Table 4.1b

Orion A W(10) G 209.0 —19.4

n_α	Frequency (GH_Z)	θ_{HPW} in arc min	η_B (beam efficiency)	$T_L \Delta V \pm 3\sigma$ (K KH_Z)	References
75	15.3	1.3	.5	22.41 ± 6.62	Kuiper & Evan (1978)
85	10.5	3	.76	22.85 ± 2.56	Dupree (1974)
		2.8	.70	19.54 ± 5.44	Balick et al.(1974)
		2.8	.58	24.53 ± 3.80	Jaffe & Pankonin (1978)
92	8.3	4.0	.53	18.54 ± 5.34	Chaisson (1974)
94	7.8	4.2	.53	11.57 ± 3.5	Dupree (1974)
109	5.0	6.45x6.3	.81	12.18 ± 3.94	Palmer (1968)
		6.45x6.3	.81	9.82 ± 2.5	Churchwell (1970)
		2.6	.58	13.98 ± 1.5	Jaffe & Pankonin (1978)
134	2.7	11	.76	7.23 ± 4.2	Dupree (1974)
157	1.68	18	.70	19.24 ± 6.0	Churchwell & Edrich (1974)
158	1.65	18	.70	6.05 ± 2.5	Churchwell (1970)
166	1.425	21	.70	8.08 ± 1.87	Dupree (1974)
		21	.70	6.02 ± 2.2	Chaisson & Lada (1974)

Table 4.1b (Contd.)

n_α	Frequency (GH_Z)	θ_{HPW} in arc min	η_B (beam efficiency)	$T_L \Delta V \pm 3\sigma$ (K KH_Z)	References
168	1.375	21	.70	9.57 ± 2.2	Simpson (1970)
183	1.064	28	.66	3.38 ± 2.44	Dupree (1974)
210	.695	42	.77	2.8 ± 3.64	Dupree (1974)
220	.614	31	.49	1.07 ± .5	Pedlar & Davis (1972)

Table 4.1c

W3 (IC 1795); G 133.7 + 1.2

n_α	Frequency (GH_Z)	θ_{HPW} in arc min	η_β (beam efficiency)	$T_L \Delta V \pm 3\sigma$ (K KH_Z)	References
76	14.7	2.3	.5	20.06 ± 8.32	Rickard et al. (1977)
85	10.5	3	.76	14.68 ± 1.75	Churchwell (1970)
		3	.76	18.88 ± 3.14	Cited by Rickard et al (1977)
92	8.3	4.0	.53	5.25 ± 2.4	Chaisson (1974)
94	7.8	4.2	.53	2.88 ± 1.08	Chaisson (1971)
109	5.0	6.45x6.3	.81	7.82 ± 3.16	Palmer (1968)
		6.45x6.3	.81	9.82 ± 2.5	Churchwell (1970)
		2.6	.65	20.78 ± 2.36	Pankonin et al.(1977)
134	2.7	11	.76	3.2 ± 1.2	Dupree (1974)
		4.8	.65	15.21 ± 3.90	Wilson et al.(1975)
157	1.68	18	.70	5.52 ± 1.42	Churchwell & Edrich (1970)
		18	.70	2.88 ± 1.68	Chaisson (1972)
158	1.65	18	.7	2.91 ± .74	Chaisson et al.(1972)
		7.8	.65	14.26 ± 1.30	Pankonin et al.(1977)
166	1.425	21	.70	3.8 ± 1.8	Dupree (1974)
		8.7	.70	9.3 ± .84	Pankonin et al.(1977)
168	1.375	21	.70	1.59 ± .52	Simpson (1970)
183	1.064	28	.66	< 3.50	Rickard et al.(1977)
198	.841	36	.67	< 1.84	Rickard et al.(1977)

Table 4.2

Comparison of ratio of intensities of α and β lines of carbon

Source	Lines	$T_L(n\alpha)/T_L(n'\beta)$		
		Observed values (ref.)	Calculated	
			Solar abundance	Depleted abundance
NGC 2024	85α/107β	-	2.1	3.0
	109α/137β	2.8(1)	3.0 (3.3, ref.2)	3.4
	157α/197β	9.8(2)	9.1 (7.0, ref.2)	8.9
Orion A	85α/107β	2.9(3)	2.3	3.1
	109α/137β	~3 to 4(4)	3.0	3.5
	166α/211β	~6 (5)	5.9	5.8
W3	85α/107β	-	2.8	3.1
	109α/137β	3 (2)	3.4	3.5
	158α/199β	7.3(2)	7.3	7.3

Reference: 1. Cesarsky (1971), 2. Pankonin et al. (1977),
3. Ahmad (1976a), 4. Palmer(1968), 5. Simpson (1970).

Table 4.3

Ratio's of line intensities $T_L(X)\ \Delta\nu_L(X)/T_L(C)\Delta\nu_L(C)$ of carbon and heavy elements

Source	Lines	Observed (Ref.)	Calculated (Solar abundance)					Calculated (Depleted abundance)				
			S	Si	Mg	Fe	Σx	S	Si	Mg	Fe	Σx
NGC2024	92α	.10(1)	.10	.23	.20	.15	.68	.22	.035	.04	.014	.30
	134α	.10(2)	.14	.34	.26	.21	.95	.33	.05	.06	.016	.44
	157α	.19(3)	.30	.58	.44	.40	1.72	.44	.07	.09	.008	.61
	158α	.14(5)	.30	.58	.44	.40	1.72	.44	.07	.09	.008	.61
	166α	.18(3)] .23(4)]	.32	.62	.47	.44	1.85	.49	.08	.09	.008	.63
Orion A	85α	.21(7)	.06	.15	.15	.10	.46	.22	.03	.04	.01	.32
	92α	.38(8)	.07	.16	.16	.12	.49	.24	.04	.05	.01	.34
	109α	.23(9)	.10	.20	.20	.15	.65	.27	.04	.05	.01	.37
	158α	.21(8)	.13	.26	.25	.19	.83	.25	.04	.05	.01	.35
	166α	.35(8)	.14	.28	.26	.20	.88	.28	.04	.05	.01	.38
W3	92α	.36(1)	.09	.20	.18	.14	.61	.24	.04	.05	.005	.34
	109α	.50(3)	.10	.20	.19	.14	.63	.28	.04	.05	.005	.38
	157α	.42(6)	.12	.24	.23	.18	.77	.43	.07	.09	.008	.60
	158α	.25(3)] .32(5)]	.12	.24	.23	.18	.77	.44	.07	.09	.008	.61
	166α	.14(3)] .12(4)]	.125	.25	.24	.18	.80	.48	.08	.09	.008	.62

1. Chaisson(1974), 2. Wilson et.al.(1975), 3. Pankonin et al.(1977), 4. Pedlar & Hart (1974), 5. Chaisson et al.(1972), 6. Chaisson (1972), 7. Ahmad (1976b), 8. Chaisson (1973), 9. Jaffe & Pankonin (1978).

Table 4.4

Comparison of line intensities of carbon and "narrow" hydrogen, $T_L(H)\,\Delta\nu_L(H)/T_L(C)\,\Delta\nu_L(C)$

Source	Transition	Observed (ref.)	Calculated	
			Solar	Depleted
NGC 2024	94α	.90(6)	.32	.64
	134α	.80(1)	.31	.62
	157α	.67(2) .67(4)	.31	.62
	166α	.58(2) .80(3)	.31	.62
W3	134α	.60(1)	.30	.61
	157α	.45(5)	.28	.60
	158α	.76(2)	.28	.60
	166α	1.2(2) 1.33(3)	.28	.60

1. T. Wilson et al.(1975), 2. Pankonin et al. (1977),
3. Pedlar & Hart (1974), 4. Ball et al.(1970),
5. Chaisson (1972), 6. Chaisson (1971).

Table 4.5

Best fit model Parameters derived from carbon intensities

Source	Position	Solar abundance				Depleted abundance			
		n_H	angular size	Depth L (pc)	E.M.of H II region	n_H	angular size	Depth L (pc)	E.M.of H II region
NGC2024	Background	5×10^4	3.2	.027	8×10^5	2×10^6	2.4	.0015	10^6
	Foreground	6×10^4	1.73	.042	8×10^5	5×10^5	4.5	.007	8×10^5
Orion A	Background	10^5	3.2	.04	2×10^7	2.5×10^6	7.3	.001	2×10^7
	Foreground	2×10^4	6.15	.23	10^5	5×10^4	6.5	.096	10^6
W3	Background	4×10^5	1.1	.006	10^7	2.5×10^6	3.5	.001	2×10^6
	Foreground	5×10^4	1.54	.088	5×10^5	2×10^5	3.8	.021	10^6

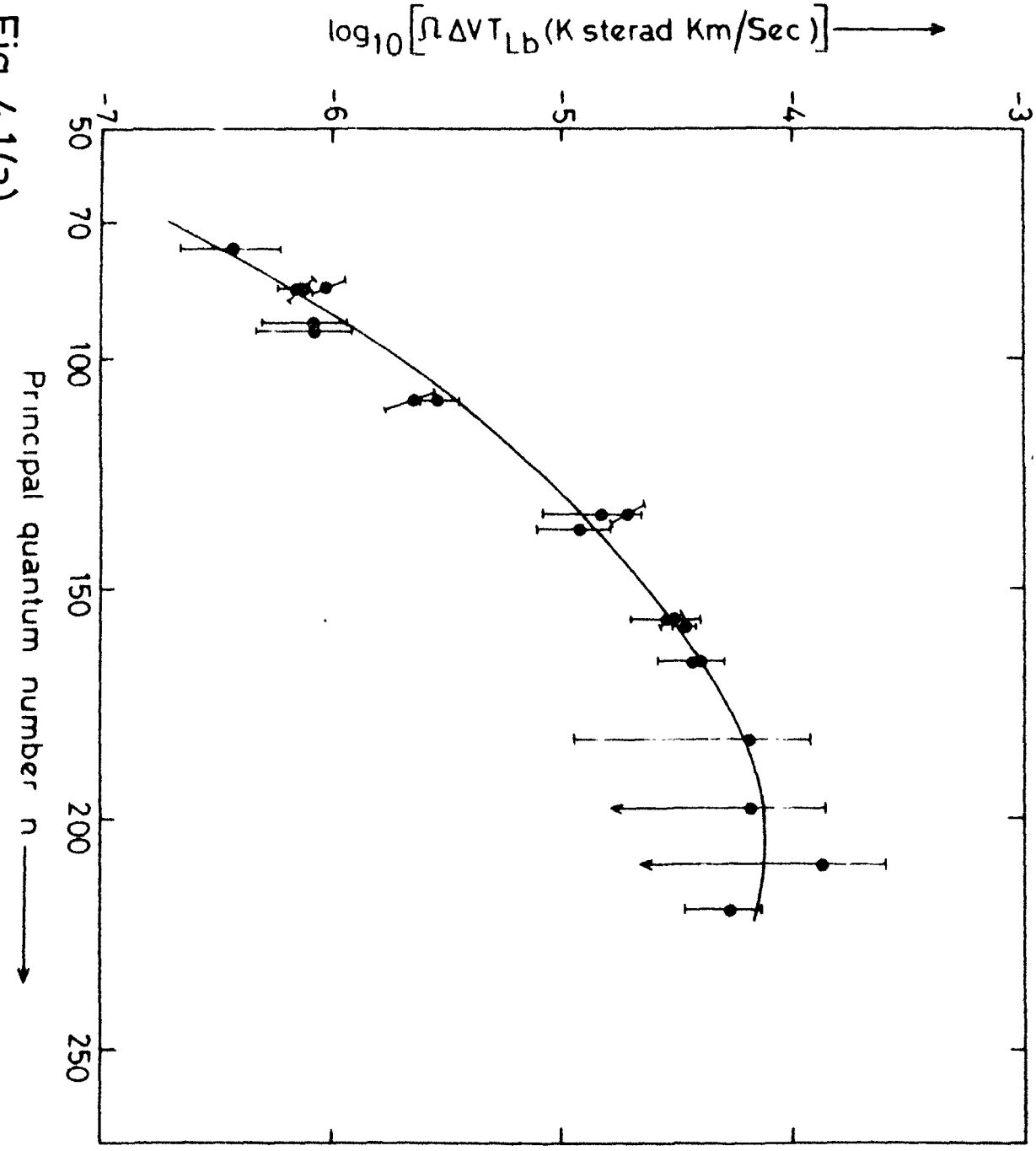
$\log_{10}[\Omega \Delta V T_{Lb}$ (K sterad Km/Sec)]
-7
-6
-5
-4
-3
50
70
100
150
200
250
Principal quantum number n

Fig. 4.1(a)

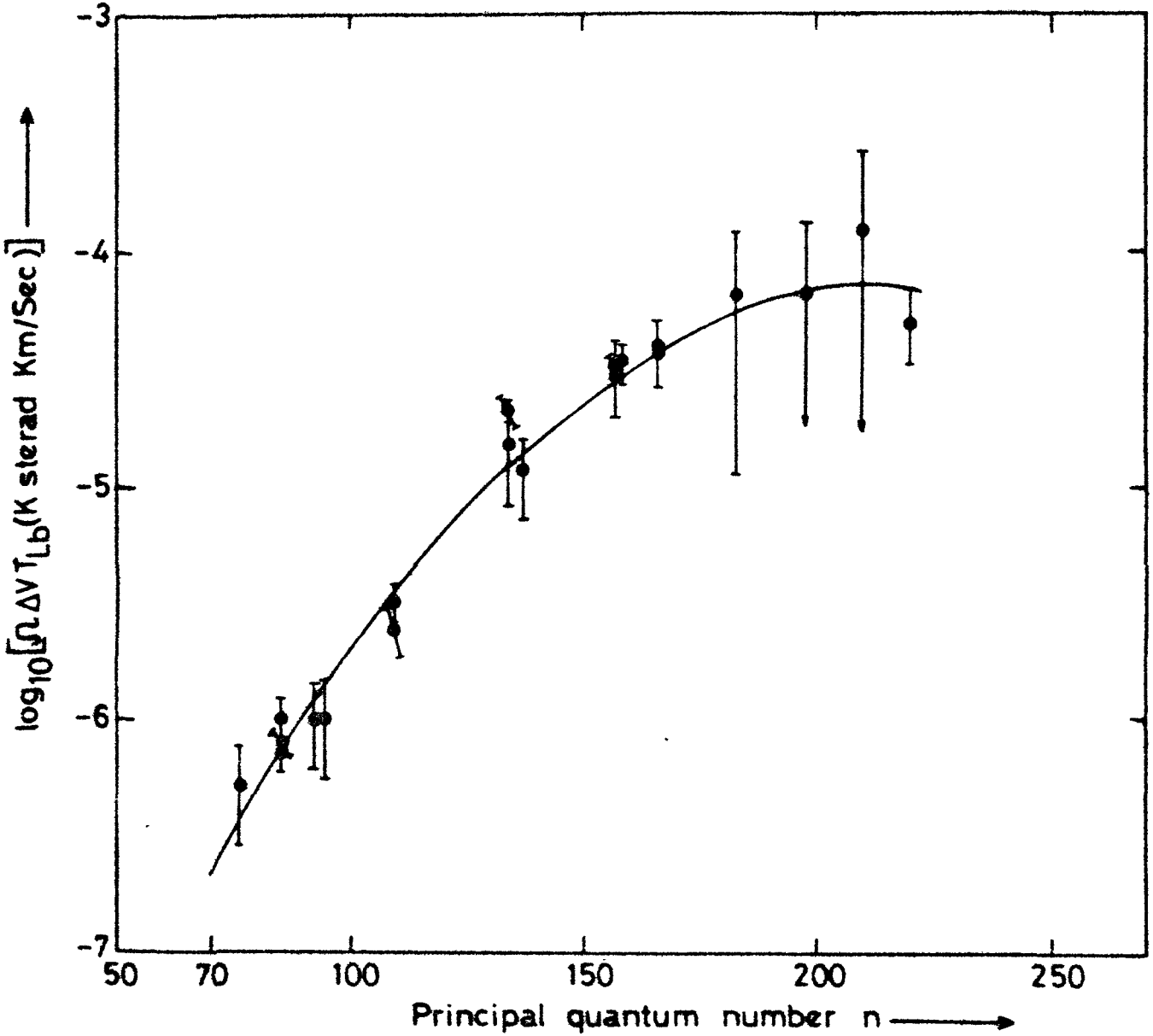
-3
-4
-5
-6
-7
50
70
100
150
200
250
$\log_{10}[\Omega.\Delta V T_{LB}(K\ sterad\ Km/Sec)]$
Principal quantum number n

Fig. 4.1(b)

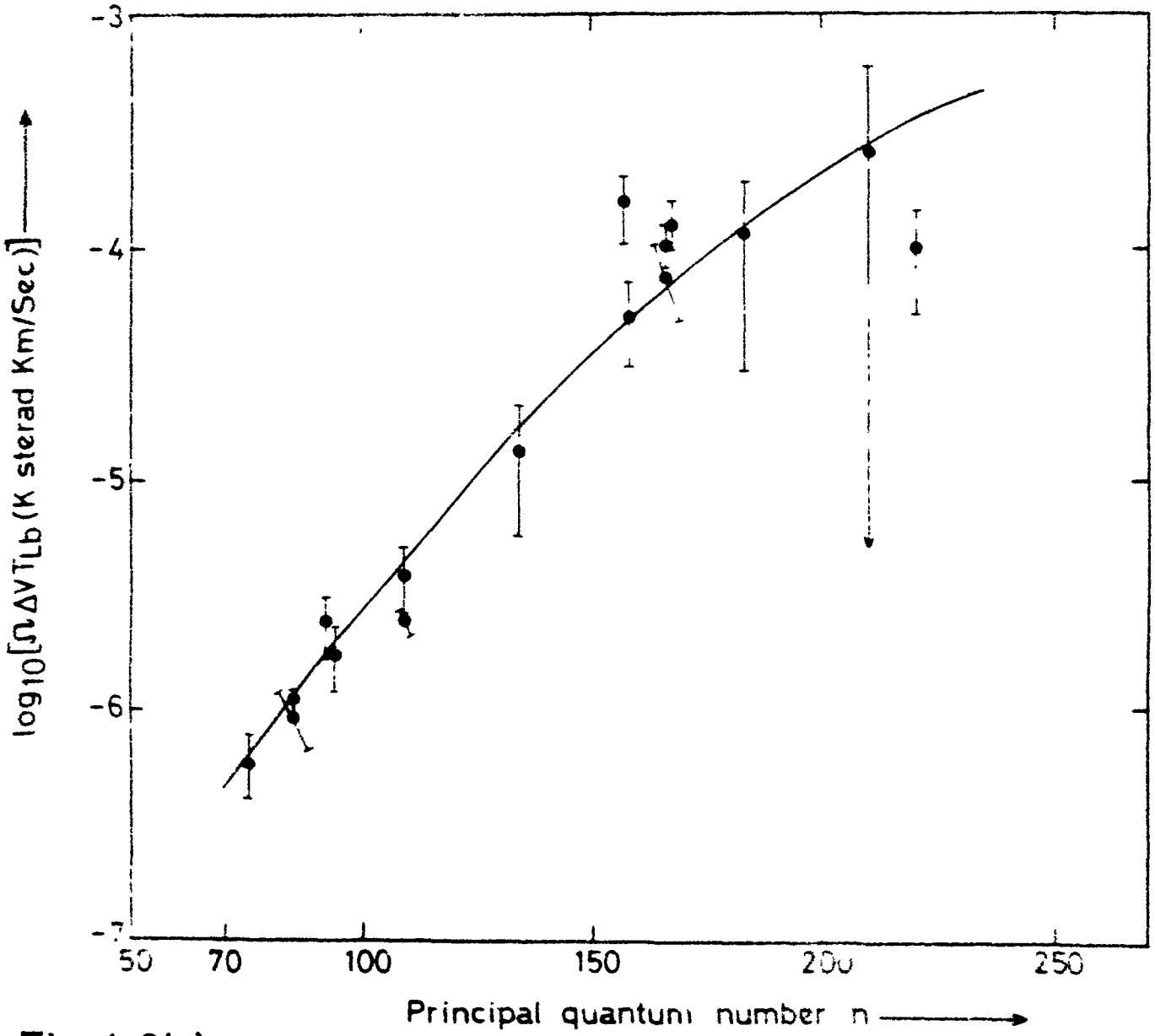
-3
-4
-5
-6
-7
50
70
100
150
200
250
log10[Ω.ΔVTLb (K sterad Km/Sec)]
Principal quantum number n

Fig. 4·2(a)

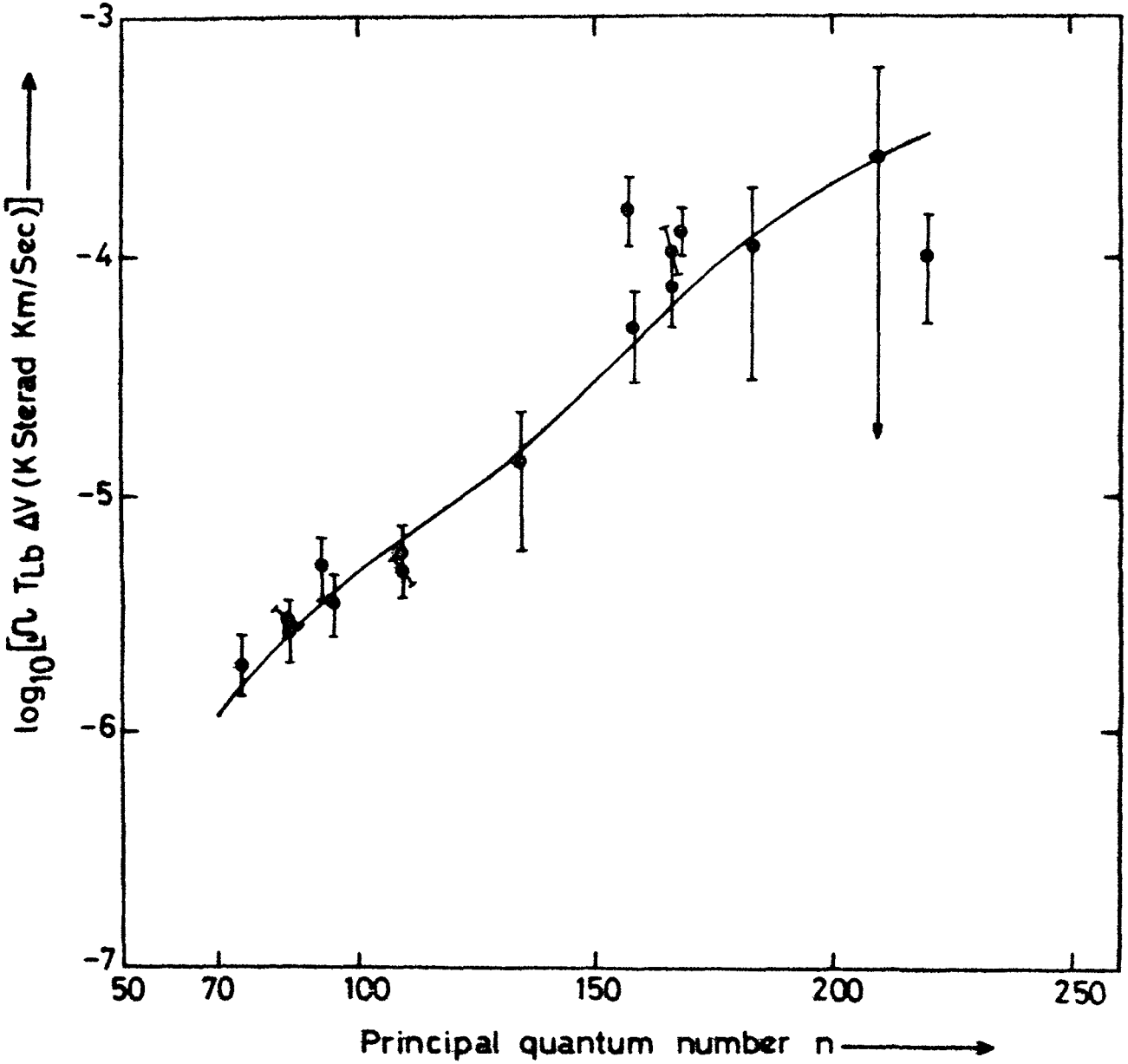
-3
-4
-5
-6
-7
50
70
100
150
200
250
log10[∫n TLb ΔV (K Sterad Km/Sec)]
Principal quantum number n

Fig.4.2(b)

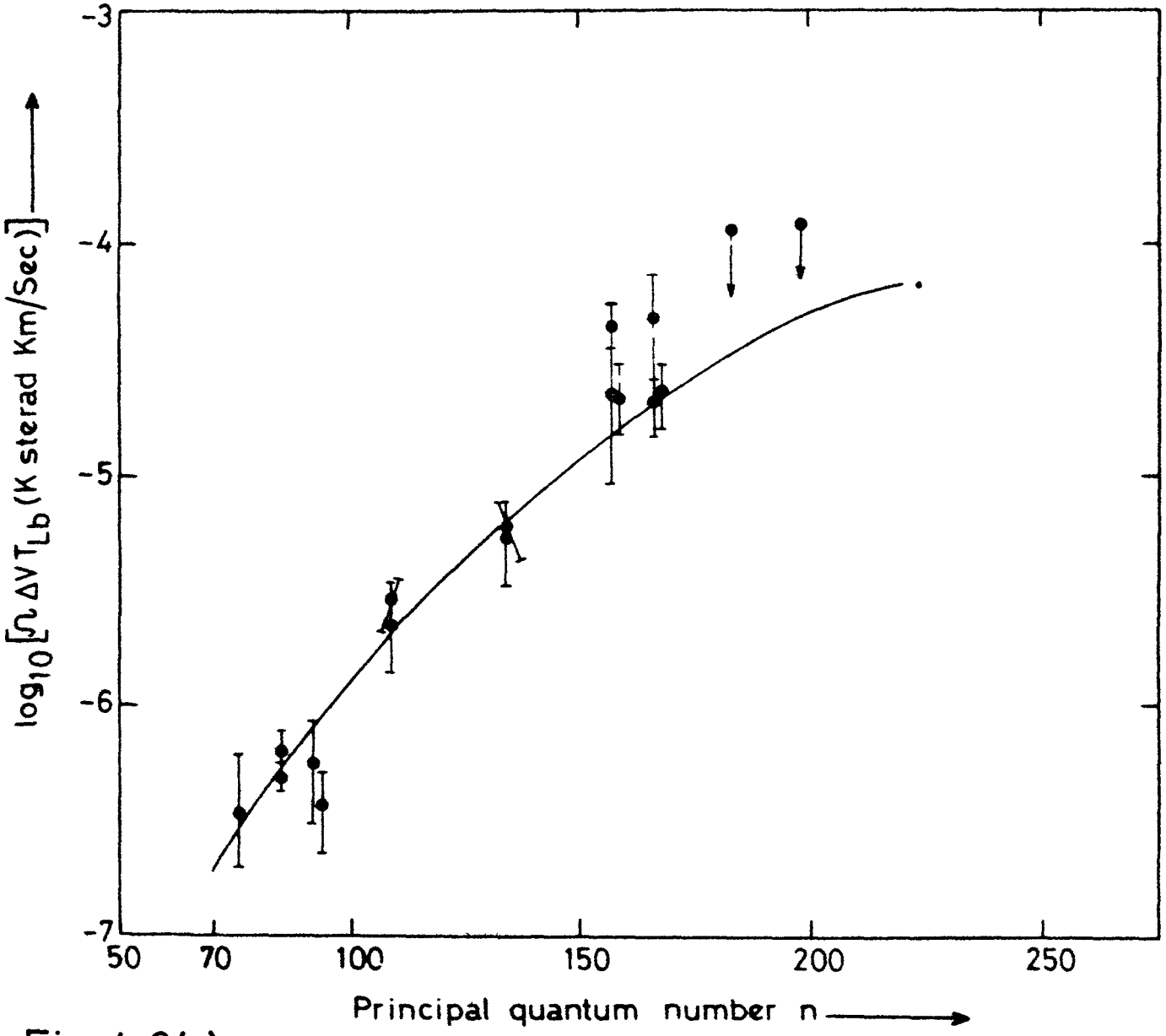
-3
-4
-5
-6
-7
50
70
100
150
200
250
$\log_{10}[\int \Delta V T_{Lb}$ (K sterad Km/Sec)]
Principal quantum number n

Fig. 4.3(a)

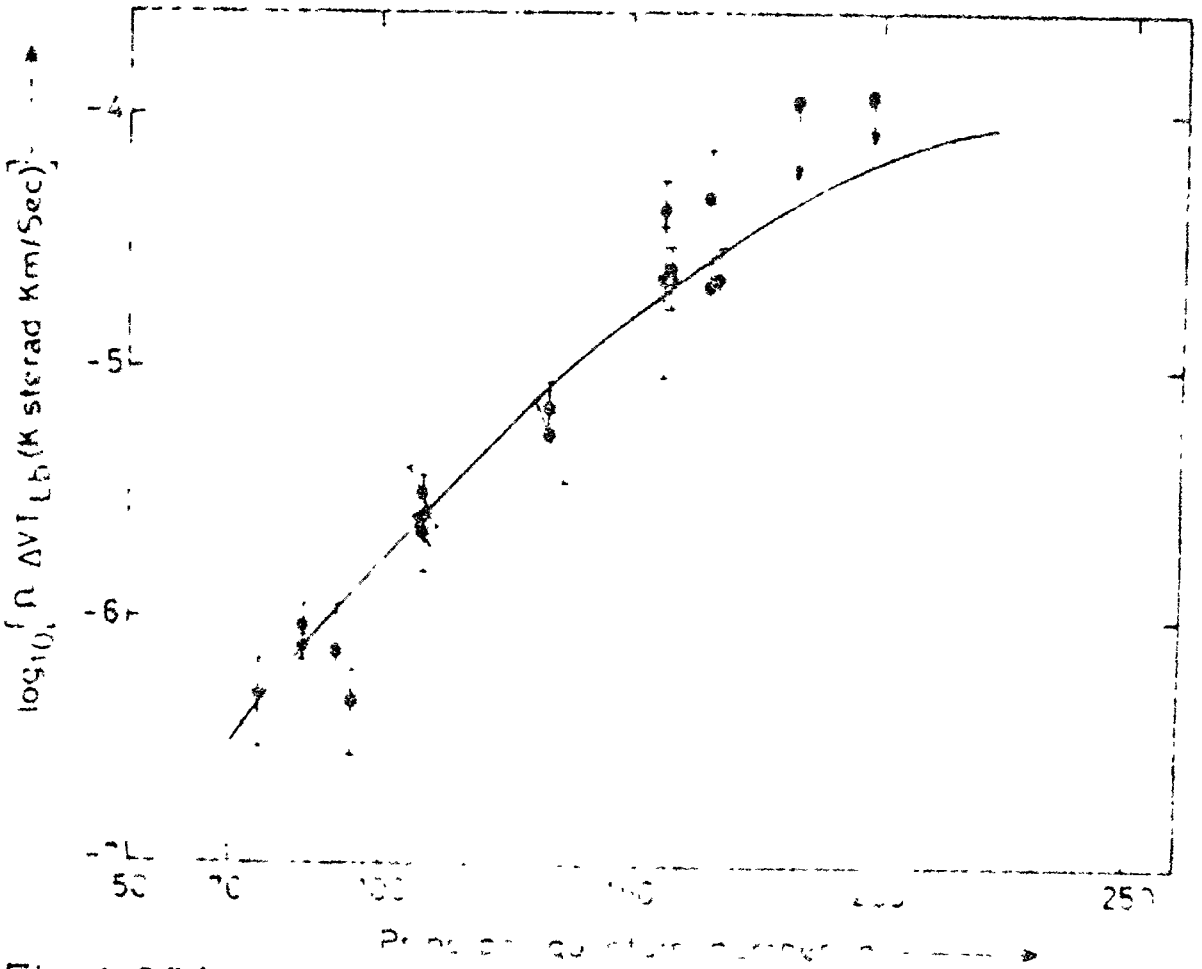

Fig. 4.3(b)

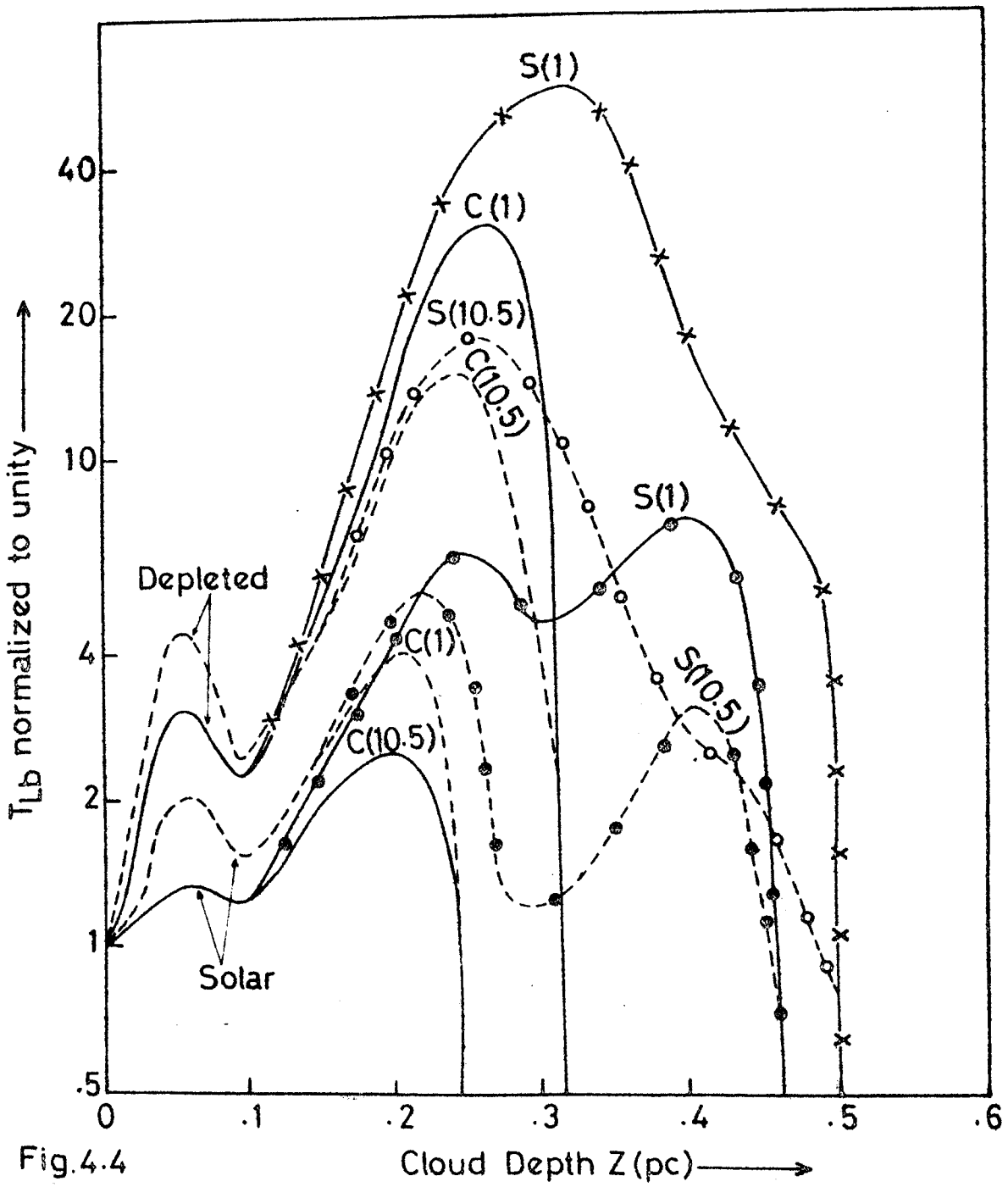
S(1)
C(1)
S(10.5)
C(10.5)
S(1)
S(10.5)
C(1)
C(10.5)
Depleted
Solar
40
20
10
4
2
1
.5
0
.1
.2
.3
.4
.5
.6
T_{Lb} normalized to unity
Cloud Depth Z (pc)

Fig.4.4

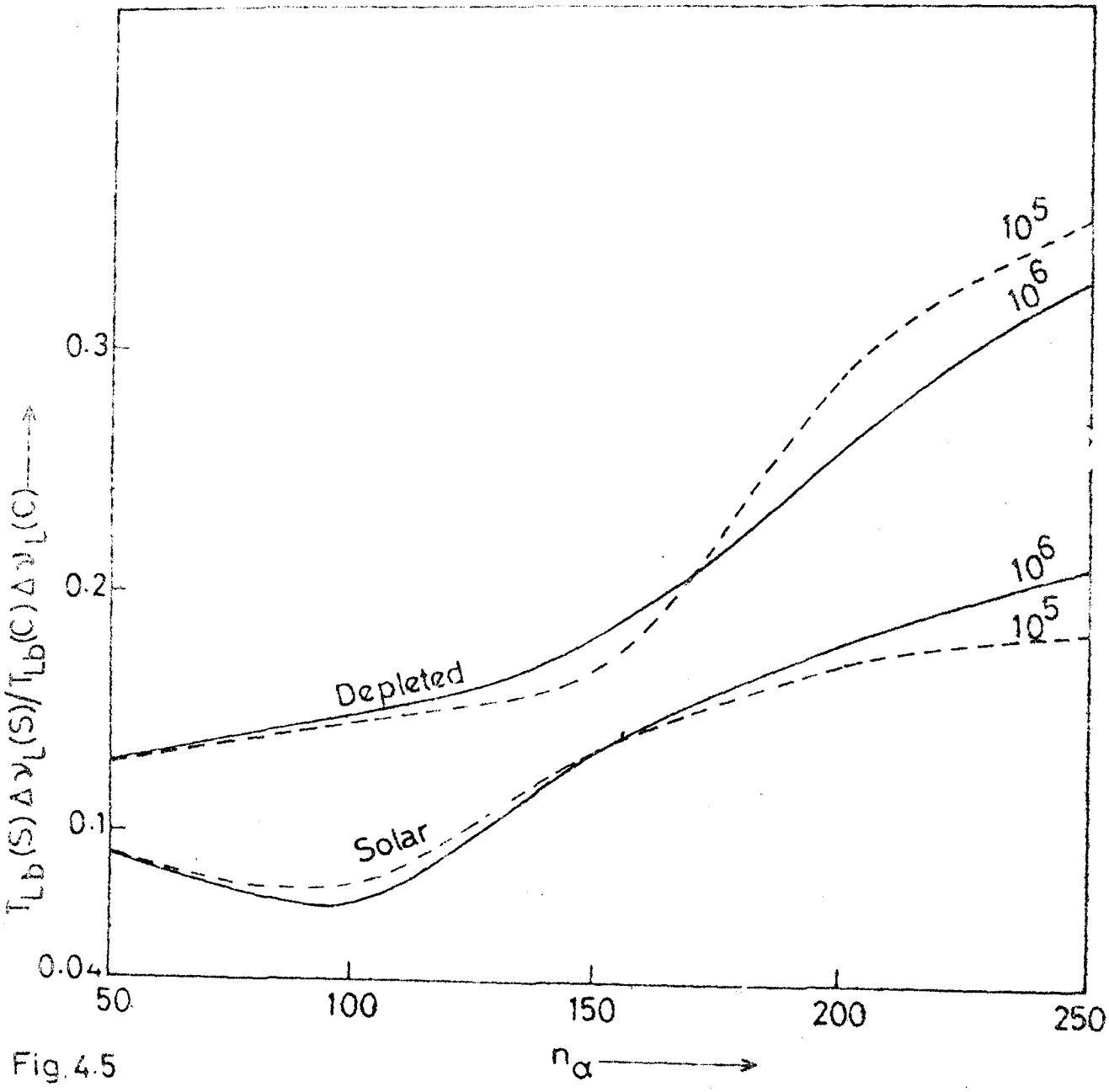
0.3
0.2
0.1
0.04
50
100
150
200
250
n_α
$T_{Lb}(S)\,\Delta\nu_L(S)/T_{Lb}(C)\,\Delta\nu_L(C)$
Depleted
Solar
10^5
10^6
10^6
10^5

Fig. 4.5

FIGURE CAPTIONS

Fig.4.1. Comparison for observed brightness of α lines of carbon for NGC 2024, in units of the product of the line width in km/sec and source size in steradian, with theoretical results (a) for solar abundance (b) for depleted abundance.

Fig.4.2. Comparison of observed brightness of α -lines of carbon for Orion A, in units of the product of the line width in km/sec and source size in Steradian, with the theoretical results for (a) solar abundance (b) depleted abundance.

Fig.4.3. Comparison of observed brightness of α lines of carbon for W3, in units of the product of the line width in km/sec and source size in Steradian, with the theoretical results (a) for solar abundance (b) for depleted abundances

Fig.4.4. Variation of line brightness temperature (T_{Lb}) as a function of position in the cloud for solar and depleted abundances of C(carbon) and S (sulfur) at 1 GH_Z and 10.5 GH_Z.

Fig.4.5. Variation of line intensity ratio of S to C as a function α transitions (n_α) for solar and depleted abundances and two assumed emission measures (10^5 and 10^6 Pc cm^{-6}) of H II region.

CHAPTER 5

SUMMARY AND CONCLUSION

During the last decade the physics of formation and transfer of radio-recombination lines in cold gas has been thoroughly described and many troublesome problems have been solved. But detailed theoretical attempts were not made for cool region to explain the high ionisation rate of hydrogen. The rate is calculated here using reaction of ClII with H_2, and we also establish here a relationship between the regions emitting the narrow recombination lines of hydrogen, carbon and other heavy elements. It is now widely recognised that observed line emission depends sensitively upon the density, temperature and their gradients (Brown et al.1978), but these lines from cool regions have not been interpreted in terms of gradients of density and temperature. We have therefore carried out line-intensities calculation taking into account the density and temperature structure of the cold clouds in interstellar medium.

Here the basic difference from earlier attempts lies in the fact that a detailed chemical balance is set up between formation and destruction mechanisms of a particular species to deduce the density (abundance) structures of electrons, important atomic, ionic and of molecular species in the cloud. Also a thermal balance between cooling and heating is considered to deduce the temperature structure of the region in question. Investigations

on the importance of far infra-red radiations from dust grains of HII regions on the cooling in HI region at low temperature is also reported here.

The line intensities are calculated assuming the plane-parallel geometry and dividing the cloud into equally thick, isothermal and homogeneous thin slabs. A best fit is carried out taking the hydrogen density n_H, emission measure (EM) of the associated HII regions and cloud size as independent and free parameters, instead of electron density n_e and temperature T_e (which in turn depend upon n_H) as was done by earlier research workers. Further in addition to 3^oK general background radiation the continuum radiation from HII region and also from dust grain are taken into consideration to calculate the intensity of recombination lines.

The following conclusions may be drawn from our calculations. Some of which are corroborated by experimental evidence.

i) The regions of ionised carbon(CII) and partially ionised hydrogen (H^o) are well separated from the adjacent molecular region other than H_2. They are themselves not only associated with each other but have also some region in common (Diagram 1). Experimentally observed small difference in radial velocities of C and H (MacCleod et al 1975, Wilson et al 1975) favours the above argument. The H^o region appears to be located between HII and CII regions but nearer to the outer boundary of

the HII regions. Thus it explains the radial velocity of narrow hydrogen line which is slightly displaced towards the central velocity of HII region (Pankonin et al.1977). Intensity ratio of hydrogen to carbon can easily be explained with the help of ionisation of hydrogen through chlorine chemistry (Qaiyum and Ansari 1979) and a detailed calculation favours a depletion of carbon. Further observations of hydrogen recombination lines are needed for a definite conclusion. It may added that intensity ratio of hydrogen to carbon decreases with increasing n_H. Therefore at high density of n_H the narrow hydrogen lines may be absent.

ii) The spatial extension of ionised carbon and other heavy elements are not identical but heavy elements are ionised to a greater depth having some domain common with the molecular region (Figures 2.1(a) and (b), Diagram 1). For the same conclusion see Pankonin et al.(1977). Small difference in the radial velocties obtained from recombination lines of any element also favours a close association of these regions. Further on the basis of our calculation of ionisation structure (Figures 2.1(a) and(b)) it may be argued that physical conditions derived from the heavy element lines will be closer to that observed from the molecular lines.

The theoretical blend emission $\sum_X T_L(X)\,\Delta\nu_L(X) \,/\, T_L(C)\,\Delta\nu_L(C)$ does not give appreciably higher value than the observed ratio of intensity of the lines of the unknown element to that of

carbon. We conclude that the unknown element may be identified as sulphur, the others being heavily depleted. This conclusion is also consistent with the general depletion feature obtained for ζOph and λSco (Morton 1974, York 1975).

iii) Theoretically two regions of neutral hydrogen have been identified having column densities $\backsim 2\times10^{21}$ cm^{-2} and $\backsim 2\times10^{20}$ cm^{-2} for $n_H \gtrsim 10^4$ cm^{-3}. The former having greater column density is close to the HII region and also closely associated with the CII, H^o and also the region of heavy elements. The latter is only associated with the molecular region. Compare the observational evidence that two or more components of neutral hydrogen exist, having column densities $\backsim 3\times10^{21}$ cm^{-2} and $\backsim 2.9\times10^{20}$ cm^{-2} (Radhakrishnan et al.1972) and the former region has radial velocity very near to those obtained from the recombination lines of any element, thus corroborating a close association of these regions.

iv) The interpretation of recombination lines favours two or more components contributing to the line emission. The components are found to have hydrogen density in the range 2×10^4 to 4×10^5 cm^{-3} for solar abundance and 5×10^4 to 2×10^6 cm^{-3} for depleted abundance; both the abundances fit to the observation within experimental error. High frequency lines are found being emitted from the background component (high density) while low frequency lines are emitted predominantly from the foreground

component of low density. Theoretically it is found that OH and H_2CO molecules may be predominantly from the low density region while contribution to column density of CO is equally from both the regions. Radial velocities patterns of the molecules and CII lines favours this prediction (Pankonin et al. 1977). Moreover, calculated column density of OH is also in agreement with the observed value for $n_H \gtrsim 10^4$ cm^{-3}.

v) As mentioned in the preceding para in the case of depleted abundance, a higher density of hydrogen is required to explain the frequency pattern of the recombination lines of carbon. Therefore a slightly more depletion than assumed here will require a value of $n_H > 10^6$ cm^{-3} to interpret the recombination line intensities of carbon. But for this density $n_H > 10^6$ cm^{-3} the temperature obtained in the outer region of the cloud will be $\gtrsim$ 300 K (Qaiyum and Ansari 1983a). At these or slightly higher density and temperature the detection probability of the recombination lines will be very low and they may not be obsevable. Further for $n_H > 10^6$ cm^{-3} the beam dilution would also be insurmountable. Therefore in the regions, where carbon is heavily depleted and even though they are associated with the HII regions, the carbon line emission could not be detected. This may be one of the reasons of the absence of the carbon recombination lines in the neighbourhood of many HII regions.

As a wealth of data is available for other clouds, a detailed study will be carried out on the basis of the present work, to interpret the line emission and also to deduce the characteristics of the regions. Then with a comprehensive study we may conclude fairly well about the degree of depletion of elements and also about the most efficient source of ionisation of hydrogen described here. Further, a line-profile study of CO molecule for these regions will clarify the understanding of the region and will also lead to ideas about the velocity field and kinematics of the clouds.

******

REFERENCES

Ahmad, I.A., 1976a. Ap. J., 205, 379.

Ahmad, I.A., 1976b. Ap. J., 209, 462.

Allen, M. & Robinson, G.W., 1976. Ap. J., 207, 745.

Allison, A.C. & Dalgarno, A., 1970. Atomic Data, 1, 289.

Auer, L.H. & Mihalas, D., 1972. Ap. J.Suppl., 24, 205.

Balick, B., Gammon, R.H. & Doherty, L.H., 1974. Ap. J., 188, 45.

Ball, J.A., Cesarsky, D.A., Dupree, A.K., Goldberg, L. &
Lilley, A.E., 1970. Ap. J., 162, L 25.

Barlow, M.J. & Silk, J., 1976. Ap. J., 207, 131.

Barsuhn, J., 1977. Astron. Astrophys.Suppl. Series, 28, 453.

Bates, D.R. & Dalgarno, A., 1962. 'Atomic and Molecular
Processes', ed. D.R. Bates, New York Academic Press.

Biondi, M.A., 1969. Canadian J. Chemistry, 47, 1711.

Black, J.H., 1975. Ph.D. Thesis, Harvard University.

Black, J.H. & Dalgarno, A., 1973. Ap. J., 184, L101.

Black, J.H. & Dalgarno, A., 1977. Ap. J.Suppl.Series, 34, 405.

Bohlin, R.C., 1975. Ap. J., 164, 387.

Breig, E. & Lin, C.C., 1966. Phys. Rev., 151, 67.

Brocklehurst, M., 1971. Mon. Not. R. Astro.Soc., 153, 471.

Brocklehurst, M. & Salem, M., 1977. Computer Physics Commun.,
13, 39.

Brocklehurst, M. & Seaton, M.J., 1972. Mon. Not. R. Astron. Soc.,
157, 179.

Brown, R.L., Lockman, F.J. & Knapp, G.R., 1978. Ann. Rev. Astron. Astrophys., 16, 445.

Carter, S.L. & Kelley, H., 1976. Phys. Rev. A, 13, 1388.

Cesarsky, D.A., 1971. Ap. J. Letters, 167, L89.

Chaisson, E.J., 1971. Ap. J., 170, 81.

Chaisson, E.J., 1972. Nature Phys. Sci., 239, 83.

Chaisson, E.J., 1973. Ap. J., 182, 767.

Chaisson, E.J., 1974. Astron. J., 79, 555.

Chaisson, E.J. & Good, L.E., 1972. Ap. J. Letters, 171, 161.

Chaisson, E.J. & Lada, C.J., 1974. Ap. J., 189, 227.

Chaisson, E.J., Black, J.H., Dupree, A.K. & Cesarsky, D.A., 1972. Ap. J. Letters, 173, L131.

Chapman, R.D. & Henry, R.J.W., 1971. Ap. J., 168, 169.

Chapman, R.D. & Henry, R.J.W., 1972. Ap. J., 173, 243.

Chu, Shih-I & Dalgarno, A., 1975. Proc. Roy. Soc. London., A342, 191.

Churchwell, E.B., 1970. Ph.D. Thesis, Indiana University,U.S.A.

Churchwell, E.B. & Edrich, J., 1970. Astron. Astrophys., 6,261.

Churchwell, E., Mezger, P.G. & Huchtmeier, W., 1974. Astron. Astrophys.,32, 283.

Clavel, J., Viala, Y.P. & Bell, N., 1978. Astron.Astrophys., 65, 435.

Cook, G.R., Mezger, P.H. & Ogawa, M., 1965. Canadian J.Phys., 43, 1706.

Cravens, T.E. & Dalgarno, A., 1978. Ap. J., 219, 750.

Dalgarno, A. & McCray, R.A., 1972. Ann. Rev.Astron. Astrophys., 10, 375.

Dalgarno, A., Black, J.H. & Weisheit, J.C., 1973. Astrophys. Letters, 14, 77.

de Jong, T., 1972. Astron.Astrophys., 20, 263.

de Jong, T., 1977. Astron. Astrophys.,55, 137.

de Jong, T., Chu, Shih-I & Dalgarno, 1975. Ap. J., 199, 69.

de Jong, T., Dalgarno, A. & Boland, W., 1980, Astron.Astrophys., 91, 68.

Draine, B.T., 1978. Ap. J. Suppl., 36, 595.

Dravskikh, Z.V. & Dravskikh, A.F., 1964. Astron. Tsirk., No.282.

Dubau, J. & Wells, J., 1973. J. Phys. B., 6, L31.

Dubrovskii, G.V. & Ob'edkov, V.D., 1967. Soviet Astron. A.J., 11, 305.

Dupree, A.K., 1974. Ap. J., 187, 25.

Elander, N., & Smith, W.H., 1973. Ap. J., 184, 663.

Elitzur, M. & de Jong, T. 1978. Astron.Astrophys. 67, 323.

Fehsenfeld, F.C., 1976. Ap. J., 209, 638.

Fehsenfeld, F.C. & Ferguson, E.E., 1973. J. Geophys. Res., 78, 1699.

Flower, D.R. & Launay, J.M., 1977. J. Phys. B: Atom.Molecul. Phys., 10, L229.

Gee, C.S., Percival, I.C., Lodge, J.G. & Richards, D., 1976. Mon. Not. R. Astron. Soc., 175, 209.

Gerola, H. & Glassgold, A.E., 1978. Ap. J. Suppl., 37, 1.

Glassgold, A.E. & Langer, W.D., 1974. Ap. J., 193, 73.

Glassgold, A.E. & Langer, W.D., 1976. Ap. J., 206, 85.

Goldreich, P. & Kwan, J., 1974. Ap. J., 193, 73.

Goldsmith, P.F. & Langer, W.D., 1978. Ap. J., 222, 881.

Green, S. & Thaddeus, P., 1976. Ap. J., 205, 766.

Habing, H.J., 1968. B.A.N., 19, 421.

Herbst, E., 1976. Ap. J., 205, 94.

Herbst, E., 1978. Ap. J., 222, 506.

Herbst, E. & Klemperer, W., 1973. Ap. J., 185, 505.

Henry, R.J.W., 1970. Ap.J., 161, 1153.

Hoang-Binh, D. & Walmsley, C.M., 1974. Astron.Astrophys., 35, 49.

Hudson, R.D., 1971. Rev. Geophys. Space Phys., 9, 305.

Huntress, W.T., 1977. Ap. J. Suppl., 33, 495.

Huntress, W.T. & Anicich, V.G., 1976. Ap. J., 208, 237.

Jaffe, D.T. Pankonin, V., 1978. Ap. J., 226, 869.

Johnsen, R. & Biondi, M.A., 1974. J. Chem. Phys., 61, 2112.

Jura, M., 1974. Ap. J., 190, L34.

Jura, M., 1976. Ap. J., 204, 12.

Jura, M. & York, D.G., 1978. Ap. J., 219, 861.

Kardashev, N.S., 1959. Soviet Astr-A.J., 3, 813.

Katayama, D.H., Huffman, R.E. & O'Bryan, C.L., 1973.
J. Chem. Phys., 59, 4309.

Kelley, H., 1973. Phys. Rev. A., 6, 1048.

Kim, J.K., Theard, L.P. & Huntress, W.T., 1975.
J. Chem. Phys., 62, 45.

Kuiper, T.B.H. & Evans II, N.J., 1978. Ap. J., 219, 141.

Langer, W.D., 1976. Ap. J., 206, 699.

Launay, M.J. & Roueff, E., 1977a. Astron.Astrophys., 56, 289.

Launay, J.M. & Roueff, E., 1977b. J. Phys. B: Atom. Molecul.
Phys., 10, 879.

Leu, M.T., Biondi, M.A. & Johnsen, R. 1973. Phys. Rev., A8, 413.

Leung, C.M. & Liszt, H.S., 1976. Ap. J., 208, 732.

Lillie, C.F. & Witt, A.W., 1976. Astron.Astrophys., 25, 397.

Macleod, J.M., Doherty, L.H. & Higgs, L.A., 1975. Astron.
Astrophys., 42, 195.

Matsunaga, F.M. & Watanabe, K., 1967. Science of Light, 16, 31.

McGowan, J.W., 1979. (Cited in de Jong et al. 1980).

McGuire, E.J., 1968. Phys. Rev., 175, 20.

Menzel, D.H., 1968. Nature, 218, 756.

Mitchell, G.F., Ginsburg, J.L. & Kunze, P.J., 1978.
Ap. J. Suppl., 38, 39.

Morton, D.C., 1974. Ap. J. Letters, 193, L35.

Mul, P.M. & McGowan, J. Wm., 1979. Ap. J. Letters, 227, L157.

O'Donnell, E.J. & Watson, W.D., 1974. Ap. J., 192, 29.

Oppenheimer, M. & Dalgarno, A., 1974. Ap. J., 192, 29.

Oppenheimer, M., 1975., Ap. J., 196, 251.

Palmer, P.E., 1968. Ph.D.Thesis, Harvard University.

Palmer, P., Zuckerman, B., Penfield, H., Lilley, A.E. &
Mezger, P.G. 1967. Nature, 215, 40.

Panagia, N. & Walmsley, C.M., 1978, Astron.Astrophys.,
70,411.

Pankonin, V., 1980. 'Radio Recombination Lines',
D. Reidel Publ., p.111.

Pankonin, V. & Walmsley, C.M., 1976. Astron.Astrophys.,
48, 341.

Pankonin, V., Walmsley, C.M., Wilson, T.L. & Thomasson, P.,
1977. Astron. Astrophys., 57, 341.

Peach, G., 1967. Mem. R.A.S., 71, 29.

Pedlar, A. & Davies, R.D., 1972. Mon.Not.R.Astron.Soc.,
159, 129.

Pedlar, A. & Hart, L., 1974. Mon.Not.R.Astron., 168, 577.

Pengelly, R.M. & Seaton, M.J., 1964. Mon.Not.R.Astro.Soc.,
127, 165.

Penston, M.V., 1970. Ap. J.,162, 771.

Prasad, S.S. & Huntress, W.T., 1979. Ap. J., 228, 123.

Qaiyum, A., 1976. 'M.Phil.dissertation', A.M.U., Aligarh.

Qaiyum, A. & Ansari, S.M.R., 1979. Mon.Not.R.astr.Soc.,186,621.

Qaiyum, A. & Ansari, S.M.R., 1983a. Mon. Not. R. Astro.Soc. (In press).

Qaiyum, A. & Ansari, S.M.R., 1983b. (Submitted for publication) Publication of Astronomical Society of Japan.

Radhakrishnan, V., Goss, W.M, Murray, J.D. & Brook, J.W., 1972. Ap. J. Suppl., 24, 49.

Raftery, J. & Richards, W.G., 1973. J.Phys.B., 6, 1301.

Raouf, A.S.M., Jones, J. D.C., Lister, D.G., Birkinshaw, K. & Twiddy, N.D., 1980. J. Phys. B.: Atom.Molecul. Phys., 13, 2581.

Rickard, L.J., Zuckerman, B., Palmer, P. & Turner, B.E., 1977. Ap. J., 218, 659.

Salem, M., 1975. Mon. Not. R. Astro. Soc., 173, 513.

Saraph, H.E., Seaton, M.J. & Shemming, J., 1969. Phil.Trans. Roy. Soc., 264A, 77.

Sarazin, C.L., 1976. Ap. J., 204, 68.

Savage,B.D., 1975. Ap . J., 199, 92.

Scville, N.J. & Solomon, P.M., 1974. Ap. J.(Letters), 187,L67.

Seaton, M.J., 1955. Ann. Ap., 18, 188.

Seaton, M.J., 1958. Rev. Mod.Phys., 30, 1095.

Seaton, M.J., 1959. Mon. Not. R.Astro.Soc., 119, 81.

Seaton, M.J., 1964. Mon.Not.R.Astron.Soc., 127, 177.

Seaton, M.J., 1980. 'Radio Recombination Lines', D. Reidel Publ., 3.

Simpson, J.P., 1970. Astrophys. Letters, 7, 43.

Smith, D. & Adams, N.G., 1978. Ap. J. Letters, 220, L87.

Smith, D. & Adams, N.G., 1981. Mon.Not.R.Astro.Soc., 197, 377.

Smith, W.H. & Sweibel, E.G. 1976., Ap.J., 207, 758.

Solomon, P.M. & Klemperer, W., 1972. Ap.J., 178, 389.

Spitzer, L. Jr., 1949. Ap. J., 109, 337.

Spitzer, L., 1968. 'Diffuse Matter in Space'(New York: Interscience).

Spitzer, L. Jr. & Jenkins, E.B., 1975. Ann. Rev. Astron. Astrophys., 13, 133.

Spitzer, L. and Tomasko, M.G., 1968. Ap. J., 152, 971.

Stecher, T.P. & Williams, D.A., 1967. Ap. J., 149, L29.

Stephens, T.L. & Dalgarno, A., 1972. J. Quant. Spectrosc. Radiat. Transfer, 12, 569.

Summers, H.P., 1969. Ph.D.Thesis, Cambridge.

Ungerecht, H. & Walmsley, C.M., 1978. Astron.Astrophys., 80, 325.

Viala, Y.P., Bel, N. & Clavel, J., 1979. Astron.Astrophys., 73, 174.

Walker, T.E.H. & Kelly, H.P., 1972. Chem.Phys.Letters, 16, 511.

Watson, W.D., 1972. Ap. J., 176, 103.

Watson, W.D., 1974. 'Atomic and Molecular Physics and the Interstellar Matter', LES HOUCHES Session XXVI, p.177.

Weiss, M.J., Lawrence, G.M. & Young, R.A., 1970. J.Chem.Phys., 52, 2867.

Werner, M.W., 1970. Astrophys. Lett., 6, 81.

Westbrook, W.E., Werner, M.W., Elias, J.H., Gezari, D.Y., Hauser, M.G., Lo, K.Y. & Neugebauer, G., 1976. Ap.J.,209, 94.

Wild, J.P., 1952. Ap. J., 115, 206.

Wilson, T.L, Thomasson, P. & Gardner, F.F., 1975. Astron. Astrophys., 43, 167.

Winnewisser, G., Mezger, P.G. & Breuer, H.D., 1974. Top.Curr. Chem., 44, 1.

Witt, A. & Johnson, M.W., 1973. Ap. J., 181, 363.

York, D.G., 1975. Ap. J. Letters, 196, L103.

Zuckerman, B. & Ball, J.A., 1974. Ap. J., 190, 35.

****

LIST OF PUBLICATIONS

1. "Improved Calculation of the Ionisation Equilibrium of Ca and Na in HI Regions."
   Bull. Astron. Soc. India (1974), 2, 41.
2. "Chlorine Chemistry as a Possible Source of Ionisation of Interstellar Hydrogen."
   Mon. Not. R. Astron. Soc. (1979), 186, 621.
3. "Temperature Distribution in the Transition Region and Inner Corona".
   Solar Physics. (1979), 62, 93. (not Concerned with this Thesis)
4. "A Non-isothermal Calculation of Radio-Recombination Line-intensities of NGC2024, Orion A and W3".
   Mon. Not. R. Astron. Soc. (1983) (In Press).
5. "Influence of the Far Infra-red Radiation Field from the Grains in the HII Region on the Cooling at Low Temperature".
   Publication of Astron. Soc. Japan (Submitted)

[No. 2 – 5 inserted in the flap at the back]

****